# QUANTUM OPTICAL COHERENCE: APPLICATIONS IN PHOTON SWITCHING, CONTROL OF SPONTANEOUS EMISSION AND ATOM LOCALIZATION

A Dissertation

by

SHUAI YANG

Submitted to the Office of Graduate and Professional Studies of
Texas A&M University
in partial fulfillment of the requirements for the degree of

DOCTOR OF PHILOSOPHY

| | |
|---|---|
| Chair of Committee, | M. Suhail Zubairy |
| Committee Members, | Goong Chen |
| | Marlan O. Scully |
| | Alexei Sokolov |
| Head of Department, | George R. Welch |

December 2013

Major Subject: Physics

ABSTRACT

Quantum interference and coherence lead to many interesting phenomenon and applications in quantum optics. In this dissertation, we study the quantum coherent properties in the following systems and aspects. We first investigate the optical bistability in a combined cavity-cold atoms system. In such a system the atom-photon interaction provides an optical lattice to the atoms and affects the mechanical motion of the atoms while atoms induce a position dependent phase shift on the cavity field. This highly nonlinearity induces optical bistability of intra-cavity photon number with respect to the pumping light added along the cavity axis. We show that the presence of this bistability can be controlled by a second pumping field added perpendicular to the cavity axis. It is also found that the critical input intensity of switching from one branch of bistability to the other depends on the the way of the field being added. This behavior is similar to the anomalous switching of the dispersive optical bistability of atomic media in the cavity. We also study the effect of counter-rotating terms in the control of spontaneous emission. We make use of a unitary transformation method and investigate the effect of dynamic energy shifts on the spontaneous emission modification via quantum interference in a four-level atomic system. We show that the counter-rotating terms, which are normally neglected in the usual investigation of atomic systems, do produce a significant influence on the evolution of the atomic amplitudes and the emission spectrum. This effect of counter-rotating terms can be observed in the time scale of the decay rate even when the dipole moments of the two upper levels are orthogonal to each other. The effect of counter-rotating terms on the spontaneous emission in a 3-D anisotropic photonic crystal is also discussed. It is shown that the behavior of the emission is similar to the

case making rotating wave approximation, i.e., the localized and propagating fields are also separated by two characteristic atomic transition frequencies. However, the two characteristic frequencies are shifted due to the full Lamb shift which is obtained with counter-rotating terms being included in the Hamiltonian. We also utilize the unitary transformation method to show how the Lamb shift in a multi-level atom can be controlled by a driving field. Finally, we propose a subwavelength atom localization scheme for an atom located in a standing-wave field. The strategy is based on the observation that the photon statistics of resonance fluorescence depends on the position-dependent Rabi frequency.

*To Evan*

# ACKNOWLEDGEMENTS

I would like to take this opportunity to thank the people who have inspired and supported me throughout my PhD studies. First, I would like to express my greatest gratitude to my advisor, Prof. M. Suhail Zubairy. Suhail has amazing physics intuition and insight. His caring, patience, and excellent guidance insured my research and always helped me from going in wrong directions to search for answers. Beyond academic support and guidance, the more valuable things I learned from him are his professional manner and optimistic attitude.

Next, I would like to extend my gratitude to Prof. Mohammad Al-Amri, Prof. Shi-Yao Zhu and Prof. Jörg Evers for offering their expertise and physics insight through many stimulating discussions. I would also like to thank my dissertation committee Prof. Marlan Scully, Prof. Alexei Sokolov and Prof. Goong Chen for providing me valuable suggestions.

I am grateful to work with several wonderful and talented current and former group members Dr. Qing-qing Sun, Prof. Jun Xu, Ze-yang Liao, Dr. Ke-yu Xia, Dr. Zheng-hong Li, Dr. Li-gang Wang, Wen-chao Ge, and Jabir Hakami. Additional gratitude is offered to many other friends and colleagues. I have enjoyed discussing physics with Dr. Meng Gao, Dr. Xiong-jun Liu, Dr. Xin Liu, Kai Wang, Dr. Da-wei Wang, Lu-qi Yuan, Dr. Xi Wang, Dr. Miao-chan Zhi, Dr. Eyob Sete, and Dr. Dong Sun.

Finally, but most importantly, I would like to thank my family. I appreciate my parents for their unconditional and endless love and support. I wish to thank my wife Siyi for her assistance and faith in me. Their constant support make what I am today.

TABLE OF CONTENTS

Page

ABSTRACT . . . . . ii

DEDICATION . . . . . iv

ACKNOWLEDGEMENTS . . . . . v

TABLE OF CONTENTS . . . . . vi

LIST OF FIGURES . . . . . viii

1. INTRODUCTION . . . . . 1

2. OPTICAL BISTABILITY AND DICKE PHASE TRANSITION OF COLD ATOMS IN A CAVITY . . . . . 7

2.1 Introduction . . . . . 7
2.2 The combined cavity-cold atoms system . . . . . 9
2.3 Controllable optical bistability . . . . . 15
2.3.1 Optical bistability . . . . . 15
2.3.2 The role of the atom-atom interaction . . . . . 23
2.3.3 Influence of the parallel pump on the Dicke phase transition . 24
2.3.4 Summary . . . . . 29
2.4 Anomalous switching of the optical bistability . . . . . 30
2.4.1 Anomalous switching . . . . . 30
2.4.2 Explanation . . . . . 32
2.4.3 Effect of initial condition and damping rate . . . . . 36
2.4.4 Summary . . . . . 38
2.5 Degenerate Fermi gas in a cavity . . . . . 39
2.5.1 Motivation and the system . . . . . 39
2.5.2 Phase transition and the analogy to the Dicke Hamiltonian . . 41
2.6 Summary . . . . . 47

3. CONTROL OF SPONTANEOUS EMISSION: EFFECT OF COUNTER-ROTATING TERMS . . . . . 48

3.1 Introduction . . . . . 48
3.2 The unitary transformation method . . . . . 50
3.3 Effect of energy shifts on the spontaneous emission modification via quantum interference . . . . . 53
3.3.1 Motivation . . . . . 53

3.3.2 Model and calculation . . . 54
3.3.3 Results . . . 61
3.3.4 Experiment proposal . . . 66
3.3.5 Summary . . . 67
3.4 Effect of counter-rotating terms on the spontaneous emission in an anisotropic photonic crystal . . . 67
3.4.1 Motivation . . . 67
3.4.2 Model and calculation . . . 68
3.4.3 Results . . . 72
3.4.4 Summary . . . 77
3.5 Control of Lamb shift by a driving field . . . 78
3.5.1 Motivation . . . 78
3.5.2 Level shifts in a coherently driven atom . . . 79
3.5.3 Summary . . . 88
4. SINGLE ATOM LOCALIZATION VIA RESONANCE FLUORESCENCE PHOTON STATISTICS . . . 89
4.1 Introduction . . . 89
4.2 Localization scheme . . . 90
4.3 Photon statistics in resonance fluorescence . . . 92
4.4 Results and discussion . . . 94
4.4.1 Position-dependent resonance fluorescence photon statistics . . . 94
4.4.2 Conditional position probability distribution . . . 95
4.4.3 Strategy . . . 99
4.4.4 Effect of the detector efficiency . . . 101
4.5 Summary . . . 104
5. CONCLUSION . . . 105
REFERENCES . . . 110
APPENDIX A. DERIVATION OF THE DISCRETE MODE HAMILTONIAN 125
APPENDIX B. DERIVATION OF THE FERMION HAMILTONIAN . . . 127
B.1 Commutation relation $[\hat{d}_q, \hat{d}_q^\dagger]$ . . . 127
B.2 Effective Hamiltonian . . . 127
APPENDIX C. TRAPPING CONDITION WITHOUT THE RWA . . . 130
APPENDIX D. LAPLACE TRANSFORM AND ENERGY SHIFTS . . . 132
D.1 Calculation of $\Gamma$ . . . 132
D.2 The inverse Laplace transform . . . 133
D.3 Energy shifts . . . 135

LIST OF FIGURES

FIGURE Page


2.1 A schematic of the combined cavity-cold-atoms system . . . . . 9

2.2 The cavity photon numbers as a function of the input pump along the cavity axis. For (a) → (c), the parameters are $N = 4.8 \times 10^4, \tilde{U}_0 = 0.25, \tilde{\delta}_c = 1.2 \times 10^3, \tilde{\kappa} = 0.4 \times 10^3$, and (a) $\tilde{\eta}_\perp = 0$, (b) $\tilde{\eta}_\perp = 0.1$, (c) $\tilde{\eta}_\perp = 0.5$. For (d) → (f), the parameters are $N = 1 \times 10^4, \tilde{U}_0 = 0.5, \tilde{\delta}_c = 1.1 \times 10^3, \tilde{\kappa} = 0.2 \times 10^3$, and (a) $\tilde{\eta}_\perp = 0$, (b) $\tilde{\eta}_\perp = 0.4$, (c) $\tilde{\eta}_\perp = 1$. For each cases, we neglect the atom-atom interaction since we want to make a direct comparison with the DMP method. . . . . 16

2.3 The cavity photon numbers as a function of the input pump along the cavity axis by the 3-level DMP method. The parameters are $N = 4.8 \times 10^4, \tilde{U}_0 = 0.25, \tilde{\delta}_c = 1.2 \times 10^3, \tilde{\kappa} = 0.4 \times 10^3$, and (a) $\tilde{\eta}_\perp = 0$, (b) $\tilde{\eta}_\perp = 0.1$, (c) $\tilde{\eta}_\perp = 0.5$. . . . . 20

2.4 The cavity photon numbers as a function of the input pump along the cavity axis. The parameters are $N = 4.8 \times 10^4, \tilde{U}_0 = 0.25, \tilde{\delta}_c = 1.2 \times 10^3, \tilde{\kappa} = 0.4 \times 10^3$, and (a) $\tilde{\eta}_\perp = 0$, (b) $\tilde{\eta}_\perp = 0.1$, (c) $\tilde{\eta}_\perp = 0.5$. . 21

2.5 (a) and (c) The cavity output photon number $n_{out}$ as a function of the trial input photon number $n_{tr}$. (b) and (d) show $\langle \cos(2kx) \rangle$ as a function of the parallel pumping strength. The parameters are $N = 4.8 \times 10^4, \tilde{U}_0 = 0.25, \tilde{\delta}_c = 1.2 \times 10^3, \tilde{\kappa} = 0.4 \times 10^3$, and (a) and (b) $\tilde{\eta}_\perp = 0$, (c) and (d) $\tilde{\eta}_\perp = 0.5$. The curves in (a) and (c) correspond to $\tilde{\eta}_\parallel = (0.5, 0.9, 1.2, 1.4, 1.6) \times 10^3$, respectively. . . . . 22

2.6 The influence of the atom-atom interaction for the bistability. The two lines with the same color correspond to the two branches of the bistable behavior for a given value of $Ng_c = 0, 10, 20, 30, 40, 50$, and 60, from bottom to top. Other parameters are $N = 4.8 \times 10^4, \tilde{U}_0 = 0.25, \tilde{\kappa} = 0.4 \times 10^3$, $\tilde{\eta}_\perp = 0$ and $\tilde{\delta}_c = 1.1 \times 10^3$ . . . . . 25

2.7 The cavity photon number as a function of the input pump perpendicular to the cavity axis. The parameters are $N = 1 \times 10^4$, $\tilde{U}_0 = 0.5$, $\tilde{\delta}_c = 1.1 \times 10^3$, $\tilde{\kappa} = 0.2 \times 10^3$, $Ng_c = 0$, and (a) $\tilde{\eta}_\parallel = 0$, (b) $\tilde{\eta}_\parallel = 50$, (c) $\tilde{\eta}_\parallel = 1 \times 10^3$, and (a) $\tilde{\eta}_\parallel = 1.5 \times 10^3$. . . . . 26

2.8 The regions of lower branch, bistability, and upper branch of the cavity photon number. The parameters are $N = 1 \times 10^4$, $\tilde{U}_0 = 0.5$, $\tilde{\delta}_c = 1.1 \times 10^3$, $\tilde{\kappa} = 0.2 \times 10^3$, and $Ng_c = 0$. . . . . 30

2.9 Steady-state intra-cavity photon number as a function of the input pump intensity. The parameters are $N = 4.8 \times 10^4$, $U_0 = 0.25\omega_r$, $\delta_c = 1.2 \times 10^3\omega_r$, $\kappa = 0.4 \times 10^3\omega_r$. The input pump intensity is also in the unit of $\omega_r$. The critical switching points are $\eta_A = 1322\omega_r$ and $\eta_B = 1013\omega_r$ for the steady state. The critical anomalous switching points are $\eta_C = 1222\omega_r$ and $\eta_D = 1143\omega_r$. . . . . 31

2.10 Intra-cavity photon number as a function of time. Initially there is no pump field and the condensate is the homogeneous state. Then the pump field is turned on immediately with values (a) $500\omega_r$, (b) $1100\omega_r$, (c) $1500\omega_r$ and (d) $1250\omega_r$. The parameters are $N = 4.8\times10^4$, $U_0 = 0.25\omega_r$, $\delta_c = 1.2 \times 10^3\omega_r$, $\kappa = 0.4 \times 10^3\omega_r$. The time is in the unit of $1/\omega_r$. . . . . 33

2.11 The potential $V(X)$. The lines from top to bottom correspond to difference pump fields, (1) $500\omega_r$, (2) $1100\omega_r$, (3) $1250\omega_r$ and (4) $1500\omega_r$. The parameters are $N = 4.8 \times 10^4$, $U_0 = 0.25\omega_r$, $\delta_c = 1.2 \times 10^3\omega_r$, $\kappa = 0.4 \times 10^3\omega_r$. . . . . 34

2.12 Intra-cavity photon number as a function of time for different initial conditions. (a) The initial state is the steady state corresponding to $\eta = 800\omega_r$. Then the pump field is tuned sharply to $\eta = 1250\omega_r$. (b) The initial state is the steady state corresponding to $\eta = 1600\omega_r$. Then the pump field is tuned to $\eta = 1100\omega_r$ abruptly. The other parameters are $N = 4.8 \times 10^4$, $U_0 = 0.25\omega_r$, $\delta_c = 1.2 \times 10^3\omega_r$, $\kappa = 0.4 \times 10^3\omega_r$. The time is in the unit of $1/\omega_r$. . . . . 37

2.13 Intra-cavity photon number as a function of time with damping. Initially there is no pump field and the condensate is the homogeneous state. Then the pump field is turned on immediately with $\eta = 1250\omega_r$. The damping rates are (a) $0.05\omega_r$ and (b) $0.02\omega_r$. The other parameters are $N = 4.8\times10^4$, $U_0 = 0.25\omega_r$, $\delta_c = 1.2\times10^3\omega_r$, $\kappa = 0.4\times10^3\omega_r$. The time is in the unit of $1/\omega_r$. . . . . 38

2.14 The phase transition of different quantities. (a) The intra-cavity photon number. (b) The eigenstate energy. (c) The average value of $\cos(k_c x)$. The horizontal coordinate of the black vertical line is calculated from equation (2.59). . . . . 46

3.1 Atomic transitions in the dressed state picture. . . . . 55

3.2 Evolution of the population with $a_1(0) = a_2(0) = 1/\sqrt{2}$. The parameters are $\omega_{a_1 b} = 10^4\gamma_{a_1}$, $\Delta_1 = -\Delta_2 = 5\gamma_{a_1}$, and $\gamma_{a_2} = \gamma_{a_1}$. The driving fields are (a) $\Omega_1 = \Omega_2 = 0$, (b) $\Omega_1 = \Omega_2 = 1.5\gamma_{a_1}$, and (c) $\Omega_1 = \Omega_2 = 5\gamma_{a_1}$. . . . . 62

3.3 Spontaneous emission spectrum for $a_1(0) = a_2(0) = 1/\sqrt{2}$. The parameters are $\omega_{a_1 b} = 10^4\gamma_{a_1}$ and $\omega_{12} = \gamma_{a_2} = \gamma_{a_1}$. Red dashed line, $\Omega_1 = \Omega_2 = 0$; blue solid line, $\Omega_1 = \Omega_2 = \gamma_{a_1}$. . . . . 62

3.4 Evolution of the population in the upper levels for $a_1(0) = a_2(0) = 1/\sqrt{2}$. The parameters are $\omega_{a_1 b} = 10^4\gamma_{a_1}$, $\Delta_1 = -\Delta_2 = 5\gamma_{a_1}$, $\Omega_1 = \Omega_2 = 5\gamma_{a_1}$, and $\gamma_{a_2} = \gamma_{a_1}$. . . . . 63

3.5 Spontaneous emission spectrum. The parameters are $\omega_{a_1 b} = 10^4\gamma_{a_1}$, (a) $\Omega_1 = \Omega_2 = \Delta_1 = -\Delta_2 = \gamma_{a_2} = \gamma_{a_1}$, (b) $\Omega_1 = \Delta_1 = \gamma_{a_2} = \gamma_{a_1}$, $\Delta_2 = -4\gamma_{a_1}$, $\Omega_2 = 2\gamma_{a_1}$. The atom is initially in level $|a_1\rangle$ for (a) and $(1/\sqrt{2})(|a_1\rangle + |a_2\rangle)$ for (b). . . . . 64

3.6 Evolution of the population in the upper levels when the two dipoles are orthogonal. The initial state is $(1/\sqrt{2})(|a_1\rangle + |a_2\rangle)$. The parameters are $\omega_{a_1 b} = 10^4\gamma_{a_1}$, $\Delta_1 = -\Delta_2 = 5\gamma_{a_1}$, $\gamma_{a_2} = \gamma_{a_1}$. The driving fields are (a) $\Omega_1 = \Omega_2 = 2\gamma_{a_1}$ and (b) $\Omega_1 = \Omega_2 = 0$. . . . . 65

3.7 Spontaneous emission spectrum when the two dipoles are orthogonal. The parameters are $\omega_{a_1 b} = 10^4\gamma_{a_1}$, $\Omega_1 = \Omega_2 = \Delta_1 = -\Delta_2 = \gamma_{a_2} = \gamma_{a_1}$. The atom is initially in level $|a_1\rangle$. . . . . 65

3.8 The squared amplitude of the localized mode and the propagating mode as function of detuning of resonant frequency from photonic band edge $\omega_1 c$ with $\omega_c = 200\beta$. The top figure corresponds to the case with RWA. The bottom figure corresponds to the case without making RWA. The three ranges I, II and III correspond to the localized modes, diffusion modes and propagating modes, respectively . . . . . 73

3.9 The time evolution of the upper-level population with $\omega_c = 200\beta$. figure (a) $\omega_{1c} = 0.041436\beta$, (b) $\omega_{1c} = 0.055\beta$, and (c) $\omega_{1c} = 0.07072\beta$, respectively. . . . . 75

3.10 The steady-state atomic population in the upper level with respect to the detuning with $\omega_c = 200\beta$. . . . . 75

3.11 The atom configuration. . . . . 79

3.12 Additional Lamb shift by the driving field. . . . . 86

3.13 Schematic of Feynman's interpretation of the Lamb shift. . . . . 88

4.1 The photon statistics $p(n|x)$ for fixed atom positions (a) $kx = 0$, (b) $kx = \pi/20$, (c) $kx = \pi/8$, and (d) $kx = \pi/2$. The other parameters are $\Omega_0 = 10\beta$ and $\beta t = 10$. . . . . 94

4.2 The conditional position probability distribution $p(x|n)$ versus normalized position of the atom inside the standing-wave field ($kx = -\pi$ to $\pi$) for (a) $n = 0$, (b) $n = 1$, (c) $n = 5$, (d) $n = 7$, (e) $n = 10$, and (f) $n = 15$. The other parameters are the same as in figure 4.1. . . . . 96

4.3 The conditional position probability distribution for different number of measurements when the atom is located at (a) $kx = \pi/20$, (b) $kx = \pi/10$ and (c) $kx = \pi/4$. The red dashed lines correspond to the case when one measurement is made. The blue solid lines correspond to the case when 10 measurements are made in (a) and (b) and the case when 100 measurements are made in (c). The other parameters are the same as in figure 4.1. . . . . 97

4.4 (a) The estimated position of the atom within unit wavelength domain of the standing-wave field and (b) deviation from the estimated position versus number of photons measured. The other parameters are the same as in figure 4.1. . . . . 99

4.5 The deviation from the estimated position of the atom versus detector measuring time when no photon is recorded. The other parameters are the same as in figure 4.1. . . . . 101

4.6 The position probability distribution for no counting $p(x|0)$ versus $kx$ for (a) different detector efficiencies (i) $\eta = 0.2$ (ii) and $\eta = 1.0$. The driving field strength $\Omega_0 = 3\beta$ and the measuring time $\beta t = 3$. (b) different combinations of the driving field strength and the measuring time (i) $\Omega_0 = 3\beta$, $\beta t = 3$ and (ii) $\Omega_0 = 10\beta$, $\beta t = 10$. Here $\eta = 0.2$. . . 103

D.1 (a) The integration contour of Eq. (D.3). (b) The integration contour of Eq. (D.5) . . . . . 135

# 1. INTRODUCTION

Since the birth of quantum mechanics, interference has been described as the real quantum mystery. R. Feynman, referred in the following way to the phenomenon of interference: "it has in it the heart of quantum mechanics", and it is really "the only mystery" of quantum mechanics [1].

In quantum optics, interference continuously plays roles in many phenomenons [2]. The understanding of such phenomenons stimulates the progress and development of the field. In early studies, quantum interference is concerned with coherence and correlation phenomena in radiation fields and between their sources. The Hanbury-Brown-Twiss experiment studied the correlation in the photo-current fluctuations from two detectors and observed the photon bunching phenomenon [3]. The quantum formulation of optical coherence theory by R. Glauber elucidated the two-time correlation function and predicates the photon anti-bunching [4]. The experimental verification of the photon anti-bunching of the light generated in resonance fluorescence from a two-level atom showed the nonclassical effect in optics for the first time [5].

Modern studies of interference and coherence in quantum optics involve a series of interesting topics, such as the property and application of squeezed states of radiation fields [6, 7], electromagnetic induced transparency [8, 9], and lasing without inversion [10, 11, 12]. The study of quantum interference also twists with some fundamental concepts of quantum physics. For example, spontaneous emission, which describes the process that an excited light source such as an atom, jumps to a lower energy state and emit a photon, stimulated the birth of modern quantum mechanics and quantum electrodynamics. It is shown that quantum interference can lead to

spontaneous emission suppression, spectral narrowing, population trapping, and the phase control of spontaneous emission [13, 14, 15, 16, 17, 18, 19, 20, 21, 22, 23, 24].

Rapid developed techniques in quantum optics and atomic physics provide powerful probes for many seminal discoveries and applications. The developments in these topics also enriched the contents of quantum optics. The appearance of optical interference also arose in these versatile toolboxes. For example, The multi-photon entanglement technique not only enables the testing of fundamental quantum mechanics issues such as complementarity and hidden variables but also provides basic resources for quantum communication and computation process [25]. The standing light wave generates a periodic potential structure for atoms and can be used to build atom interferometer [26].

Progresses in experimental techniques also twist atomic, molecular and optical physics with other physics branches. For example, laser cooling combined with the evaporation cooling techniques enable experimental observation of Bose-Einstein condensation (BEC) in 1995 [27, 28]. Since then, "atomic physics and quantum optics has met condensed matter physics" [29]. Particularly, the interference of counter-propagating laser lights which are far detuned from an atomic resonance creates a spatially periodic polarization pattern called optical lattice. The resulting periodic potential can be used to trap neutral atoms. Cooled atoms congregate in the locations of potential minima and resembles a crystal lattice. The dynamics of atoms in the lattice can be easily controlled through adjusting several of the lattice parameters as the intensity and the configuration. In addition, well developed Feshbach resonance technique enables the tailoring of the collisional properties of certain types of atoms. Therefore, optical lattice offers a clean platform and provides for a plethora of possibilities to study quantum properties of many-body strongly correlated systems. The physics of cold atoms touches the same frontiers of condensed matter and high

energy physics [30].

In this dissertation, we study the applications of quantum interference and coherence in the following aspects.

- Optical bistability in a cavity-cold atoms system

  In free space, the light fields which build the optical lattice are usually treated classically and independently of the atoms. This approximation requires intense light, far detuned from any atomic transition. Of course this assumption fails when the light is enhanced by an optical resonator. In this case, the field itself becomes a dynamical quantity which depends on the atomic distribution. As all atoms are coupled to the same field modes, this immediately introduces substantial long range interactions, which cannot be ignored as in free space. In such a system, many interesting phenomenons and applications have been proposed and investigated theoretically and experimentally. For example, with well chosen parameters, the long range force induces coherently driven atoms to self-organize in regular patterns [31, 32, 33, 34, 35, 36]. Such a self-organization phase transition can be mapped to the Dicke quantum phase transition [37, 38, 39, 40, 41]. In addition, the center-of-mass oscillation of the ultra-cold atoms can be identified as the vibration of a quantum mirror. Therefore, the coupling of the center-of-mass freedom of the atoms and the cavity optical field can realize the optomechanical systems [42, 43].

  In our research, we mainly focus on the optical property of the combined cavity-cold atoms system. The atom-photon interaction provides the optical lattice to the atoms and affects the mechanical motion of the atoms. In turn, atoms induce a position dependent phase shift on the cavity field. This highly intrinsic nonlinearity leads bistability for both the intra-cavity photon number and

atomic state. We will investigate the switching behavior of the optical bistability and show how the switching from one branch of the bistability to the other depends on the manner of adding the laser light [44]. We will also explore how the bistability can be controlled [45]. Especially, if in a high-Q optical resonator, our scheme provides a candidate for controllable optical switch of a few photons. These studies are presented in section 2.

- Effect of counter-rotating terms in the control of spontaneous emission

  Quantum interference has been recognized as a significant mechanism for the modification of spontaneous emission [13, 14, 15, 16, 17, 18, 19, 20, 21, 22, 23, 24]. The spontaneously generated coherence can lead to suppression, spectral narrowing, and population trapping [13, 14, 15, 16, 17, 18, 19, 20, 21], phase control of spontaneous emission [22, 23], and enhancement of Kerr nonlinearity [24]. Particularly in a V-type atom, the quantum interference due to the spontaneous emission of two atomic levels coupled to a common lower level through the interaction with the same vacuum modes can lead to quenching of the spontaneous emission from the two upper levels [13]. If the two upper levels are driven to another level by a strong laser field, complete quenching of spontaneous emission is possible under certain conditions [14, 18].

  In previous studies of quantum interference of the spontaneous emission of two atomic levels coupled to a common lower level, the rotating wave approximation (RWA) is usually assumed. However, the validity of RWA is questionable. The interference between the decay rates of the two levels (real parts of the dynamical equations) is investigated, while the energy shifts (imaginary parts of the dynamical equations), are discarded. This is because the imaginary parts are divergent because of the free electron self-energy. In addition, calculation of

the energy shifts cannot neglect the contribution of the counter-rotating terms.

In section 3, we utilize the unitary transformation method proposed in Ref. [46, 47] to study the spontaneous emission without making RWA. The unitary transformation method transforms the Hamiltonian to the RWA form while including the effect of the counter-rotating terms and subtracting the free electron self-energy from the Hamiltonian. We first show the interference effect of the energy shifts in a four-level atom. This effect will be revealed even if the two dipole transitions from the upper levels to the ground level are orthogonal [48]. We then show two other applications of the unitary transformation method. One is the spontaneous emission in a photonic crystal without making RWA [49]. The other one is a scheme to control Lamb shift by a driving field [50].

- Single atom localization via resonance fluorescence photon statistics

  When a low monochromatic resonant excitation field is applied on a atom, the atom absorbs a photon at the excitation frequency, and energy conservation demands that the emitted photon have the same frequency. The emitted fluorescence has the same spectral profile as the excitation. In a strong resonant field, when the excitation intensity increases and the Rabi frequency associated with the driving field becomes comparable to, or larger than, the atomic linewidth, non-linear scattering occurs. The atom can coherently interact many times with the laser field before spontaneously radiating a photon. Therefore, Rabi oscillations show up not only in the population of the atomic levels (the inversion) but also as a modulation of the quantum dipole moment. This in turn leads to sidebands emerging in the spectrum of the emitted radiation which is the so-called "dynamic Stark splitting" [51]. In addition to that, the

fluorescent light exhibits certain nonclassical properties including photon antibunching and squeezing [5]. Antibunching implies sub-Poissonian statistics, in the sense that the probability distribution $p(n)$ is narrower than a Poisson distribution with the same mean $\langle n \rangle$. So the probability distribution $p(n)$ of the number of photons $n$ emitted by a driven two-level atom in some given time interval $T$ in the steady state shows a sub-Poissonian photon statistic [52, 53, 54].

In section 4, we propose a scheme to localize a single atom fixed in a standing wave based on the photon statistics in resonance fluorescence [55]. The photon number statistics depends on the atom position through the position-related Rabi oscillations introduced by the standing-wave field. So the recorded photon number will provide us information on the position of the atom. Furthermore, as the standing wave is a sinusoid function, the change in the Rabi frequency at the nodes is sharp, which means a tiny change in the position will cause a dramatic response of the statistics. The accuracy of the localization would be high close to the nodes.

# 2. OPTICAL BISTABILITY AND DICKE PHASE TRANSITION OF COLD ATOMS IN A CAVITY *

## 2.1 Introduction

Recently, an ultra cold atomic ensemble located in a small volume ultra-high finesse optical cavity has been studied from many different points of view. In the large detuning limit from the atomic resonance, the dispersive regime is realized. The atom-photon interaction provides an optical lattice to the atoms and affects the mechanical motion of the atoms. In turn, atoms induces a position dependent phase shift on the cavity field. This highly intrinsic nonlocal nonlinearity is quite different from the usual local atom-atom interactions and induces a lot of interesting results such as self-organization of atoms [31, 32, 33, 34, 35, 36], optical bistability [56, 57, 58, 59, 60], cavity-enhanced super-radiant Rayleigh scattering [61], mapping between the atoms ensemble-cavity system and the canonical optomechanical system [42, 43], and analogy of the Dicke quantum phase transition [37, 38, 39, 40, 41].

We first focus on the optical bistability. The optical bistability of the intra-cavity photon number is typically studied for a system with only one pumping field, which is along the cavity axis. We consider a system with transverse pumping also. We show that the bistable behavior can be controlled by this transverse pumping field. For low transverse pumping, the intra-cavity photon number shows clear bistability for a particular range of the input pump along the cavity axis. When increasing the transverse pumping field, the range of the bistable behavior is diminished. In

*Reprinted with permission from "Controllable optical switch using a Bose-Einstein condensate in an optical cavity," by Shuai Yang, M. Al-Amri, Jörg Evers, and M. Suhail Zubairy, 2011, *Phys. Rev. A*, vol. 83, p. 053821, copyright [2011] by American Physical Society, and "Anomalous switching of optical bistability in a Bose-Einstein condensate," by Shuai Yang, M. Al-Amri, and M. Suhail Zubairy, 2013, *Phys. Rev. A*, vol. 83, p. 033836, copyright [2013] by American Physical Society.

particular, above a critical value of the transverse pumping, the bistable behavior disappears. This result provides the possibility of realizing a controllable optical switch. For this, the two stable branches of the output photon number conditioned on the parallel input field act as the optical switch. The transverse pump can then be used to enable or disable this switch. If the switch is disabled, only one of the two possible switch states can be realized, independent of the input field. We verify the operation of the switch using numerical solutions of the underlying Gross-Pitaevskii (GP) equation, and additionally we interpret the results based on a discrete mode approximation (DMA) method [59].

We then study the dynamic behavior of the optical bistability induced by the pumping field along the cavity axis. We investigate switching behavior of the intracavity photon number from one branch to the other. We find that the way of adding the field is crucial to the switching close to the critical transition point. If the pump field is added adiabatically, the jumping happens exactly at the critical point [59]. If the pump field is added abruptly, the system may jump to the upper branch even if the pump field intensity is less than the critical transition point. This behavior is similar to the anomalous switching of the dispersive optical bistability [62, 63]. We analyze the physics of this anomalous switching and examine the effect of the initial condition and the possible damping.

At last we study the phase transition of cold atoms when a pumping field is added perpendicularly to the cavity. It has been shown both theoretically and experimentally that this phase transition of an BEC can be identified as the Dicke quantum phase transition [40, 41]. We propose an interesting scheme which realizes an effective Dicke Hamiltonian with a quantum-degenerate Fermi gas in an optical cavity. Unlike the Boson case, where the atom-atom interaction affects the critical value of the transition, the atom-atom interaction is negligible in Fermi gases due to

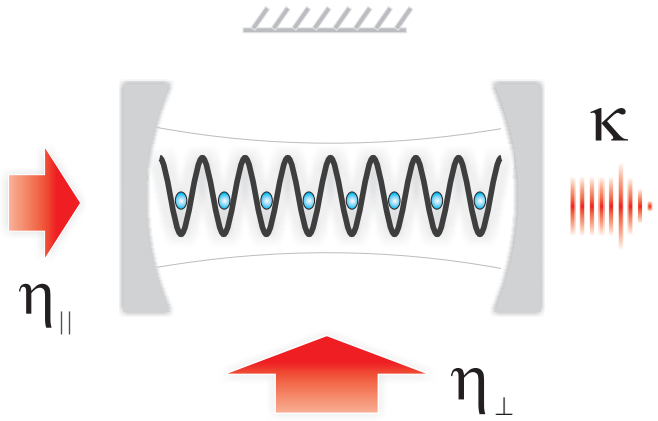


Figure 2.1: A schematic of the combined cavity-cold-atoms system

the Pauli exclusion principle.

This section is organized as follows. In 2.2, we present our system. In 2.3, we investigate the steady-state bistability and show how this bistability can be controlled. In 2.4, we study the dynamic switching between the two bistable branches. In 2.5, we present the Dicke quantum phase transition of a degenerate Fermi gas in an optical cavity.

## 2.2 The combined cavity-cold atoms system

The system we consider is a gas of $N$ ultra-cold two-level atoms with mass $m$ and transition frequency $\omega_a$ located inside a high-Q optical cavity with length $L$ and cavity mode frequency $\omega_c$, see figure 2.1. The ground state and excited state are labeled as $|g\rangle$ and $|e\rangle$, respectively. Two external pumping laser fields at frequency $\omega_p$ are added as shown in figure 2.1, one along the cavity axis and the other perpendicular to the cavity axis. And the two pump fields are polarized along the same axis.

With the rotating-wave and electric-dipole approximations been made, the single

atom Hamiltonian is described by

$$\hat{H}^1 = \hat{H}^1_A + \hat{H}^1_R + \hat{H}^1_{A-P} + \hat{H}^1_{A-R} \tag{2.1}$$

where $\hat{H}^1_A$, $\hat{H}^1_R$, $\hat{H}^1_{A-P}$, and $\hat{H}^1_{A-R}$ are the Hamiltonians for the atom, cavity field, coupling between the atom and the pumping field, and interaction between the atom and cavity field, respectively. Explicitly, they are written as

$$\hat{H}^1_A = \frac{\hat{\mathbf{p}}^2}{2m} + V_e(\mathbf{x})|e\rangle\langle e| + V_g(\mathbf{x})|g\rangle\langle g| + \hbar\Delta_a|e\rangle\langle e|\,, \tag{2.2a}$$

$$\hat{H}^1_R = \hbar\Delta_c\hat{a}^\dagger\hat{a} - i\hbar\eta_\parallel(\hat{a} - \hat{a}^\dagger)\,, \tag{2.2b}$$

$$\hat{H}^1_{A-P} = -i\hbar\Omega(\mathbf{x})(|e\rangle\langle g| - |g\rangle\langle e|)\,, \tag{2.2c}$$

$$\hat{H}^1_{A-R} = -i\hbar g(\mathbf{x})(|e\rangle\langle g|\hat{a} - |g\rangle\langle e|\hat{a}^\dagger)\,. \tag{2.2d}$$

where $\Delta_a = \omega_a - \omega_p$ and $\Delta_c = \omega_c - \omega_p$ are the atom-pump detuning and the cavity-pump detuning, respectively. Here $\eta_\parallel$ is the pumping field amplitude of the parallel driving laser, $\Omega(\mathbf{x})$ is the Rabi frequency of the transverse pump field which we take classically, and $g(\mathbf{x})$ denotes the coupling constant of the atom and cavity photon.

For the $N$ atoms system, we apply the second quantization formalism to the atomic Hamiltonian, e.g.,

$$\begin{aligned}\hat{H}_A &= \int d^3\mathbf{x}\Bigg[\hat{\Psi}^\dagger_g(\mathbf{x})\left(-\frac{\hbar^2}{2m}\nabla^2 + V_g(\mathbf{x})\right)\hat{\Psi}_g \\ &\quad + \hat{\Psi}^\dagger_e(\mathbf{x})\left(-\frac{\hbar^2}{2m}\nabla^2 + V_e(\mathbf{x}) + \hbar\Delta_a\right)\hat{\Psi}_e\Bigg]\end{aligned} \tag{2.3}$$

where $\hat{\Psi}_g(\mathbf{x})$ and $\hat{\Psi}_e(\mathbf{x})$ denote the atomic field operators for annihilating an atom at position $\mathbf{x}$ in the ground state and excited state respectively. Here we consider

the Bosons case, e.g.,

$$\left[\hat{\Psi}_j(\mathbf{x}), \hat{\Psi}^\dagger_{j'}(\mathbf{x}')\right] = \delta^3(\mathbf{x}-\mathbf{x}')\delta_{jj'}\,, \tag{2.4a}$$

$$\left[\hat{\Psi}_j(\mathbf{x}), \hat{\Psi}_{j'}(\mathbf{x}')\right] = \left[\hat{\Psi}^\dagger_j(\mathbf{x}), \hat{\Psi}^\dagger_{j'}(\mathbf{x}')\right] = 0 \tag{2.4b}$$

The field operator is not changed, i.e.,

$$\hat{H}_R \;= \hbar\Delta_c \hat{a}^\dagger\hat{a} - i\hbar\eta_\parallel(\hat{a}-\hat{a}^\dagger)\,, \tag{2.5}$$

The interaction between the laser field and the atom and the coupling of the cavity field with the atoms are described by

$$\hat{H}_{A-P} = -i\hbar\int d^3\mathbf{x}\hat{\Psi}^\dagger_g(\mathbf{x})\Omega(\mathbf{x})\hat{\Psi}_e(\mathbf{x}) + h.c.\,, \tag{2.6a}$$

$$\hat{H}_{A-R} = -i\hbar\int d^3\mathbf{x}\hat{\Psi}^\dagger_g(\mathbf{x})g(\mathbf{x})\hat{a}^\dagger\hat{\Psi}_e(\mathbf{x}) + h.c.\,. \tag{2.6b}$$

In the many particle system, we also need to consider the two-body interaction which is modeled by a short- range pseudo-potential and characterized by the $s$-wave scattering length $a_s$. Therefore, the atom-atom interaction Hamiltonian is

$$\hat{H}_{A-A} \;=\; \frac{\hbar g_c}{2}\int d^3\mathbf{x}\hat{\Psi}^\dagger_g(\mathbf{x})\hat{\Psi}^\dagger_g(\mathbf{x})\hat{\Psi}_g(\mathbf{x})\hat{\Psi}_g(\mathbf{x})\,, \tag{2.7}$$

where $g_c = 2\pi\hbar a_s/m$.

With the well defined second quantized Hamiltonian, the Heisenberg equation

give us the the evolution of the atomic field operators,

$$\frac{\partial\hat{\Psi}_g(\mathbf{x})}{\partial t} = i\left[\frac{\hbar}{2m}\nabla^2 - \frac{V_g(\mathbf{x})}{\hbar} - \frac{g_c}{\hbar}\hat{\Psi}_g^\dagger(\mathbf{x})\hat{\Psi}_g(\mathbf{x})\right]\hat{\Psi}_g(\mathbf{x}) - \left[g(\mathbf{x})\hat{a}^\dagger + \Omega(\mathbf{x})\right]\hat{\Psi}_e(\mathbf{x}) \tag{2.8a}$$

$$\frac{\partial\hat{\Psi}_e(\mathbf{x})}{\partial t} = i\left[\frac{\hbar}{2m}\nabla^2 - \frac{V_e(\mathbf{x})}{\hbar} - \Delta_a\right]\hat{\Psi}_e(\mathbf{x}) + \left[g(\mathbf{x})\hat{a} + \Omega(\mathbf{x})\right]\hat{\Psi}_g(\mathbf{x}) \tag{2.8b}$$

And the evolution of the cavity field is described by

$$\frac{\partial\hat{a}}{\partial t} = -i\Delta_c\hat{a} + \eta_\parallel - \int d^3\mathbf{x} g(\mathbf{x})\hat{\Psi}_g^\dagger(\mathbf{x})\hat{\Psi}_e(\mathbf{x}) \tag{2.9}$$

In the large detuning limit, we can adiabatically eliminate the excited state from the dynamics of our system. In this limit, we can also neglect the kinetic energy term and the trapping potential. Therefore, we assume the field $\hat{\Psi}_g(\mathbf{x})$ and $\hat{a}$ vary much slower than the time scale of $1/\Delta_a$, so

$$\hat{\Psi}_e(\mathbf{x}) = -\frac{i}{\Delta}\left[g(\mathbf{x})\hat{a} + \Omega(\mathbf{x})\right]\hat{\Psi}_g(\mathbf{x}) \tag{2.10}$$

Inserting this expression of $\hat{\Psi}_e(\mathbf{x})$ into equations 2.8a and 2.10, we have

$$\begin{aligned}\frac{\partial\hat{\Psi}_g(\mathbf{x})}{\partial t} = {} & i\left[\frac{\hbar}{2m}\nabla^2 - \frac{V_g(\mathbf{x})}{\hbar} + \frac{\Omega(\mathbf{x})^2}{\Delta_a} + \frac{\Omega(\mathbf{x})g(\mathbf{x})}{\Delta_a}(\hat{a}+\hat{a}^\dagger) + \frac{g(\mathbf{x})^2}{\Delta_a}\hat{a}^\dagger\hat{a}\right. \\ & \left. - \frac{g_c}{\hbar}\hat{\Psi}_g^\dagger(\mathbf{x})\hat{\Psi}_g(\mathbf{x})\right]\hat{\Psi}_g(\mathbf{x}) \qquad (2.11a) \\ \frac{\partial\hat{a}}{\partial t} = {} & -i\left[\Delta_c - \frac{1}{\Delta_a}\int d^3\mathbf{x} g(\mathbf{x})\hat{\Psi}_g^\dagger(\mathbf{x})^2\hat{\Psi}_g^\dagger(\mathbf{x})\hat{\Psi}_g(\mathbf{x})\right]\hat{a} \\ & + i\frac{1}{\Delta_a}\int d^3\mathbf{x}\Omega(\mathbf{x})g(\mathbf{x})\hat{\Psi}_g^\dagger(\mathbf{x})\hat{\Psi}_g(\mathbf{x}) + \eta_\parallel \qquad (2.11b)\end{aligned}$$

The effective Hamiltonian for the combined condensate-field system can therefore

be written as

$$\begin{aligned}\hat{H}_{\text{eff}} &= \int d^3(\mathbf{x})\hat{\Psi}_g^\dagger(\mathbf{x})\Bigg[\frac{\mathbf{p}^2}{2m} + V_g(\mathbf{x}) - \frac{\hbar\Omega(\mathbf{x})^2}{\Delta_a} + \frac{\hbar\Omega(\mathbf{x})g(\mathbf{x})}{\Delta_a}(\hat{a}+\hat{a}^\dagger) \\ &\quad + \frac{\hbar g(\mathbf{x})^2}{\Delta_a}\hat{a}^\dagger\hat{a}\Bigg]\hat{\Psi}_g(\mathbf{x}) + \frac{\hbar g_c}{2}\int d^3\mathbf{x}\hat{\Psi}_g^\dagger(\mathbf{x})\hat{\Psi}_g^\dagger(\mathbf{x})\hat{\Psi}_g(\mathbf{x})\hat{\Psi}_g(\mathbf{x}) \\ &\quad + \hbar\Delta_c\hat{a}^\dagger\hat{a} - i\hbar\eta_\parallel(\hat{a}-\hat{a}^\dagger) \end{aligned} \tag{2.12}$$

For the sake of simplicity, we consider the dynamics in the dimension $x$ along the cavity axis. The cavity field mode function is then described simply by $\cos(kx)$, with the wave vector $k$. Therefore, $g(\mathbf{x}) \equiv g_0\cos(kx)$ and $\Omega(\mathbf{x}) \equiv \Omega_p$ is taken as a constant. The model applies to a cigar-shaped BEC, which is tightly confined in the transverse directions by strong dipole or magnetic trap, such that the transverse size of the condensate is smaller than the waist of the cavity field. And we further neglect the external trapping field,

$$\begin{aligned}\hat{H} = \int dx\hat{\Psi}^\dagger(x)\Bigg[&-\frac{1}{2m}\frac{d^2}{d^2x} + U_0\cos^2(kx)\hat{a}^\dagger\hat{a} + \eta_\perp\cos(kx)(\hat{a}^\dagger+\hat{a}) \\ &+ \frac{g_c}{2}\hat{\Psi}^\dagger(x)\hat{\Psi}(x)\Bigg]\hat{\Psi}(x) + \Delta_c\hat{a}^\dagger\hat{a} - i\eta_\parallel(\hat{a}^\dagger-\hat{a}).\end{aligned} \tag{2.13}$$

Here we neglect the subscript $g$ in the atomic field operator. The atom-cavity photon interaction induces an additional potential $U_0\cos^2(kx)\hat{a}^\dagger\hat{a}$ for the atoms where $U_0 = -g_0^2/\Delta_a$ is maximal light shift per photon that an atom may experience. Scattering between the transverse pump field and the cavity mode is described by $\eta_\perp\cos(kx)(\hat{a}^\dagger+\hat{a})$ where $\eta_\perp = g_0\Omega_p/\Delta_a$ is the maximum scattering rate,

In the mean-field approximation, we take the matter-wave field and the cavity electromagnetic field as classic fields, i.e., $\hat{\Psi}(x,t) \sim \Psi(x,t)$ and $\hat{a} \sim \alpha$. The Gross-

Pitaevskii (GP) equation for the condensate then becomes

$$i\frac{\partial\Psi(x,t)}{\partial t}=\left[-\frac{1}{2m}\frac{d^2}{d^2x}+U_0\cos^2(kx)|\alpha|^2+\eta_\perp\cos(kx)(\alpha+\alpha^*)+g_c|\Psi(x,t)|^2\right]\Psi(x,t), \tag{2.14}$$

and the corresponding equation of motion for the cavity field is

$$\begin{aligned}\frac{\partial\alpha}{\partial t}=&-i\left[\Delta_c+U_0\int dx|\Psi(x,t)|^2\cos^2(kx)\right]\alpha-\kappa\alpha\\&-i\eta_\perp\int dx|\Psi(x,t)|^2\cos(kx)+\eta_\parallel.\end{aligned} \tag{2.15}$$

Here we have included the cavity loss $\kappa$ which is the dominant dissipation process since the spontaneous emission is suppressed under the large atom-pump detuning approximation.

In experiments, the cavity damping is much faster than the mechanical motion of the condensate, such that the cavity field can follow the condensate adiabatically. We can therefore assume the steady state for the cavity field in the GP equation, i.e.,

$$\alpha=\frac{\eta_\parallel-i\eta_\perp\int dx|\Psi(x,t)|^2\cos(kx)}{i\left[\Delta_c+U_0\int dx|\Psi(x,t)|^2\cos^2(kx)\right]+\kappa}. \tag{2.16}$$

Substituting equation (2.16) into equation (2.14), we obtain a highly nonlocal and nonlinear GP equation. We choose the imaginary-time propagation method [64] to solve this equation numerically. The strategy is to first replace the real time $t$ with $\tau=it$. Then we choose a trial function $\psi(x,t)$ for the GP equation solution, which can be expanded as as linear combination of all eigenfunctions of the Hamiltonian

$\hat{H}$,

$$\psi(x, \tau t) = \sum_i \phi_i(x) e^{-iE_i t} = \sum_i \phi_i(x) e^{-E_i \tau} \,. \tag{2.17}$$

Evolving the state in imaginary time, the excited states with larger $E_i$ will decay exponentially faster than the ground state. After each small step of the propagation along the imaginary time, we normalize the eigenfunction, which eventually leads to an increase of the ground state contribution of the evolved state. Ideally, after a certain evolution period, only the ground state survives.

## 2.3 Controllable optical bistability

### *2.3.1 Optical bistability*

The cavity photon number is given by

$$n = |\alpha|^2 = \frac{\eta_\parallel^2 + \left[\eta_\perp \int dx |\Psi(x,t)|^2 \cos(kx)\right]^2}{\left[\Delta_c + U_0 \int dx |\Psi(x,t)|^2 \cos^2(kx)\right]^2 + \kappa^2}. \tag{2.18}$$

The integrals in the above equation depend on the photon number through the GP equation (2.14). To the lowest order, we can expect a linear dependence. However equation (2.18) is a third order equation in $n$, such that in general three roots exist. This leads to the appearance of bistability. The bistable behavior relative to the parallel pump strength for the case without the transverse pumping has been studied in [59]. In our setup, we add a transverse pumping field which provides a second source of cavity photons. As studied in [36], the self-organization mechanism helps the atoms being accumulated to the optical potentials generated by the cavity photons. At a certain transition point, the cavity photon number undergoes a sharp change with the increasing of transverse pumping field. From this general

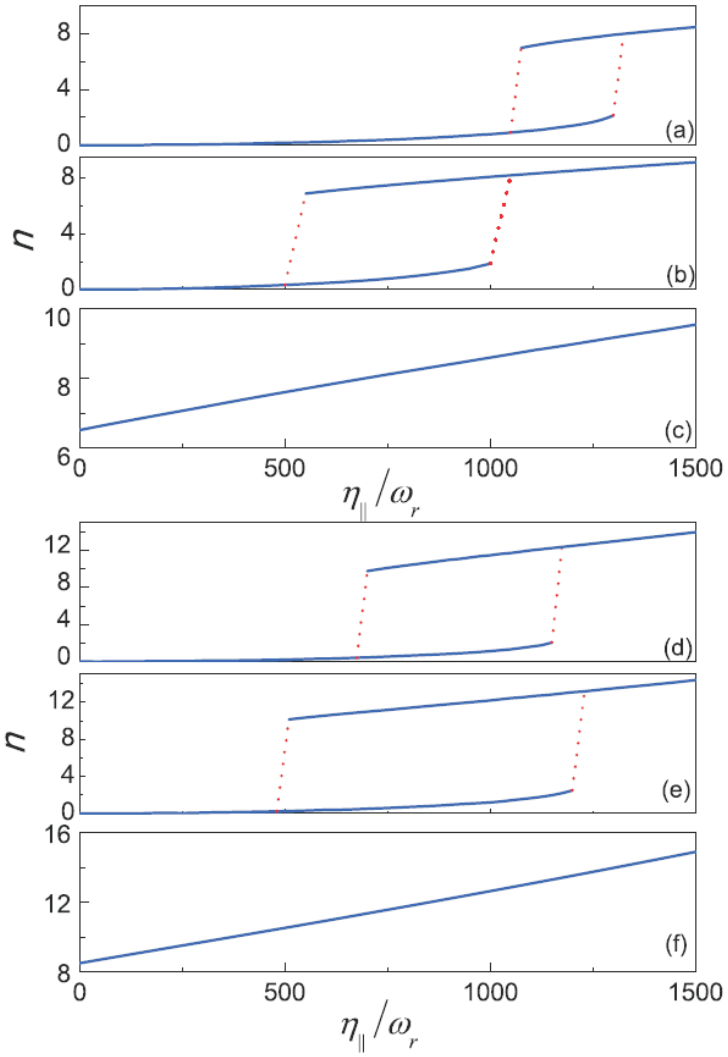


Figure 2.2: The cavity photon numbers as a function of the input pump along the cavity axis. For (a) $\rightarrow$ (c), the parameters are $N = 4.8 \times 10^4, \tilde{U}_0 = 0.25, \tilde{\delta}_c = 1.2 \times 10^3, \tilde{\kappa} = 0.4 \times 10^3$, and (a) $\tilde{\eta}_\perp = 0$, (b) $\tilde{\eta}_\perp = 0.1$, (c) $\tilde{\eta}_\perp = 0.5$. For (d) $\rightarrow$ (f), the parameters are $N = 1 \times 10^4, \tilde{U}_0 = 0.5, \tilde{\delta}_c = 1.1 \times 10^3, \tilde{\kappa} = 0.2 \times 10^3$, and (a) $\tilde{\eta}_\perp = 0$, (b) $\tilde{\eta}_\perp = 0.4$, (c) $\tilde{\eta}_\perp = 1$. For each cases, we neglect the atom-atom interaction since we want to make a direct comparison with the DMP method.

behavior, we expect that the bistability of the parallel pump will be suppressed if the transverse pumping field alone fills the cavity with enough photons to establish the upper branch of the bistability. In figure 2.2, we plot the cavity photon number as a function of the parallel pumping field with different but fixed perpendicular pumping field. It is clear that the bistability of the cavity photon number with the change of parallel pumping field can be controlled by the perpendicular pumping field. This phenomenon provides a candidate for a controllable optical switch, with the parallel pump field as the input and perpendicular pump field as the control.

In order to interpret the physics behind our findings we in addition to the numerical GP calculation introduce the discrete mode approximation for the atom modes at current step [59]. The ground state of the condensate with no pumping field is a homogeneous macroscopic state with zero-momentum. The effect of the transverse pumping field is to diffract this ground state into the symmetric superposition of the $\pm\hbar k$ momentum states. By absorption and stimulated emission of cavity photons the condensate can be excited to the superposition of $\pm 2\hbar k$ momentum states from the ground state. Taking into account the lowest order perturbation to the uniform condensate wave function,we select the subspace expanded by the basis functions

$$\phi_0 = \sqrt{1/L}\,, \tag{2.19a}$$

$$\phi_1 = \sqrt{2/L}\cos(kx)\,, \tag{2.19b}$$

$$\phi_2 = \sqrt{2/L}\cos(2kx)\,. \tag{2.19c}$$

Substituting $\hat{\Psi}(x) = \sum_{i=0}^{2} \phi_i \hat{c}_i$ into the Hamiltonian, we obtain (see Appendix )

$$\begin{aligned}\hat{H} = \; & \hbar\omega_r \hat{c}_1^\dagger \hat{c}_1 + 4\hbar\omega_r \hat{c}_2^\dagger \hat{c}_2 + \frac{\hbar U_0}{4}\hat{a}^\dagger \hat{a}\Big[\sqrt{2}(\hat{c}_0^\dagger \hat{c}_2 + \hat{c}_2^\dagger \hat{c}_0) + 2N + \hat{c}_1^\dagger \hat{c}_1\Big] \\ & + \frac{\hbar\eta_\perp}{2}(\hat{a}^\dagger + \hat{a})\Big[\sqrt{2}(\hat{c}_0^\dagger \hat{c}_1 + \hat{c}_1^\dagger \hat{c}_0) + (\hat{c}_1^\dagger \hat{c}_2 + \hat{c}_2^\dagger \hat{c}_1)\Big]\end{aligned}$$

$$+ \hbar\Delta_c \hat{a}^\dagger \hat{a} + \hbar\eta_\parallel (\hat{a}^\dagger + \hat{a}) \,, \tag{2.20}$$

where $\omega_r = \hbar k^2/2m$ is the atomic recoil energy and

$$N = \hat{c}_0^\dagger \hat{c}_0 + \hat{c}_1^\dagger \hat{c}_1 + \hat{c}_2^\dagger \hat{c}_2 \tag{2.21}$$

is the total number of the atoms. Note that if there is no pump field along the cavity axis, then we assume the two modes approximation, i.e., $\hat{c}_2^\dagger = \hat{c}_2 = 0$. In this case, we recover the Dicke Hamiltonian considered in Ref. [41]. On the other hand, if we take the transverse pump field to be zero, which means there is no excitation proportional to $\cos(kx)$, we recover the cavity optomechanical like Hamiltonian as in Ref. [43].

Applying the mean-field approximation $\hat{c}_i \sim \sqrt{N} Z_i$, $\hat{a} \sim \alpha$, the equation of motion for the condensate can be found as

$$i\frac{d}{d\tilde{t}} Z = H(\alpha_{ph})\, Z = \left[H_0 + |\alpha_{ph}|^2 H_1 + 2\mathrm{Re}(\alpha_{ph}) H_2\right] Z, \tag{2.22}$$

with $Z = (Z_0, Z_1, Z_2)^T$ and

$$H_0 = \begin{pmatrix} 0 & 0 & 0 \\ 0 & 1 & 0 \\ 0 & 0 & 4 \end{pmatrix}, H_1 = \frac{\tilde{U}_0}{4} \begin{pmatrix} 0 & 0 & \sqrt{2} \\ 0 & 1 & 0 \\ \sqrt{2} & 0 & 0 \end{pmatrix}, H_2 = \frac{\tilde{\eta}_\perp}{2} \begin{pmatrix} 0 & \sqrt{2} & 0 \\ \sqrt{2} & 0 & 1 \\ 0 & 1 & 0 \end{pmatrix}, \tag{2.23}$$

where $\tilde{t} = \omega_r t$, $\tilde{U}_0 = U_0/\omega_r$ and $\tilde{\eta}_\perp = \eta_\perp/\omega_r$ are rescaled dimensionless quantities.

Since

$$\int dx |\Psi(x,t)|^2 \cos(kx)$$

$$
\begin{aligned}
&= N\int dx\left[\sqrt{\frac{1}{L}}Z_0+\sqrt{\frac{2}{L}}\cos(kx)Z_1+\sqrt{\frac{2}{L}}\cos(2kx)Z_2\right]^2\cos(kx)\\
&= N\left(\sqrt{2}Z_0Z_1+Z_1Z_2\right)=\frac{1}{\tilde{\eta}_\perp}NZ^\dagger H_2Z,
\end{aligned}
\tag{2.24}
$$

and

$$
\begin{aligned}
&\int dx|\Psi(x,t)|^2\cos^2(kx)\\
&= N\int dx\left[\sqrt{\frac{1}{L}}Z_0+\sqrt{\frac{2}{L}}\cos(kx)Z_1+\sqrt{\frac{2}{L}}\cos(2kx)Z_2\right]^2\cos^2(kx)\\
&= \frac{1}{2}N\left(1+\frac{1}{2}Z_1^2+\sqrt{2}Z_0Z_2\right)=\frac{1}{2}N+\frac{1}{\tilde{U}_0}NZ^\dagger H_1Z,
\end{aligned}
\tag{2.25}
$$

the coherent photon amplitude is

$$
\begin{aligned}
\alpha &= \frac{\eta_\parallel - iW_0\int dx|\Psi(x,t)|^2\cos(kx)}{i\left[\Delta_c+U_0\int dx|\Psi(x,t)|^2\cos^2(kx)\right]+\kappa}\\
&= \frac{\tilde{\eta}_\parallel - iNZ^\dagger H_2Z}{i(\tilde{\Delta}_c'+NZ^\dagger H_1Z)+\tilde{\kappa}},
\end{aligned}
\tag{2.26}
$$

where $\tilde{\delta}_c=(\Delta_c+\frac{1}{2}NU_0)/\omega_r$ and $\tilde{\kappa}=\kappa/\omega_r$.

Next, we determine the atomic condensate ground state $Z_s(t)=Z_se^{-iE_0\tilde{t}}$, where

$$
\left[H_0+|\alpha_{ph}|^2H_1+2\mathrm{Re}(\alpha_{ph})H_2\right]Z_s=E_0Z_s. \tag{2.27}
$$

This is a nonlinear problem because the Hamiltonian $H$ depends on the eigenstate $Z_s$ through $\alpha_{ph}$. The procedure is to first take an arbitrary trial photon amplitude $\alpha_{tr}$, and then solve the ground state of the Hamiltonian $H(\alpha_{tr})$. Next, we substitute the solution $X_s$ to equation (2.26) and get an output photon amplitude $\alpha_{out}$. If $\alpha_{out}=\alpha_{tr}$, we get a self-consistent solution. Figure 2.3 shows distinct bistable

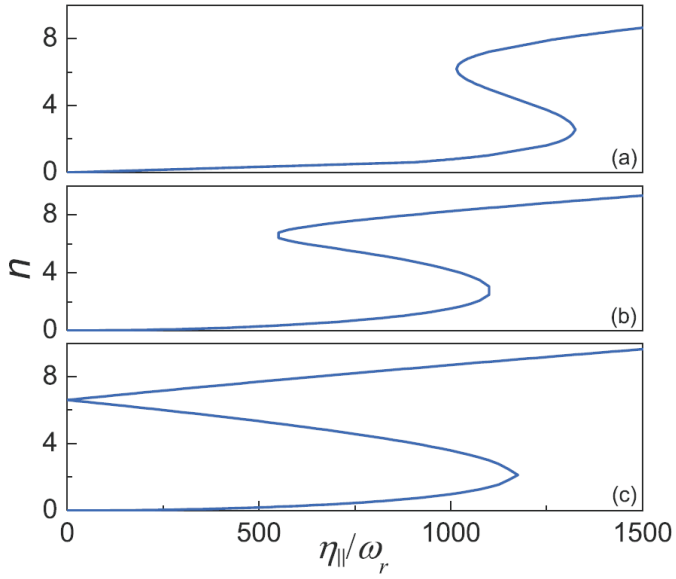


Figure 2.3: The cavity photon numbers as a function of the input pump along the cavity axis by the 3-level DMP method. The parameters are $N = 4.8 \times 10^4, \tilde{U}_0 = 0.25, \tilde{\delta}_c = 1.2 \times 10^3, \tilde{\kappa} = 0.4 \times 10^3$, and (a) $\tilde{\eta}_\perp = 0$, (b) $\tilde{\eta}_\perp = 0.1$, (c) $\tilde{\eta}_\perp = 0.5$.

behavior of the cavity photon number as a function of the input pump along the cavity axis for different transverse pumping field. Qualitative differences to figure 2.2 arise since the method described above can only solve for the eigenvalues, but cannot discriminate whether the state is stable or not. In contrast, the GP method leads to stable solutions due to the intrinsic properties of the imaginary time method. If we use the GP results as the start trial photon amplitude, we obtain results as shown in figure 2.4. It can be seen that the DMA and the GP method agree well. As we include more states in the DMA basis, the results of the approximate method approach those of the exact solution of the GP equation.

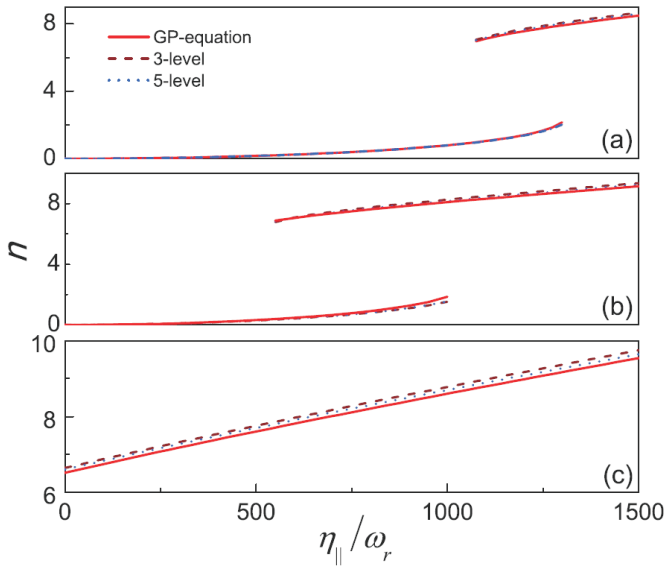


Figure 2.4: The cavity photon numbers as a function of the input pump along the cavity axis. The parameters are $N = 4.8\times10^4, \tilde{U}_0 = 0.25, \tilde{\delta}_c = 1.2\times10^3, \tilde{\kappa} = 0.4\times10^3$, and (a) $\tilde{\eta}_\perp = 0$, (b) $\tilde{\eta}_\perp = 0.1$, (c) $\tilde{\eta}_\perp = 0.5$.

When there is no perpendicular pumping,$H_2 = 0$, the cavity photon number

$$n = |\alpha|^2 = \frac{\tilde{\eta}_\parallel{}^2}{(\tilde{\delta}_c + NZ^\dagger H_1 Z)^2 + \tilde{\kappa}^2}, \tag{2.28}$$

Here $Z^\dagger H_1 Z$ is a function of the cavity photon number, and can be expand linearly as $Z^\dagger H_1 Z \simeq \beta n$, to the lowest order. So

$$n = \frac{n_{in}}{1 + (\tilde{\delta}_c + N\beta n)^2/\tilde{\kappa}^2}, \tag{2.29}$$

where $n_{in} = \tilde{\eta}_\parallel{}^2/\tilde{\kappa}^2$.

This equation can be mapped exactly to the relation of dispersive optical bistability [65]. The scattering of photons due to the atomic gases causes an extra optical length and thus a phase change, which depends on the field intensity and produces

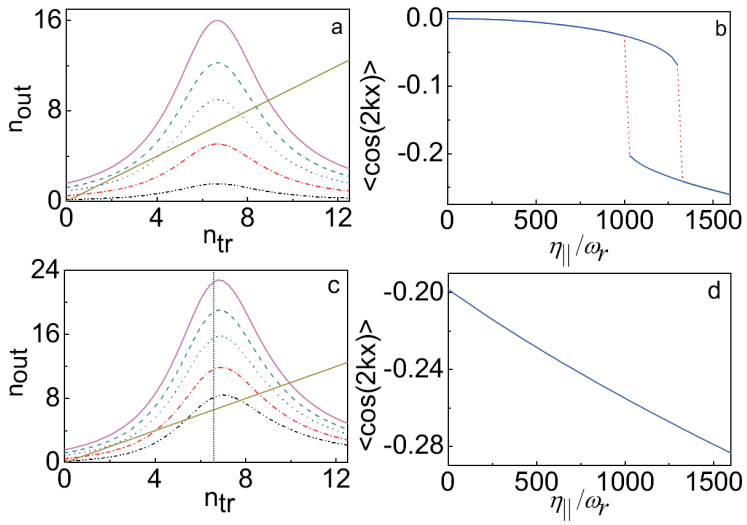


Figure 2.5: (a) and (c) The cavity output photon number $n_{out}$ as a function of the trial input photon number $n_{tr}$. (b) and (d) show $\langle\cos(2kx)\rangle$ as a function of the parallel pumping strength. The parameters are $N = 4.8 \times 10^4, \tilde{U}_0 = 0.25, \tilde{\delta}_c = 1.2 \times 10^3, \tilde{\kappa} = 0.4 \times 10^3$, and (a) and (b) $\tilde{\eta}_\perp = 0$, (c) and (d) $\tilde{\eta}_\perp = 0.5$. The curves in (a) and (c) correspond to $\tilde{\eta}_\parallel = (0.5, 0.9, 1.2, 1.4, 1.6) \times 10^3$, respectively.

the bistable states. In figure 2.5(a) we plot the right hand side of equation (2.28), which can be interpreted as the output cavity photon number $n_{out}$ predicted from equation (2.28) given the input trial photon number ntr. The intersection points of $n_{out}(n_{tr})$ and the bisection of the first quadrant determined by $n_{out} = n_{tr}$ provide a graphic solution for the cavity photon number. The bistable behavior emerges when there are more than one intersections. One can easily find that the upper branch corresponds to the intersections on the right side of the peaks, where the number of cavity photons is sucient to excited the condensate to $\phi_2$ with certain extent, see figure 2.5(b). This can be understood from the fact that the bistability comes mainly from the value of $\beta$ and the quadratic form of the denominator in the right hand side of equation (2.29).

If the perpendicular pumping is added, a new channel for the introduction of

cavity photons is set up. It can be easily seen that the perpendicular pumping enters the Hamiltonian, like the parallel pumping term, as a displacement operator. The difference is that the pumping rate now depends on the feedback of the atoms and thus the cavity photon number, while it is constant for the parallel pumping. The reason is that the scattering rate of the perpendicular photon depends on the configuration of the condensate. This point also distinguishes our system from the classical case in which the change of the media's configuration can be neglected and the scattering rate of the perpendicular pumping would be a constant too. With the perpendicular field, we find

$$n = \frac{n_{in} + (N\beta' n)^2/\tilde{\kappa}^2}{1 + (\tilde{\delta}_c + N\beta n)^2/\tilde{\kappa}^2}, \tag{2.30}$$

where $X^\dagger H_2 X \simeq \beta' n$. Comparing figure 2.5(c) with figure 2.5(a), we find that the output photon number as a function of the input photon number $n_{out}(n_{in})$ is not modified much from the case without parallel pumping. However, the condensate can now be excited from the homogeneous state $\phi_0$ to $\phi_2$ through scattering of two perpendicular pump photons into the cavity even if no parallel pumping is added. This leads to a non-zero intercept of the vertical axis in figure 2.5(d). Accordingly, potential intersection points located at the left wing of the curves $n_{out}(n_{tr})$ in figure 2.5(c) can not be accessed if a sufficient number of cavity photons is introduced due to the perpendicular pumping, since this leads to a displacement of the cavity photon number to a larger values. In particular the value of $n_{out}$ at $n_{tr} = 0$ determines a cutoff which explains the disappearance of the bistability, see figure 2.5(c).

### *2.3.2 The role of the atom-atom interaction*

So far, we have neglected the atom-atom interaction by considering the case $g_c = 0$. But in the real systems, this coupling is usually present. And it is helpful

to stabilize the homogeneous phase when the pump power is low. Collision between atoms with positive scattering length tends to diffuses the atoms away from each other. Therefore, the optical lattice generated by the cavity photons can rearrange the atoms only if it is strong enough to overcome the diffusion caused by the atom-atom interaction. Thus, with repulsive atom-atom interactions, more photons are needed to produce a deeper trap to confine the atoms. From this argument we expect that the bistability will still be present with atom-atom interactions, but the parallel pumping field strength needs to be increased to overcome the interaction. This would lead to a shifting of the bistability transition to higher values along the parallel pump axis. At the same time, the higher photon number at the transition point also shifts the upper branch up. This is confirmed in figure 2.6 Since the critical point of the self organization increases with $Ng_c$ as shown in equation(2.34), in turn stronger transverse input is required to remove the bistability.

### *2.3.3 Influence of the parallel pump on the Dicke phase transition*

Defining

$$\theta = \langle \cos(kx) \rangle \,, \tag{2.31a}$$

$$\beta = \langle \cos^2(kx) \rangle \,, \tag{2.31b}$$

the optical lattice potential generated by the cavity photons can be written as

$$V(x) = U_0 \cos^2(kx)|\alpha|^2 + \eta_\perp \cos(kx)(\alpha + \alpha^*) = V_1 \cos(kx) + V_2 \cos^2(kx), \tag{2.32}$$

with

$$V_1 = 2\eta_\perp \frac{\eta_\parallel \kappa - \eta_\perp \theta(\Delta_c + NU_0\beta)}{(\Delta_c + NU_0\beta)^2 + \kappa^2} \,, \tag{2.33a}$$

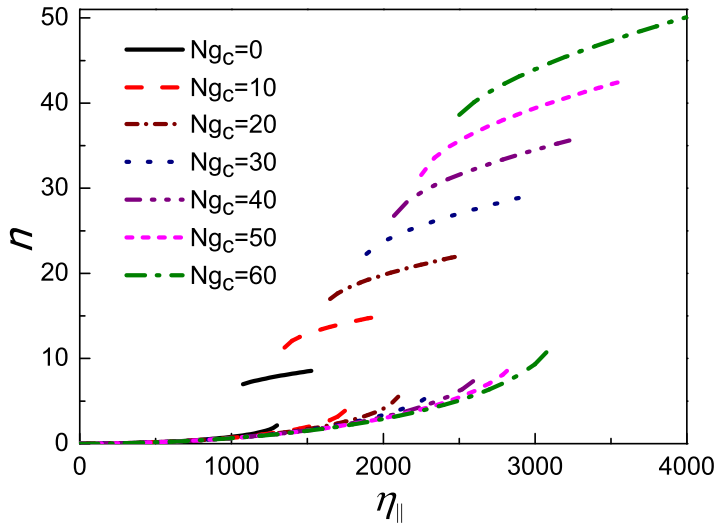


Figure 2.6: The influence of the atom-atom interaction for the bistability. The two lines with the same color correspond to the two branches of the bistable behavior for a given value of $Ng_c = 0, 10, 20, 30, 40, 50,$ and 60, from bottom to top. Other parameters are $N = 4.8 \times 10^4, \tilde{U}_0 = 0.25, \tilde{\kappa} = 0.4 \times 10^3$, $\tilde{\eta}_\perp = 0$ and $\tilde{\delta}_c = 1.1 \times 10^3$

$$V_2 = U_0 \frac{\eta_\parallel^2 - (\eta_\perp \theta)^2}{(\Delta_c + NU_0\beta)^2 + \kappa^2} \,. \tag{2.33b}$$

As discussed previously [36] for the case without pumping along the cavity axis, the steady-state of the condensate atoms is either a homogeneous distribution or a $\lambda$-periodic ordered pattern. The two regimes correspond to different transverse pumping strengths and are well separated by a critical point. This sharp transition could be traced back to a self-organization mechanism [36] as follows. If there is no parallel pumping, and if $\Delta_c + NU_0\beta > 0$, the sign of the potential $V_1$ becomes the opposite of the sign of $\theta$. Therefore, if more atoms happen to be close to the odd(even) sites than to the even(odd) sites due to fluctuations, the produced potential $V_1 \cos(kx)$ will have minima at the odd(even) sites and attracts even more atoms there, leading to an amplification of the fluctuation and thus to organization.

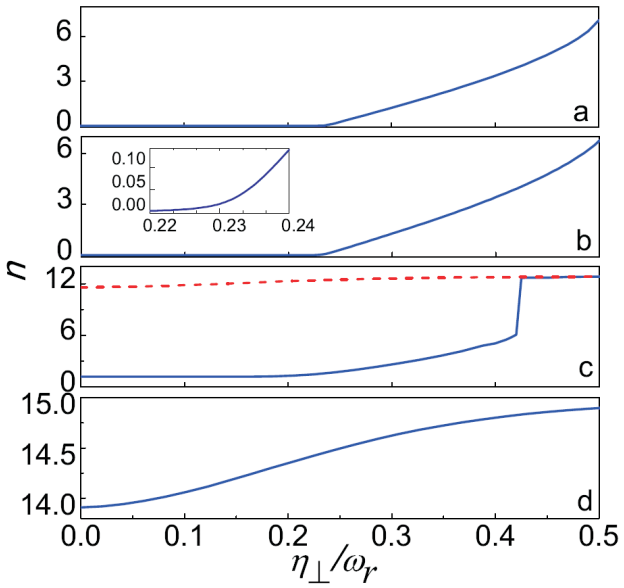


Figure 2.7: The cavity photon number as a function of the input pump perpendicular to the cavity axis. The parameters are $N = 1 \times 10^4$, $\tilde{U}_0 = 0.5$, $\tilde{\delta}_c = 1.1 \times 10^3$, $\tilde{\kappa} = 0.2 \times 10^3$, $Ng_c = 0$, and (a) $\tilde{\eta}_\parallel = 0$, (b) $\tilde{\eta}_\parallel = 50$, (c) $\tilde{\eta}_\parallel = 1 \times 10^3$, and (a) $\tilde{\eta}_\parallel = 1.5 \times 10^3$.

It follows that apart from the reorganization of the wave function, if the pumping strength is increased over some critical value, the intra-cavity photon number also shows an abrupt change at the threshold pump power, see figure 2.7(a). This phase transition has been shown to be analogous to the Dicke quantum phase transition [40, 41]. The critical transition point is determined by

$$\sqrt{N}\eta_\perp = \sqrt{\frac{(\Delta_c + NU_0/2)^2 + \kappa^2}{2\Delta_c + NU_0}}\sqrt{\omega_r + 2Ng_c}\,. \tag{2.34}$$

When an extra input pump field is added along the cavity axis, the feedback mechanism works a little different. The parallel pumping provides another channel for cavity photons and forms an additional $\lambda/2$ periodic potential to confine the atoms. Thus the atoms to the lowest order are in a state $\psi_0$, which is a coherent superposition of the homogeneous state and $\phi_2$. In contrast, without the parallel pump field, the condensate initially is in the homogeneous state only. Furthermore, for the case without parallel pumping field, the initial homogeneous state is always a self-consistent solution for the combined GP equation and amplitude equation, even with perpendicular pumping. However, this is not true if the parallel pumping is added. Then the initial state $\psi_0$ is not a self-consistent solution for the GP equation as long as perpendicular pumping is added. Therefore a gradual increase of the perpendicular pumping from zero also leads to a gradual buildup of the $\lambda$ periodic potential $V_1$ if a parallel pumping field is applied. From this we expect that no phase transition occurs if the parallel pumping is added. This expectation is confirmed by our numerical calculations. Figure 2.7(b) shows a smooth change of the cavity photon number as we increase $\eta_\perp$ when a parallel pumping $\eta_\parallel = 50$ is added. And, since $\eta_\parallel\kappa > |\eta_\perp\theta(\Delta_c + NU_0\beta)|$ if $\eta_\perp$ is small, the sign of $V_1$ is positive at the beginning. So the effect of $V_1$ is to weaken the odd peaks of the $\lambda/2$ periodic potential

and strengthen the even peaks. Thus the atoms will be gradually confined at the odd sites. Alternatively, the sign of $-\eta_\perp\theta(\Delta_c + NU_0\beta)$ will be positive if $\Delta_c + NU_0\beta$ is positive. Then the $\lambda$ periodic potential will be enhanced as the atoms been attracted at the odd sites. Thus in this case the atoms will be fixed at the odd sites. We thus find that with parallel pumping, the parameters of the system uniquely determine the structure of the condensate after the reorganization. This is in contrast to the case without parallel pumping in which the atoms can be attracted to either of the two equivalent but spatially offset lattice configurations depending on an initial symmetry-breaking due to fluctuations.

We recall the fact that bistability can be observed for some particular values of $\eta_\parallel$ and $\eta_\perp$, as explained in Sec. III. Thus if we increase the pump strength along the cavity axis further, bistability is also expected with the change of transverse pumping, see figure 2.7(c). Above a certain critical value of $\eta_\parallel$, the $\lambda/2$-periodic potential will dominate and there is no bistability, see figure 2.7(d). So the controllable optical switch can also operate with the parallel pumping as the control and the perpendicular pumping as the signal.

The exact critical point at which the bistable behavior disappears is determined by the highly nonlinear equation

$$\alpha = \frac{\eta_\parallel - i\eta_\perp g(\alpha)}{i\left[\Delta_c + U_0 f(\alpha)\right] + \kappa}\,, \tag{2.35}$$

where

$$f(\alpha) \equiv \int dx |\Psi(x,t)|^2 \cos^2(kx)\,, \tag{2.36a}$$

$$g(\alpha) \equiv \int dx |\Psi(x,t)|^2 \cos(kx)\,, \tag{2.36b}$$

for which only numerical result can be searched. Close to the critical points, the numerical analysis is complicated by the fact that the ground state and the first excited state become almost degenerate [36]. This increases the likelihood of numerical errors and reduces the eciency of the algorithm. As a solution, we applied an "adiabatic" evolution of the system, namely, once a wave-function is found, we use it as the next trial amplitude after a small parameter change. Figure 2.8 depicts the regions of the lower branch, bistability, and the upper branch in the parameter space spanned by the two pump fields. We see that for lower pumping fields in both parallel and perpendicular directions, the cavity photon number is mainly in the lower branch. For some intermediate values of the pumping fields, there is bistability for the cavity photon number. If we further increase either the parallel pumping field or the perpendicular pumping field, the cavity photon number is in the upper branch and the bistability disappears. The vertical cross sections of figure 2.8 at $\eta_\perp = 0, 0.1$ and 1.0, and horizontal cross sections at $\eta_\parallel = 0, 50, 1000$, and 1500 coincide with figure 2.2(d)-(f) and figure 2.7, respectively.

### *2.3.4 Summary*

In summary, we have discussed theoretically the bistable behavior of the cavity photon number for a combined cavity-BEC system. We showed that one can use a perpendicular driving field as a control for bistability of the cavity photons relative to the parallel pump. If no perpendicular driving field is added, the cavity photons show strong bistable behavior for a large range of the parallel pumping field strength. However, if the perpendicular driving exceeds a critical value, this bistability will disappear. Vice versa, we can also use the parallel pumping as a control of the bistability of the perpendicular pumping. While the optical bistability with conventional media such as atomic gases and dense crystals have been suggested as

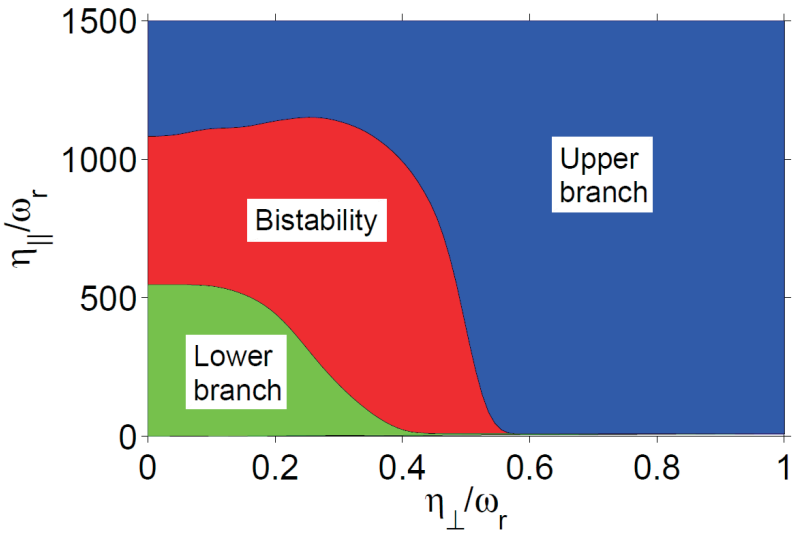


Figure 2.8: The regions of lower branch, bistability, and upper branch of the cavity photon number. The parameters are $N = 1 \times 10^4$, $\tilde{U}_0 = 0.5$, $\tilde{\delta}_c = 1.1 \times 10^3$, $\tilde{\kappa} = 0.2 \times 10^3$, and $Ng_c = 0$.

mechanism for an optical switch, this phenomenon may provide a candidate for a controlled optical switch. Further studies are needed for the physics of the dissipation channels and analysis of the switching time of the bistable behavior.

## 2.4 Anomalous switching of the optical bistability

### *2.4.1 Anomalous switching*

When there is no perpendicular pumping field, the steady-state intra-cavity photon number $n_s = |\alpha_s|^2$ shows bistability, similar to the optical bistability [59]. The bistable behavior of the intra-cavity photon number with respect to the pumping field intensity is shown in figure 2.9, where points with negative slopes correspond to unstable states. Here we would like to focus on the dynamical properties of the system. There are two different ways to add the pump field. In the first case, the pumping field is turned on adiabatically. The increase of the field intensity is so slow

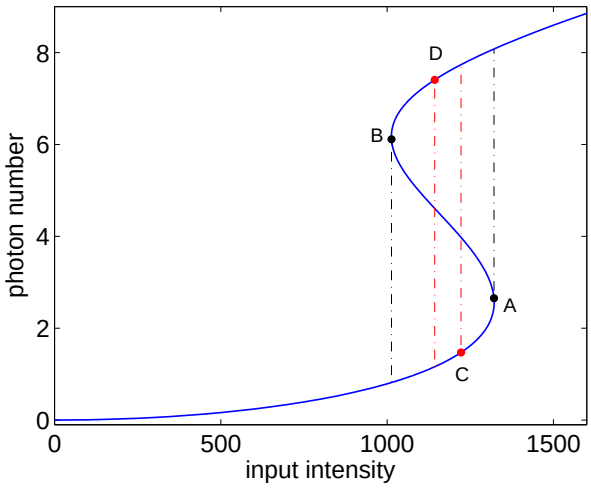


Figure 2.9: Steady-state intra-cavity photon number as a function of the input pump intensity. The parameters are $N = 4.8 \times 10^4$, $U_0 = 0.25\omega_r$, $\delta_c = 1.2 \times 10^3\omega_r$, $\kappa = 0.4 \times 10^3\omega_r$. The input pump intensity is also in the unit of $\omega_r$. The critical switching points are $\eta_A = 1322\omega_r$ and $\eta_B = 1013\omega_r$ for the steady state. The critical anomalous switching points are $\eta_C = 1222\omega_r$ and $\eta_D = 1143\omega_r$.

that the condensate and intra-cavity photon follow all the steady states corresponding to the pump field in the lower branch until the critical point $A$ in figure 2.9. When the pump field exceeds the critical point, the condensate can not follow the input field adiabatically and therefore jumps to the upper branch. This is because the steady state corresponding to the critical point $A$ in the lower branch is much different from the steady state corresponding to the current pump field in the upper branch. Since there is no damping mechanism for the condensate, the system oscillates around the upper branch [59]. In the second case, instead of adding the pumping field adiabatically, the field is added abruptly. Suppose the condensate is initially in the homogenous state $Z = (1, 0)^T$. After solving equations (2.22) and (2.26) numerically, we draw the evolution of the intra-cavity photon number $|\alpha|^2$ with respect to different pumping field intensity, as shown in figure 2.10. If the added field

stays in the purely lower branch or lies in the bistable region but not close to the critical point $A$, the intra-cavity photon number oscillates around steady state in the lower branch, see figure 2.10(a) and (b). If the input field exceeds the critical value of $A$, it will introduce oscillations between two branches, see figure 2.10(c). These oscillations have been investigated and confirmed by solving the GP equation numerically in Ref. [59].

We find that the photon number may approach the upper branch with a pump field less than the critical point $A$ if the field is turned on abruptly. This is quite different from the first case where the photon number jumps to the upper branch only if the pump field is greater than the critical value $A$. The evolution of the intra-cavity photon number when $\eta = 1250\omega_r$ is shown in figure 2.10(d). Note that the field at the critical point $A$ is $1322\omega_r$. It follows, on comparing the intra-cavity photon numbers in figure 2.9, that the intra-cavity photon number reaches the upper branch. Further numerical calculation shows that the switching happens when the added pumping field lies between point $C$ and $A$ in figure 2.9. This phenomenon reminds us the anomalous switching of the dispersive bistability for the traditional two-level atomic media in the good cavity limit [62, 63].

### *2.4.2 Explanation*

In order to understand this anomalous switching behavior, and note that there is no excitation from the homogeneous state $\phi_0$ to $\phi_1$, we proceed by introducing the quadratures of the mechanical oscillators $X = \sqrt{N/2}(Z_0^* Z_2 + Z_0 Z_2^*)$, $P = i\sqrt{N/2}(Z_2^* Z_0 - Z_0^* Z_2)$. The corresponding equations of motion are

$$\frac{dX}{dt} = 4\omega_r P\,, \tag{2.37a}$$

$$\frac{dP}{dt} = -4\omega_r X - \frac{\sqrt{N}U_0}{2}|\alpha|^2\,, \tag{2.37b}$$

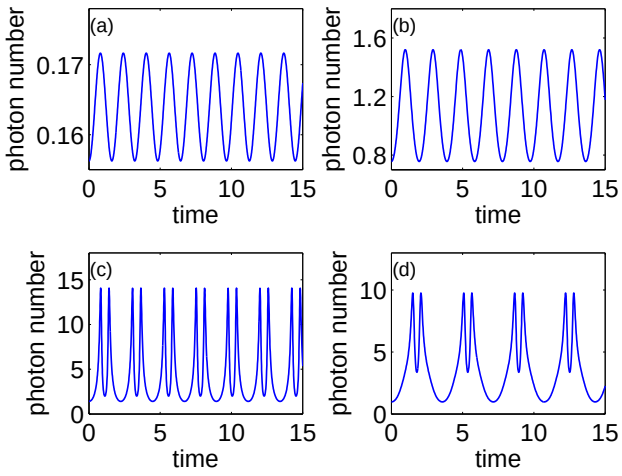


Figure 2.10: Intra-cavity photon number as a function of time. Initially there is no pump field and the condensate is the homogeneous state. Then the pump field is turned on immediately with values (a) $500\omega_r$, (b) $1100\omega_r$, (c) $1500\omega_r$ and (d) $1250\omega_r$. The parameters are $N = 4.8 \times 10^4$, $U_0 = 0.25\omega_r$, $\delta_c = 1.2 \times 10^3\omega_r$, $\kappa = 0.4 \times 10^3\omega_r$. The time is in the unit of $1/\omega_r$.

and the photon amplitude is (with $X = \frac{2\sqrt{N}}{U_0} Z^\dagger \frac{H_1}{\hbar} Z$)

$$\alpha = \frac{\eta}{i\left(\Delta_c + \frac{NU_0}{2} + \frac{\sqrt{N}U_0}{2}X\right) + \kappa}\,. \tag{2.38}$$

In deriving the above equations, we have used the fact that $|Z_1|^2 \ll |Z_0|^2 \simeq 1$. Then the evolution of the generalized displacement would be

$$\frac{d^2X}{d^2t} = -(4\omega_r)^2 X - \frac{2\sqrt{N}U_0\omega_r\eta^2}{\left(\Delta_c + \frac{NU_0}{2} + \frac{\sqrt{N}U_0}{2}X\right)^2 + \kappa^2} = -\frac{dV(X)}{dX}\,, \tag{2.39}$$

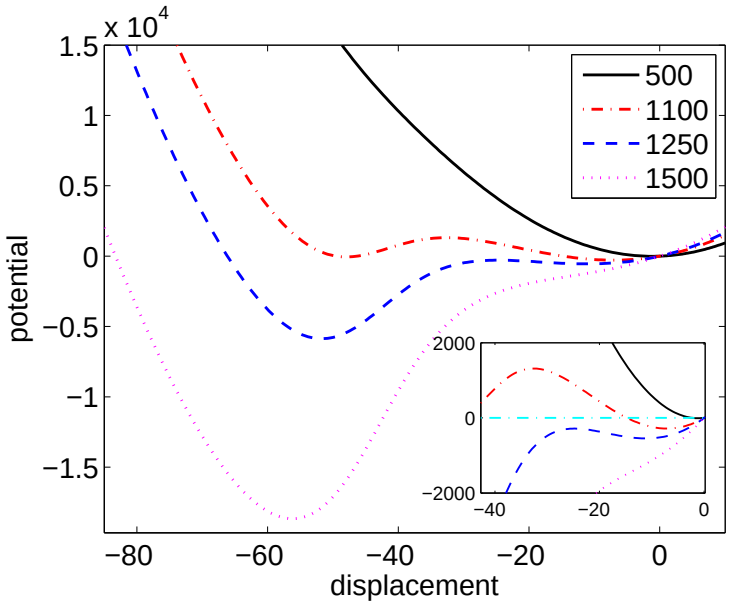


Figure 2.11: The potential $V(X)$. The lines from top to bottom correspond to difference pump fields, (1) $500\omega_r$, (2) $1100\omega_r$, (3) $1250\omega_r$ and (4) $1500\omega_r$. The parameters are $N = 4.8 \times 10^4$, $U_0 = 0.25\omega_r$, $\delta_c = 1.2 \times 10^3\omega_r$, $\kappa = 0.4 \times 10^3\omega_r$.

where

$$V(X) \equiv \int^X ds \left[ (4\omega_r)^2 s + \frac{2\sqrt{N}U_0\omega_r\eta^2}{\left(\Delta_c + \frac{NU_0}{2} + \frac{\sqrt{N}U_0}{2}s\right)^2 + \kappa^2} \right] . \tag{2.40}$$

The condensate can then be viewed as a nonlinear spring. The dynamic properties will be determined by the potential $V(X)$ and the initial condition. Figure 2.11 shows the potential function for different pump field intensity. The solid black line corresponds to the case $\eta = 500\omega_r$. We find one and only one minimum close to the origin. This minimum denotes the steady state in the purely lower branch. The potential with $\eta = 1500\omega_r$ is shown as the magenta dotted line. The single minimum is far away from the origin and corresponds to the steady state in the purely upper

branch. The red dash-dotted line ($\eta = 1100\omega_r$) and blue dashed line ($\eta = 1250\omega_r$) lie in the bistable region. The potential is double-well like and has two minimum points. The one close to the origin means the steady state in the lower branch while the other indicates the upper branch. The peak in the middle represents the unstable state.

The evolution of the condensate can then be understood as a point-like ball sliding in a one-dimension smooth bowl. The shape of the bowl is determined by the potential function $V(X)$. At $t = 0$, the shape of the bowl is harmonic-like. The initial homogenous condensate corresponds to a rest ball placed at the $X = 0$. If the field is added adiabatically, the shape of the bowl changes gradually and the ball will stay at the bottom of the bowl. Then the double well appears and the ball stays at the bottom of the right well. If the field is increased further, the left well gets deeper and the right well is raised. At the critical point, the minimum of the right well coincides with the unstable peak of the barrier in the middle. Therefore the right well disappears. The ball falls down to the left well and oscillates in the left well.

If the field is added abruptly, the shape of the bowl will be changed immediately. The ball is then released to the bowl from the initial position at $X = 0$. As the bowl is frictionless, the total energy is conserved. If the added pump field is weak, the bowl has only one minimum close to the origin, as shown in the black solid line, the ball will oscillate around this minimum, see figure 2.10(a). If the added pump field corresponds to a value in the bistable region, the potential is a double-well. There exists two cases. If the pump rate is on the left of point $C$ in figure 2.9, the peak in the middle of the double well is higher than the initial position (the red dashdotted line). Therefore, the ball will be confined in the right side of the double well. Correspondingly, the photon number will oscillate around the lower branch as shown in figure 2.10(b). If the pump field is increased between $C$ and $A$, the right

well gets deeper and the barrier in the center would be lower than the initial position (the blue dash line). In this case, the ball will not be trapped in the right well and reach the left well as well. This corresponds to the anomalous switching as shown in figure 2.10(d). Note that the barrier is not much lower than $V(X) = 0$. Therefore, the velocity of the ball when passing the barrier is small and the period of the whole oscillation is long. If the field is strong, the double wells disappear and the single minimum corresponding to the steady state in the upper branch emerges far away from the origin (the magenta dotted line). The ball will oscillate between the initial position to the other side of the bowl at the same level as the initial position. It is shown in figure 2.10(c) that the photon number oscillates between the upper branch and lower branch.

### *2.4.3 Effect of initial condition and damping rate*

With the above picture in mind, we can expect that the initial condition also plays an important role in the anomalous switching, as it determines the total energy of the system. If the initial state corresponds to a steady state in the lower branch, the initial position in the $V(X)$ line might be lower than the barrier of potential when the field is turned on, there is no anomalous switching, see figure 2.12(a). On the other hand, if the initial state corresponds to a steady state in the higher branch, the anomalous switching to the lower branch may happen close to critical point $B$, see figure 2.12(b). In figure 2.9, it shows that the photon number switches to the higher branch if the pump field is on the right of $C$ when the condensate is initially in the homogenous state. On the other hand, if the condensate is initially prepared in the steady state of $\eta = 1600\omega_r$, the anomalous switching from the higher branch to the lower branch happens when the pump field is between $B$ and $D$.

In the above analysis, we have neglected the damping effect. This needs further

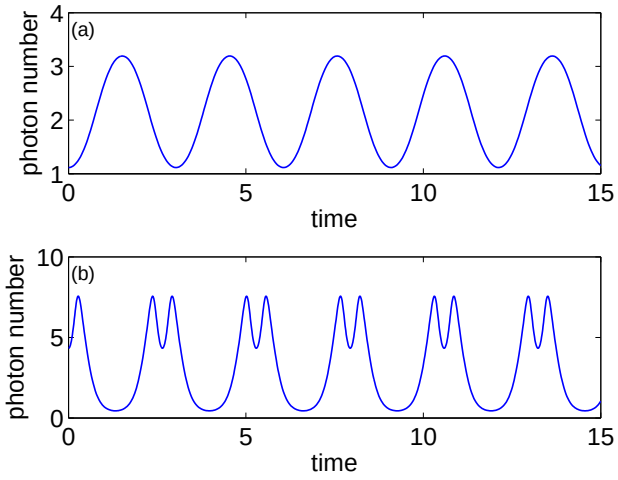


Figure 2.12: Intra-cavity photon number as a function of time for different initial conditions. (a) The initial state is the steady state corresponding to $\eta = 800\omega_r$. Then the pump field is tuned sharply to $\eta = 1250\omega_r$. (b) The initial state is the steady state corresponding to $\eta = 1600\omega_r$. Then the pump field is tuned to $\eta = 1100\omega_r$ abruptly. The other parameters are $N = 4.8 \times 10^4$, $U_0 = 0.25\omega_r$, $\delta_c = 1.2 \times 10^3\omega_r$, $\kappa = 0.4 \times 10^3\omega_r$. The time is in the unit of $1/\omega_r$.

investigation. Notice that the omitted harmonic tapping potential couples the $\pm 2\hbar k$-momentum modes to other modes and results in the damping of the above model [43, 66]. In this case we have to add a damping term in equation(2.37a). The damping introduces a loss in the total energy. Therefore, in the point-like ball picture, the surface of the bowl is frictional and the ball keeps losing energy after it is released. If the ball reaches one of the wells and lose all the kinetic energy before it overcomes the peak of the barrier, the ball then stays in that well and finally is frozen at the bottom corresponding to the steady state. Figure 2.13 shows the evolution of the intra-cavity photon number for different damping rates. We can find that the system finally approaches different branches even if it starts from the same initial states.

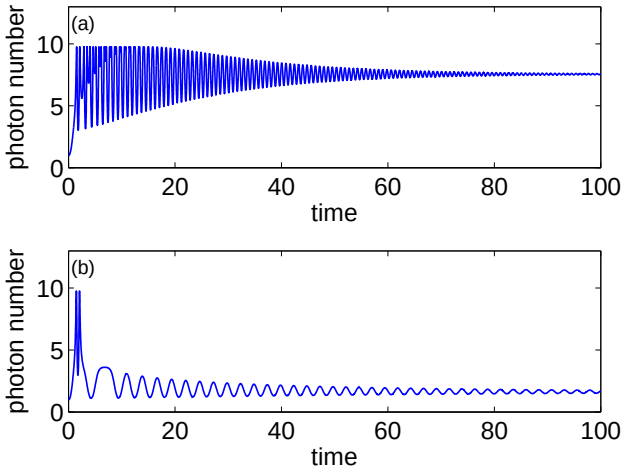


Figure 2.13: Intra-cavity photon number as a function of time with damping. Initially there is no pump field and the condensate is the homogeneous state. Then the pump field is turned on immediately with $\eta = 1250\omega_r$. The damping rates are (a) $0.05\omega_r$ and (b) $0.02\omega_r$. The other parameters are $N = 4.8 \times 10^4$, $U_0 = 0.25\omega_r$, $\delta_c = 1.2 \times 10^3\omega_r$, $\kappa = 0.4 \times 10^3\omega_r$. The time is in the unit of $1/\omega_r$.

### *2.4.4 Summary*

We have studied the nonlinear dynamics of the photon number in an optical cavity filled with a cigar-shaped Bose-Enistein condensate. We find that the way of adding the field is crucial to the switching close to the critical transition point. If the pump field is changed abruptly, the system may jump from one branch to the other even if the pump field intensity has not reached the critical transition point. The physics of this anomalous switching is that the oscillation introduced by the abrupt change of the pumping field may overcome the barrier between the two basins corresponding to the two bistable states. Different initial conditions and damping rates may affect this anomalous switching behavior.

## 2.5 Degenerate Fermi gas in a cavity

### *2.5.1 Motivation and the system*

The Dicke Hamiltonian [37] which describes the interaction of an ensemble of $N$ two-level atoms with a single mode of the electromagnetic field is a fundamental and fascinating model in quantum optics. At zero-temperature and in the thermodynamics limit, a first-order thermal phase transition happens for a critical coupling strength between the atoms and the field in the rotating wave approximation [39, 67, 68]. This transition becomes second order if the counter-rotating terms are included [69]. This phase transition associates with many interesting phenomenon such as superradiance [39, 67, 68, 69], quantum chaos [70, 71], and quantum entanglement [72, 73]. In some early studies it was claimed that the Dicke model is fictitious in the context of spins defined with atomic internal electronic degree of freedom. This is because the effect of $A^2$ term, which is neglected in the Hamiltonian, wipes away the phase transition in the vicinity of the critical point[74, 75, 76, 77, 78]. Recent interest in this problem reveals that by including certain terms of the same order as the $A^2$ terms can recover the phase transition [79, 80]. A question of interests is whether the original Dicke Hamiltonian can be realized experimentally [81, 82, 83]. It has been shown both theoretically and experimentally that the self-organization phase transition of a BEC in a cavity can be identified as the Dicke quantum phase transition [40, 41]. We propose an interesting scheme which realizes an effective Dicke Hamiltonian with a quantum-degenerate Fermi gas in an optical cavity. Unlike the Boson case, where the atom-atom interaction affects the critical value of the transition, the atom-atom interaction is negligible in Fermi gases due to the Pauli exclusion principle.

Our system is an ultracold quantum-degenerate Fermi gas loaded in an optical

ultrahigh-finesse Fabry-Perot cavity. We also consider the dynamics in the dimension $x$ along the cavity axis. The cavity field mode function is then described simply by $\cos(k_c x)$, with the wave number $k_c$ and frequency $\omega_c$. The other notations are the same as the Boson case. An external pumping laser fields at frequency $\omega_p$ is added perpendicularly to the cavity axis and we also consider the large detuning limit.. Note that here there is no pumping field along the cavity axis.

Similar to the BEC case, the Hamiltonian can be written as [35],

$$\hat{H} = \int dx \hat{\Psi}^\dagger(x) \Big[ -\frac{\hbar^2}{2m}\frac{d^2}{d^2x} + \hbar U_0 \cos^2(k_c x)\hat{a}^\dagger \hat{a} + \hbar\eta\cos(k_c x)(\hat{a}^\dagger + \hat{a}) \Big] \hat{\Psi}(x) + \hbar\Delta_c \hat{a}^\dagger \hat{a}. \tag{2.41}$$

Scattering between the transverse pump field and the cavity mode is described by $\hbar\eta\cos(k_c x)(\hat{a}^\dagger + \hat{a})$ where $\eta = g_0\Omega_p/\Delta_a$ is the maximum scattering rate, with $\Omega_a$ being the Rabi frequency of the transverse pump field. The atom-atom interaction is neglected in the Fermi gas.

For Fermions, the atomic field operator can be expanded as

$$\hat{\Psi}(x) = \frac{1}{\sqrt{L}} \sum_k \hat{f}_k e^{ikx}\,, \tag{2.42}$$

where $\hat{f}_k$ and $\hat{f}_k^\dagger$ obey the anti-commutation relations $\{\hat{f}_k, \hat{f}_{k'}^\dagger\} = \delta_{kk'}$, and $\{\hat{f}_k, \hat{f}_{k'}\} = \{\hat{f}_k^\dagger, \hat{f}_{k'}^\dagger\} = 0$.

The ground state of the identical atomic sample is a filled Fermi sea,

$$|\Psi_0^F\rangle = \prod_{k\in[-k_F,k_F]} \hat{f}_k^\dagger |0\rangle\,. \tag{2.43}$$

Here $k_i = 2\pi n_i/L$ for $n_i = 1, 2, 3, ....$ $k_F$ is the Fermi wave number $k_F = \pi N_{\max}/L$

and $N = 2N_{\max} + 1$. Upon substituting equation (2.42) into the atomic part of the Hamiltonian in equation (2.41), we have

$$\begin{aligned}\hat{H}_{\text{atom}} =& \sum_k \epsilon(k)\hat{f}_k^\dagger \hat{f}_k + \frac{\hbar N U_0}{2}\hat{a}^\dagger \hat{a} \\ &+ \frac{\hbar U_0}{4}\hat{a}^\dagger \hat{a}\sum_k (\hat{f}_{k+2k_c}^\dagger \hat{f}_k + \hat{f}_k^\dagger \hat{f}_{k+2k_c}) \\ &+ \frac{\hbar \eta}{2}(\hat{a}^\dagger + \hat{a})\sum_k (\hat{f}_{k+k_c}^\dagger \hat{f}_k + \hat{f}_k^\dagger \hat{f}_{k+k_c})\,. \end{aligned} \tag{2.44}$$

Here $\epsilon(k) = \hbar^2 k^2/2m$ is the kinetic energy. The second term describes the process of absorbing a cavity photon and reemitting it in the opposite direction. The third term describes the process of absorbing a photon from the transverse pumping mode and reemitting as cavity mode, or vice versa. Therefore, the cold atoms can suffer a recoil momentum $\pm nk_c$.

### *2.5.2 Phase transition and the analogy to the Dicke Hamiltonian*

We consider the limit of $k_c \ll k_F$, i.e., the Fermi gas is not excited too highly, only particles in the neighborhood of the Fermi surface are raised to higher levels. In this scenario, we can approximate the quadratic energy dispersion relation by its lowest order expansion, e.g., $\sum_k \epsilon(k)\hat{f}_k^\dagger \hat{f}_k \to \sum_k \hbar|k| v_F \hat{f}_k^\dagger \hat{f}_k$, where $v_F = \hbar k_F/M$ is the Fermi velocity. The excitation energies of particle-hole pair at the edges of the interval $[k_F - \delta_k, k_F]$ are $\epsilon(k_F - \delta k + nk_c) - \epsilon(k_F - \delta k) \simeq n\hbar k_c k_F$, and $\epsilon(k_F + nk_c) - \epsilon(k_F) \simeq n\hbar k_c k_F$, respectively.

Then we follow the bosonization procedures [84, 85] and introduce the density-fluctuation operator,

$$\hat{\rho}_q = \sum_k \hat{f}_k^\dagger \hat{f}_{k+q}\,, \tag{2.45}$$

where $q = nk_c$. This operator describes the superposition of particle-hole excitation with a momentum $\hbar q$. The right and left propagating density fluctuation operator can be defined as $\hat{\rho}_q^+$ and $\hat{\rho}_q^-$, corresponding to the summation of $k$ in equation (2.45) for $k > 0$ and $k < 0$, respectively. The commutation relation of $\hat{\rho}_{\pm q}^{\pm}$ leads us to define

$$\begin{aligned} \hat{d}_q &= \beta_q \hat{\rho}_q^+, \quad \hat{d}_q^\dagger = \beta_q \hat{\rho}_{-q}^+ , \\ \hat{d}_{-q} &= \beta_q \hat{\rho}_{-q}^-, \quad \hat{d}_{-q}^\dagger = \beta_q \hat{\rho}_q^- , \end{aligned} \tag{2.46}$$

where $\beta_q = \sqrt{2\pi/qL}$ is the normalization constant. The oscillation mode operator obeys the bosonic commutation relation $[\hat{d}_{\pm q}, \hat{d}_{\pm q'}^\dagger] = \delta q q'$, $[\hat{d}_{\pm q}, \hat{d}_{\pm q'}] = [\hat{d}_{\pm q}^\dagger, \hat{d}_{\pm q'}^\dagger] = 0$ [86, 87]. At the vicinity of the Fermi surface, $\sum_k \epsilon(k) \hat{f}_k^\dagger \hat{f}_k \rightarrow \sum_{q>0} \hbar v_F q (\hat{d}_q^\dagger \hat{d}_q + \hat{d}_{-q}^\dagger \hat{d}_{-q})$. Therefore, the effective Hamiltonian is

$$\begin{aligned} \hat{H} = \; & \hbar \left( \Delta_c + \frac{NU_0}{2} \right) \hat{a}^\dagger \hat{a} \hbar \omega_r (\hat{d}_{k_c}^\dagger \hat{d}_{k_c} + \hat{d}_{-k_c}^\dagger \hat{d}_{-k_c}) \\ & + 2\hbar\omega_r (\hat{d}_{2k_c}^\dagger \hat{d}_{2k_c} + \hat{d}_{-2k_c}^\dagger \hat{d}_{-2k_c}) \\ & + \frac{\hbar U_0}{4\beta_{2k_c}} \hat{a}^\dagger \hat{a} \big[ (\hat{d}_{2k_c}^\dagger + \hat{d}_{2k_c}) + (\hat{d}_{-2k_c}^\dagger + \hat{d}_{-2k_c}) \big] \\ & + \frac{\hbar \eta}{2\beta_{k_c}} (\hat{a}^\dagger + \hat{a}) \left[ (\hat{d}_{k_c}^\dagger + \hat{d}_{k_c}) + (\hat{d}_{-k_c}^\dagger + \hat{d}_{-k_c}) \right] . \end{aligned} \tag{2.47}$$

If we define the excited state of the Fermi gas $|\Psi_{\pm nk_c}^F\rangle = \hat{d}_{\pm nk_c}^\dagger |\Psi_0^F\rangle$ (n=1,2), $\hat{c}_0^\dagger = |\Psi_0^F\rangle\langle 0|$, and $\hat{c}_{n\pm}^\dagger = |\Psi_{\pm nk_c}^F\rangle\langle 0|$, then the above Hamiltonian can be written as

$$\begin{aligned} \hat{H} = \; & \hbar \left( \Delta_c + \frac{NU_0}{2} \right) \hat{a}^\dagger \hat{a} + \hbar\omega_r (\hat{c}_{1+}^\dagger \hat{c}_{1+} + \hat{c}_{1-}^\dagger \hat{c}_{1-}) \\ & + 2\hbar\omega_r (\hat{c}_{2+}^\dagger \hat{c}_{2+} + \hat{c}_{2-}^\dagger \hat{c}_{2-}) + \frac{\hbar\eta}{2\beta_{k_c}} (\hat{a}^\dagger + \hat{a}) \\ & \times \big[ (\hat{c}_+^\dagger \hat{c}_0 + \hat{c}_0^\dagger \hat{c}_+) + (\hat{c}_-^\dagger \hat{c}_0 + \hat{c}_0^\dagger \hat{c}_-) \\ & + (\hat{c}_{2+}^\dagger \hat{c}_+ + \hat{c}_+^\dagger \hat{c}_{2+}) + (\hat{c}_{2-}^\dagger \hat{c}_- + \hat{c}_-^\dagger \hat{c}_{2-}) \big] \end{aligned}$$

$$+\frac{\hbar U_0}{4\beta_{2k_c}}\hat{a}^\dagger\hat{a}\left[(\hat{c}_{2+}^\dagger\hat{c}_0+\hat{c}_0^\dagger\hat{c}_{2+})+(\hat{c}_{2-}^\dagger\hat{c}_0+\hat{c}_0^\dagger\hat{c}_{2-})\right]. \tag{2.48}$$

This approximate Hamiltonian is quite similar to the case of Bosons [45]. Note that for Bosons, the ground state corresponds to the pure condensate where all atoms are static. Therefore, the left propagating excitation with momentum $-k_c$ can be coupled with the right propagating excitation with momentum $k_c$ through the two-cavity-photon scattering. Here, for the Fermion case, the right excitation $\hat{c}_+$ and the left excitation $\hat{c}_-$ are not coupled because the two-cavity-photon scattering with recoil momentum $2k_c$ cannot overcome the wide Fermi sea as $k_c << k_F$.

After making the mean-field approximation $\hat{c}_i \sim \sqrt{N}X_i$, $\hat{a} \sim \alpha$, the equation of motion for the Fermi gas can be found as [59],

$$i\frac{d}{d\tilde{t}}X = \left[H_0 + 2\mathrm{Re}(\alpha)H_1 + |\alpha|^2 H_2\right]X, \tag{2.49}$$

with $X = (X_0, X_+, X_-, X_{2+}, X_{2-})^T$ and

$$H_0 = \begin{pmatrix} 0 & 0 & 0 & 0 & 0 \\ 0 & 1 & 0 & 0 & 0 \\ 0 & 0 & 1 & 0 & 0 \\ 0 & 0 & 0 & 2 & 0 \\ 0 & 0 & 0 & 0 & 2 \end{pmatrix}, \tag{2.50a}$$

$$H_1 = \frac{\tilde{\eta}}{2}\begin{pmatrix} 0 & 1 & 1 & 0 & 0 \\ 1 & 0 & 0 & 1 & 0 \\ 1 & 0 & 0 & 0 & 1 \\ 0 & 1 & 0 & 0 & 0 \\ 0 & 0 & 1 & 0 & 0 \end{pmatrix}, \tag{2.50b}$$

$$H_2 = \frac{\tilde{U}_0}{4}\begin{pmatrix} 0 & 0 & 0 & 1 & 1 \\ 0 & 0 & 0 & 0 & 0 \\ 0 & 0 & 0 & 0 & 0 \\ 1 & 0 & 0 & 0 & 0 \\ 1 & 0 & 0 & 0 & 0 \end{pmatrix}, \tag{2.50c}$$

where $\tilde{t} = \omega_r t$, $\tilde{\eta} = \eta/(\beta_{k_c}\omega_r)$, and $\tilde{U}_0 = \eta/(\beta_{2k_c}\omega_r)$ are rescaled dimensionless quantities.

The evolution equation of the coherent photon amplitude is

$$i\frac{d}{d\tilde{t}}\alpha = \tilde{\Delta}\alpha + NX^*H_1X + NX^*H_2X\alpha - i\kappa\alpha\,. \tag{2.51}$$

We also follow the DMA method. However, this method can only solve the eigenvalues, but cannot discriminate whether the state is stable or not. We need to perform a linear stability analysis [59]. Let $X(\tilde{t}) = X^s(\tilde{t}) + \delta X(\tilde{t})$ with $\delta X$ being an infinitesimal derivation from the eigenstate $X^s(\tilde{t})$. Upon substituting this state into the Schrödinger equation equation (2.49), we get, to the first order,

$$\begin{aligned} i\frac{d\delta X_i}{d\tilde{t}} &= \left[H_0^{ij} + 2\mathrm{Re}(\alpha)H_1^{ij} + |\alpha|^2 H_2\right]\delta X_j \\ &\quad + 2H_1^{ij}X_j^s\left[\left(\frac{\partial \mathrm{Re}(\alpha)}{\partial X_k}\right)_s \delta X_k + \left(\frac{\partial \mathrm{Re}(\alpha)}{\partial \bar{X}_k}\right)_s \delta\bar{X}_k\right] \\ &\quad + H_2^{ij}X_j^s\left[\left(\frac{\partial |\alpha|^2}{\partial X_k}\right)_s \delta X_k + \left(\frac{\partial |\alpha|^2}{\partial \bar{X}_k}\right)_s \delta\bar{X}_k\right]. \end{aligned} \tag{2.52}$$

We assume

$$\delta X(\tilde{t}) = e^{-iE_0\tilde{t}}(ue^{-i\Omega\tilde{t}} - v^*e^{-i\Omega^*\tilde{t}})\,, \tag{2.53}$$

and substitute that into equation (2.52) to get

$$M \begin{pmatrix} u \\ v \end{pmatrix} = \Omega \begin{pmatrix} u \\ v \end{pmatrix} , \tag{2.54}$$

where

$$M = \begin{pmatrix} A + B - E_0 & -B \\ B & -A - B + E_0 \end{pmatrix} , \tag{2.55}$$

and the matrices $A$ and $B$ are defined as

$$\begin{aligned} A &= H_0 + 2\mathrm{Re}(\alpha_s) H_1 + |\alpha_s|^2 H_2, \\ B_{ij} &= 2H_1^{ik} X_k^s \left( \frac{\partial \mathrm{Re}\alpha}{\partial X_j} \right)_s + H_2^{ik} X_k^s \left( \frac{\partial |\alpha|^2}{\partial X_j} \right)_s . \end{aligned} \tag{2.56}$$

If the eigenvalues $\Omega$ are all real, the eigenstate is stable; otherwise, it is unstable.

To illustrate the experimental realization, we consider a set of parameters similar to those in Refs. [86, 87]: the single atom Rabi frequency $g_0 \simeq 2\pi \times 20$MHz, the pump-atom detuning $\omega_p - \omega_a = 2\pi \times 100$GHz, which gives the coupling $U_0 \simeq 2\pi \times 5$kHz. The length of the cavity is chosen as $L = 500\mu$m, and the decay rate $\kappa = 2\pi \times 50$MHz. The wavelength of the field is taken to be $\lambda = 500$nm. The number of atoms $N = 2 \times 10^4$ and the atomic mass $M = 1.5 \times 10^{-25}$kg. Therefore $k_c/k_F \sim 0.1$. The numerical result of the photon number as a function of different pumping rate is shown in figure 2.14(a), where blue solid line and red dashed line correspond to the state and unstable states respectively. The corresponding eigenstate energy is shown in figure 2.14(b).

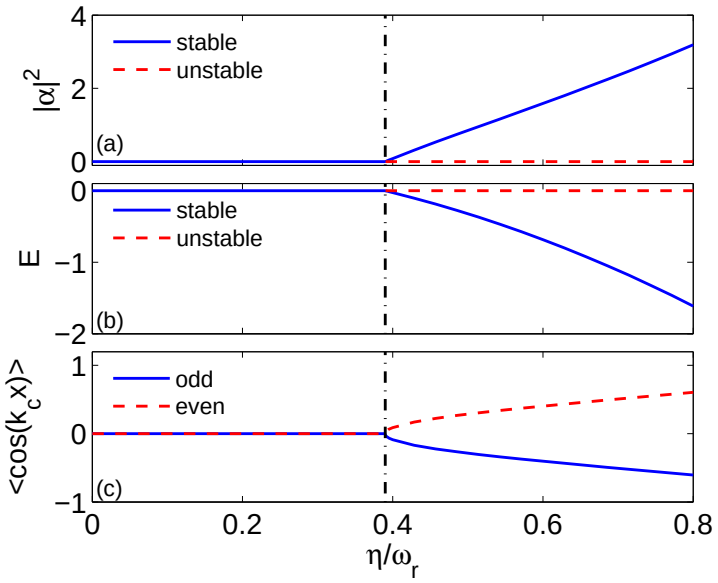


Figure 2.14: The phase transition of different quantities. (a) The intra-cavity photon number. (b) The eigenstate energy. (c) The average value of $\cos(k_c x)$. The horizontal coordinate of the black vertical line is calculated from equation (2.59).

The corresponding cavity field as

$$\alpha = \frac{NX^* H_1 X}{\kappa + i(\tilde{\Delta} + NX^* H_2 X)} \,. \tag{2.57}$$

The density waves with momentum $2\hbar\omega_r$ can be omitted in the close vicinity of the phase transition.In this case, we define $\hat{J}_z = (\hat{c}_+^\dagger \hat{c}_+ + \hat{c}_-^\dagger \hat{c}_- - 2\hat{c}_0^\dagger \hat{c}_0)/2$, $\hat{J}_+ = \hat{c}_+^\dagger \hat{c}_0 + \hat{c}_-^\dagger \hat{c}_0$, and $\hat{J}_- = \hat{c}_0^\dagger \hat{c}_+ + \hat{c}_0^\dagger \hat{c}_-$. As the Fermi gas are located in a high-finesse cavity, we can assume $\hat{c}_+ \simeq \hat{c}_-$, therefore, we have $[\hat{J}_+, \hat{J}_-] = 2\hat{J}_z$, $[\hat{J}_\pm, \hat{J}_z] = \mp \hat{J}_\pm$. The Hamiltonian is then

$$\hat{H} = \hbar\omega_0 \hat{J}_z + \hbar\omega \hat{a}^\dagger \hat{a} + \frac{\hbar\lambda}{\sqrt{N}}(\hat{J}_+ + \hat{J}_-) \,, \tag{2.58}$$

where $\omega_0 = 2\omega_r$, $\omega = \Delta_c + NU_0/2$, and $\lambda = \eta\sqrt{N}/(2\beta_{k_c})$. This Hamiltonian corresponds to the Dicke Hamiltonian and the phase transition we studied above can be identified as the quantum Dicke phase transition. The critical value of the transition is [81]

$$\lambda_c = \frac{1}{2}\sqrt{\left(\frac{\omega_0}{\omega}\right)(\kappa^2 + \omega^2)}\,. \tag{2.59}$$

It is shown in figure 2.14 that the critical value calculated from this equation and the numerical result coincide.

## 2.6 Summary

We studied the self-organization phase transition in an optical cavity filled with a cigar-shaped quantum-degenerate Fermi gas. We found that the effective Hamiltonian is of Dicke type. The corresponding phase transition can be identified with the Dicke quantum phase transition. The main advantage of Fermi gas is that the atom-atom interaction is negligible, which enables a direct comparison between the theoretical and experimental critical values.

# 3. CONTROL OF SPONTANEOUS EMISSION: EFFECT OF COUNTER-ROTATING TERMS *

## 3.1 Introduction

Spontaneous emission is one of the main and fundamental topics in quantum optics. From the fundamental point of view, it is a peculiar phenomenon which shows the quantum nature of the electromagnetic field [88, 2], as it cannot be explained within the semi-classical framework. It also leads to many useful applications and still attracts considerable interests. Many effects and techniques can be utilized to modify the spontaneous emission. For example, quantum interference has been recognized as a significant mechanism for the modification of spontaneous emission [13, 14, 15, 16, 17, 18, 19, 20, 21, 22, 23, 24]. The spontaneously generated coherence can lead to suppression, spectral narrowing and population trapping [13, 14, 15, 16, 17, 18, 19, 20, 21], phase control of spontaneous emission [22, 23], and enhancement of Kerr nonlinearity [24]. Another kind of methods focus on tailoring the mode density by embedding the atom into different surrounding environments, such as cavity electrodynamics [89] and photonic crystal [90]. Particularly, photonic crystal, which is a class of materials with composed periodic dielectric structures, has remarkable capabilities of localizing and guiding electromagnetic radiation that can be used effectively to control spontaneous emission [91, 92, 93].

In the previous studies of spontaneous emission, RWA is usually made when

*Reprinted with permission from "Control of the Lamb shift by a driving field," by Shuai Yang, Hang Zheng, Ran Hong, Shi-Yao Zhu, and M. Suhail Zubairy, 2010, *Phys. Rev. A*, vol. 81, p. 052501, copyright [2011] by American Physical Society, "Effect of energy shifts on the spontaneous emission modification via quantum interference," by Shuai Yang, Jun Xu, Shi-Yao Zhu, and M. Suhail Zubairy, 2012, *Phys. Rev. A*, vol. 85, p. 062516, copyright [2012] by American Physical Society, and "Effect of counter-rotating terms on the spontaneous emission in an anisotropic photonic crystal," by Shuai Yang, M. Al-Amri, Shi-Yao Zhu, and M. Suhail Zubairy, 2013, *Phys. Rev. A*, vol. 87, p. 033818, copyright [2013] by American Physical Society.

dealing with the interaction between the atom and the electromagnetic modes. RWA is usually a good approximation in the resonant interaction and in the long time limit in the spontaneous emission study. However, in the short-time, the dynamic evolution of the spontaneous emission with and without making RWA is different. For example, in a hydrogen atom, counter-rotating terms results a much longer quantum Zeno time and eliminates the anti-Zeno effect [46].

When studying the quantum interference of the spontaneous emission of two atomic levels coupled to a common lower level, the validity of RWA is also questionable. In previous studies of spontaneous emission quenching with RWA, the interference between the decay rates of the two levels (real parts of the dynamical equations), while the energy shifts (imaginary parts of the dynamical equations), are neglected. This is because the imaginary parts are divergent because of the free electron self-energy. In addition, calculation of the energy shifts cannot neglect the contribution of the counter-rotating terms.

For an atom embedded in a photonic crystal,the atom exchange energy back and forth with its own radiation frequently, when the atomic resonant frequency lies near the edge of a photonic band gap. This strong interaction between the atom and electromagnetic radiation induces atomic level splitting and is the origin of photon-atom bound state [94, 95, 96, 97]. However, as we know that counter-rotating terms are indispensable in explaining the Lamb shift, it will also introduce significant effect in the spontaneous emission of the atom in a photonic crystal.

In this section, we study the effect of counter-rotating terms in the control of spontaneous emission. In 3.2, we introduce the unitary transformation method proposed in Ref. [46, 47], which enable us to include the effect of the counter-rotating terms in the Hamiltonian. In 3.3, we investigate the effect of energy shifts on the spontaneous emission modification via quantum interference. In 3.4, we study the

effect of counter-rotating terms on the spontaneous emission in an anisotropic photonic crystal. In 3.5, as an application of the unitary tranformation method, we show how to control the Lamb shift by an driving field.

## 3.2 The unitary transformation method

The Hamiltonian of a multi-level atom coupled with the vacuum reservoir can be written as

$$\begin{aligned} H &= H_0 + H_1 \,, \\ H_0 &= \sum_i \hbar\omega_i |i\rangle\langle i| + \sum_k \hbar\omega_k \hat{b}_k^\dagger \hat{b}_k \,, \qquad (3.1a) \\ H_1 &= \sum_{k,i\neq j} \hbar g_{k,ij} \left(\hat{b}_k^\dagger + \hat{b}_k\right) \left(|i\rangle\langle j| + |j\rangle\langle i|\right) \,, \qquad (3.1b) \end{aligned}$$

where $H_0$ is the bare Hamiltonian of the atom and the vacuum modes, and $H_1$ describes the interaction between the atom the vacuum modes. The energy of level $i$ is $\hbar\omega_i$. $\hat{b}_k$ ($\hat{b}_k^\dagger$) is the annihilation (creation) operator of the vacuum mode $k$ with frequency $\omega_k$. The coefficient $g_{k,ij} = -e\sqrt{1/2\epsilon_0\omega_k V}\mathbf{e}_k\cdot\mathbf{p}_{ij}/m$ is the coupling constant between the atom and the vacuum field, with $\mathbf{e}_k$ being the polarization vector and $\mathbf{p}_{ij}$ being the transition matrix element of the momentum operator between the levels $i$ and $j$.

In the above Hamiltonian, all the rotating terms (energy conservation processes) and counter-rotating terms (energy nonconservation precesses) are included. One obvious effect of the counter-rotating terms is the different ground state. While $|g,0\rangle$ is the ground state of the total Hamiltonian with RWA, it is not the ground state of the full Hamiltonian with counter-rotating terms. The energy non-conserved counter-rotating terms are significant to short time evolution. They are also indispensable to explain the Lamb shift. However, the calculation including counter-rotating terms

directly is usually hard. Here we first review the unitary transformation method proposed in Ref. [46, 47].

In order to eliminate the counter-rotating terms, a unitary transformation $\exp(iS)$ is employed on the full Hamiltonian $H$, e.g.,

$$H^S = \exp(iS) H \exp(-iS)\,, \tag{3.2}$$

with

$$S = \sum_k \sum_{i \neq j} \hbar \frac{g_{k,ij}\xi_{k,ij}}{i\omega_k} \left(b_k^\dagger - b_k\right) |i\rangle\langle j|\,, \tag{3.3}$$

here

$$\xi_{k,ij} = \frac{\omega_k}{|\omega_{ij}| + \omega_k} \tag{3.4}$$

is chosen such that the counter-rotating terms cancel out. We then expand the transformed Hamiltonian $H^S$ in a power series of $g_{k,ij}$, i.e., $H^S = H_0^S + H_1^S + H_2^S + O(g_k^3)$, where $O(g_k^3)$ contains terms of order $g_k^3$ and higher, and will be neglected.

The zero order term in $g_{k,ij}$ is

$$H_0^S = \sum_i \hbar\omega_i |i\rangle\langle i| + \sum_k \hbar\omega_k \hat{b}_k^\dagger \hat{b}_k\,. \tag{3.5}$$

The first order term in $g_{k,ij}$ is

$$H_1^S = H_1 + [iS, H_0] = \sum_{k,i<j} \omega_{ji} (\hat{b}_k^\dagger |i\rangle\langle j| + \hat{b}_k |j\rangle\langle i|)\,. \tag{3.6}$$

$V_{k,ij} = 2g_{k,ij}\xi_{k,ij}/\omega_k$ is the new coupling constant.

The second order term results from

$$\begin{aligned} H_2^S &= [iS, H_1] + \frac{1}{2}[iS, [iS, H_0]] \\ &= -\sum_{k,i\neq j} \frac{g_{k,ij}^2}{\omega_k} \left[ \xi_{k,ij} - \xi_{k,ij}^2 - \frac{\xi_{k,ij}^2}{\omega_k}(\omega_j - \omega_i) \right] |i\rangle\langle i| \\ &\quad -\sum_{k,i\neq j} \sum_{l\neq i,j} \frac{g_{k,il} g_{k,lj}}{\omega_k} \left[ \xi_{k,il} + \xi_{k,lj} - \xi_{k,il}\xi_{k,lj} - \frac{\xi_{k,il}\xi_{k,lj}(2\omega_l - \omega_i - \omega_j)}{2\omega_k} \right] \\ &\quad \times |i\rangle\langle j| \,, \end{aligned} \tag{3.7}$$

where the diagonal parts mean the energy shift and the off-diagonal parts describe the indirect interaction between two states $|i\rangle$ and $|j\rangle$ through a third state $|l\rangle$. Note that these terms are linear divergent when summarizing of $k$. This is due to the self-energy of the electron which results from the exchange of virtual photons between the free electron and the vacuum. This energy is calculated as

$$E_{se}^{(ij)} = -\sum_{k,q\neq i,j} \frac{g_{k,iq} g_{k,jq}}{\omega_k} \,. \tag{3.8}$$

Subtracting the self-energy from the Hamiltonian, we have

$$H_2^S - E_{se} = \sum_i \Delta E_{nd}^{(i)} |i\rangle\langle i| + \sum_{i,j>i} \eta_{ij} (|i\rangle\langle j| + |j\rangle\langle i|) \,, \tag{3.9}$$

where

$$\Delta E_{nd}^{(i)} = \sum_k \sum_{j\neq i} \frac{g_{k,ii}^2}{\omega_k} \frac{\omega_{ji}(\omega_{ji} + \omega_k)}{(\omega_k + |\omega_{ij}|)^2} \tag{3.10}$$

denotes the non-dynamic energy shift since it is independent of any real decay pro-

cess, and

$$\eta_{ij} = \sum_{k} \eta_{k,ij} = \sum_{k,l\neq i,j} \frac{g_{k,il} g_{k,lj}}{\omega_k} \frac{2|\omega_{il}||\omega_{lj}| - \omega_{il}\omega_k - \omega_{jl}\omega_k}{2(\omega_{il} + \omega_k)(\omega_{jl} + \omega_k)} \tag{3.11}$$

is the indirect coupling parameter arising from the virtual photon processes $|i\rangle \leftrightarrow |l\rangle \leftrightarrow |j\rangle$. This interaction is important only if the direct interaction between $i$ and $j$ is absent and the energy separation between them is tiny.

In a word, three effects are seen in the transformed Hamiltonian. First, the energy levels are shifted from $\omega_i$ to $\omega_i' = \omega_i + \Delta E_{nd}^{(i)}$. Second, the coupling constant is redefined as $V_{k,ij}$. Third, indirect couplings between two levels through the virtual-photon process are introduced via $\eta$ terms. Armed with this method, we start to discuss applications.

## 3.3 Effect of energy shifts on the spontaneous emission modification via quantum interference

### *3.3.1 Motivation*

In a V-type atom, the quantum interference due to the spontaneous emission of two atomic levels coupled to a common lower level through the interaction with the same vacuum modes can lead to spontaneous emission quenching from the two upper levels [13]. If the two upper levels are driven to another level by a strong laser field, complete quenching of spontaneous emission is possible under certain conditions [14, 18]. In the previous studies, only the interference between the decay rates was investigated under the long time limit and the Markov approximation; while the dynamic energy shifts which correspond to the imaginary parts in the dynamical equations were neglected since it is impossible to take into account the phase changes due to the difficulty of including the self-energy of the free electron

before obtaining the dynamic evolution equations. In Ref. [98], Li et. al. utilized the unitary transformation method and studied the influence of the quantum interference resulting from the energy shifts on the decay rates of the two upper levels in a V-type atom. However, in this case, the dynamic shifts will take effect only if the two dipole transitions are non-orthogonal and quantum interference exists.

We consider the case of a four-level atom where the two upper levels are coupled to another level by a driving laser. In this scenario, we can compare the result, on one hand, with the result in [98], and show how the spontaneous emissions can be controlled by the driving field without making RWA. In addition, the effect of the dynamic energy shifts will be revealed even if the two dipole transitions from the upper levels to the ground level are orthogonal. On the other hand, we can compare our result with the previous studies on the quantum interference between decay channels [14, 18] and show how the evolution can be effected by the quantum interference resulting from the energy shifts.

### *3.3.2 Model and calculation*

The level diagram of our system is shown in figure 3.1. The two upper levels $|a_1\rangle$ and $|a_2\rangle$ are coupled by the same vacuum modes to the lower level $|b\rangle$ and by a strong coherent field with frequency $\nu_0$ to another upper lying level $|c\rangle$. Since we are more interested in the spontaneous emission, the Hamiltonian in the rotating frame of the the driving field can be written as

$$
\begin{aligned}
H &= H^{(0)} + H^{(1)}\,, \\
H^{(0)} &= \hbar\omega_{a_1 b}|a_1\rangle\langle a_1| + \hbar\omega_{a_2 b}|a_2\rangle\langle a_2| + \hbar(\omega_{cb}+\nu_0)|c\rangle\langle c| \\
&\quad + \sum_k \hbar\omega_k \hat{b}_k^\dagger \hat{b}_k + \hbar\Omega_1\big(|a_1\rangle\langle c| + |c\rangle\langle a_1|\big) + \hbar\Omega_2\big(|a_2\rangle\langle c| + |c\rangle\langle a_2|\big)\,, \qquad (3.12a)
\end{aligned}
$$

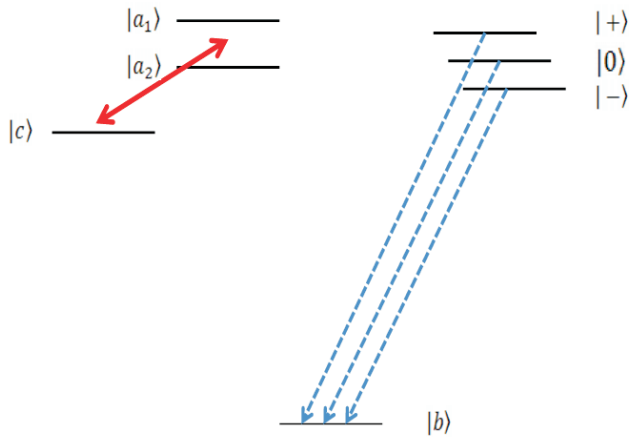


Figure 3.1: Atomic transitions in the dressed state picture.

$$H^{(1)} = \hbar \sum_k \left[ g_k^{(1)} \left( \hat{b}_k^\dagger + \hat{b}_k \right) \left( |a_1\rangle\langle b| + |b\rangle\langle a_1| \right) + g_k^{(2)} \left( \hat{b}_k^\dagger + \hat{b}_k \right) \left( |a_2\rangle\langle b| + |b\rangle\langle a_2| \right) \right], \tag{3.12b}$$

where $H^{(0)}$ is the bare Hamiltonian of the atom the vacuum modes and the driven transition between upper levels and $H^{(1)}$ describes the interaction of the atom and the vacuum modes. The interactions of the driven transitions through vacuum modes are neglected. The frequency differences between $|a_1\rangle$, $|a_2\rangle$, $|c\rangle$, and $|b\rangle$ are labeled by $\omega_{a_1 b}$, $\omega_{a_2 b}$ and $\omega_{cb}$, respectively. Here $\hat{b}_k(\hat{b}_k^\dagger)$ is the annihilation (creation) operator of the vacuum mode $k$ with frequency $\omega_k$, $\Omega_1(\Omega_2)$ is the Rabi frequency of the coupling between $|a_1\rangle(|a_2\rangle)$ and $|c\rangle$ through the coherent driving field, and $g_k^{(1)}(g_k^{(2)})$ describes the vacuum-induced coupling between $|a_1\rangle(|a_2\rangle)$ and $|b\rangle$.

Digonalizing $H^{(0)}$, we arrive at the characteristic equation

$$x_n^3 - x_n^2(\Delta_1 + \Delta_2) - x_n[\Omega_1^2 + \Omega_2^2 - \Delta_1\Delta_2)] + \Delta_1\Omega_2^2 + \Delta_2\Omega_1^2 = 0, \tag{3.13}$$

where $\Delta_1 = (\omega_{a_1 b} - \omega_{cb}) - \nu_0$ and $\Delta_2 = (\omega_{a_2 b} - \omega_{cb}) - \nu_0$ are the detunings of the driving field. We assume, for simplicity, that

$$\Delta_1 \Omega_2^2 + \Delta_2 \Omega_1^2 = 0\,, \tag{3.14}$$

then the three eigenstates are

$$|0\rangle = N_0 \left( \Omega_2 |a_1\rangle - \Omega_1 |a_2\rangle - \frac{\Omega_2}{\Omega_1} \Delta_1 |c\rangle \right), \tag{3.15a}$$

$$|\pm\rangle = N_\pm \left[ \Omega_1 \left( \mu \pm \frac{\omega_{12}}{2} \right) |a_1\rangle + \Omega_2 \left( \mu \mp \frac{\omega_{12}}{2} \right) |a_2\rangle \pm (\Omega_1^2 + \Omega_2^2) |c\rangle \right]. \tag{3.15b}$$

Here

$$\mu = \sqrt{\Omega_1^2 + \Omega_2^2 + \frac{\omega_{12}^2}{4}}\,. \tag{3.16}$$

The energy difference between the two upper levels is denoted as $\omega_{12} = \omega_{a_1 b} - \omega_{a_2 b}$. $N_0$ and $N_\pm$ are the normalization constants. The corresponding energies are

$$E_0 = \hbar(\omega_{cb} + \nu_0), \tag{3.17a}$$

$$E_\pm = \hbar \left( \omega_{cb} + \nu_0 + \frac{\Delta_1 + \Delta_2}{2} \pm \mu \right). \tag{3.17b}$$

In the dressed state basis, the Hamiltonian can be rewritten as

$$H^{(0)} = \sum_{\alpha = 0, \pm} \hbar \omega_i |i\rangle\langle i| + \sum_k \hbar \omega_k \hat{b}_k^\dagger \hat{b}_k\,, \tag{3.18a}$$

$$H^{(1)} = \sum_{i = 0, \pm} \hbar g_{k,i} \left( \hat{b}_k^\dagger + \hat{b}_k \right) \left( |i\rangle\langle b| + |b\rangle\langle i| \right), \tag{3.18b}$$

where $\hbar\omega_i \equiv E_i$, and

$$g_{k,0} = N_0\Big(\Omega_2 g_k^{(1)} - \Omega_1 g_k^{(2)}\Big)\,, \tag{3.19a}$$

$$g_{k,\pm} = N_\pm\left[\Omega_1\Big(\mu \pm \frac{\omega_{12}}{2}\Big)g_k^{(1)} + \Omega_2\Big(\mu \mp \frac{\omega_{12}}{2}\Big)g_k^{(2)}\right]. \tag{3.19b}$$

We then follow the unitary transformation method [46, 47] and include the influence of the counter-rotating terms while transforming the Hamiltonian to the RWA form. After removing the free-electron self-energy, the whole transformed Hamiltonian $H'$, to the second order of $g_k$, can be written as

$$\begin{aligned} H' \;=\; & \sum_{i=b,0,\pm} \hbar\omega_i' |i\rangle\langle i| + \sum_k \hbar\omega_k \hat{b}_k^\dagger \hat{b}_k + \sum_k \sum_{j=0,\pm} \hbar V_{k,j}\Big(|b\rangle\langle j|b_k^\dagger + |j\rangle\langle b|b_k\Big) \\ & + \sum_{i,j=0,\pm}^{i\neq j} \hbar\eta_{ij}(|j\rangle\langle i| + |i\rangle\langle j|)\,, \end{aligned} \tag{3.20}$$

where $V_{k,j} \equiv \frac{2g_{k,j}\xi_{k,j}}{\omega_k}\omega_{jb}$ and $\hbar\omega_i' = \hbar\omega_i + \Delta E_{\rm nd}^{(i)}$. Here

$$\Delta E_{\rm nd}^{(i)} = \hbar\frac{g_{k,i}^2}{\omega_k}\frac{\omega_{ib}(\omega_{ib}-\omega_k)}{(\omega_k+\omega_{ib})^2}, \qquad i \in \{0,\pm\} \tag{3.21a}$$

$$\Delta E_{\rm nd}^{(b)} = \sum_{i=0,\pm} \hbar\frac{g_{k,i}^2}{\omega_k}\frac{\omega_{ib}(\omega_{ib}+\omega_k)}{(\omega_k+\omega_{ib})^2}\,, \tag{3.21b}$$

denote the non-dynamic shifts and

$$\eta_{ij} = \sum_k \frac{g_{k,i}g_{k,j}}{\omega_k}\frac{2\omega_{ib}\omega_{jb} - \omega_k(\omega_{ib}+\omega_{jb})}{2(\omega_{ib}+\omega_k)(\omega_{jb}+\omega_k)} \tag{3.22}$$

arises from the virtual photon process $i \leftrightarrow b \leftrightarrow j$.

In the interaction picture

$$\begin{aligned}\mathscr{V} &= \sum_k \sum_{j=0,\pm} \hbar V_{k,j} \Big\{ |b\rangle\langle j| b_k^\dagger \exp[-i(\omega'_{jb} - \omega_k)t] + |j\rangle\langle b| b_k \exp[i(\omega'_{jb} - \omega_k)t] \Big\} \\ &\quad + \sum_{i,j=0,\pm}^{i\neq j} \hbar \eta_{ij} \Big[ |j\rangle\langle i| \exp(i\omega'_{ji}t) + |i\rangle\langle j| \exp(-i\omega'_{ji}t) \Big] . \end{aligned} \tag{3.23}$$

The state vector at time $t$ can be written as

$$\Psi(t) = \sum_{i=0,\pm} a_i(t)|i\rangle|\{0\}\rangle + \sum_k \beta_k(t)|b\rangle|1_k\rangle . \tag{3.24}$$

The corresponding evolution equations are

$$i\dot{a}_i(t) = \sum_{j=0,\pm}^{j\neq i} a_j(t)\eta_{ij} \exp(-i\omega'_{ji}t) + \sum_k \beta_k(t) V_{k,i} \exp[i(\omega'_{ib} - \omega_k)t] , \tag{3.25a}$$

$$i\dot{\beta}_k(t) = \sum_{i=0,\pm} a_i(t) V_{k,i} \exp[-i(\omega'_{ib} - \omega_k)t] . \tag{3.25b}$$

Integrating the equation for $\beta_k$, and then substituting into the equation for $a_i$, we have

$$\begin{aligned}\dot{a}_i(t) &= -\sum_k V_{k,i} \exp[i(\omega'_{ib} - \omega_k)t] \sum_j V_{k,j} \int_0^t dt' \exp[-i(\omega'_{jb} - \omega_k)t'] a_j(t') \\ &\quad -i \sum_{j=0,\pm}^{j\neq i} \eta_{ij} \exp(-i\omega'_{ji}t) a_j(t) . \end{aligned} \tag{3.26}$$

We can simplify the equation above by using the Markov approximation in the long time limit, which gives

$$\dot{a}_i = -\kappa_i a_i - \sum_{j=0,\pm}^{j\neq i} \kappa_{ij} \exp(i\omega'_{ij}t) a_j(t) , \tag{3.27}$$

where $\kappa_i = \sum_k V_{k,i}^2 \left[-i\mathscr{P}\frac{1}{\omega_k-\omega'_{ib}} + \pi\delta(\omega_k-\omega'_{ib})\right] = \frac{1}{2}\gamma_i + i\Delta E_{\rm dyn}^{(i)}$ with

$$\begin{aligned}
\gamma_0 = \;& N_0^2[\gamma_{a_1}\Omega_2^2 + \gamma_{a_2}\Omega_1^2 - 2p\sqrt{\gamma_{a_1}\gamma_{a_2}}\Omega_1\Omega_2]\,, && \text{(3.28a)}\\
\gamma_\pm = \;& N_\pm^2[\gamma_{a_1}\Omega_1^2(\mu \pm \frac{\omega_{12}}{2})^2 + \gamma_{a_2}\Omega_2^2(\mu \mp \frac{\omega_{12}}{2})^2 \\
& - 2p\sqrt{\gamma_{a_1}\gamma_{a_2}}\Omega_1\Omega_2(\mu^2 - \frac{\omega_{12}^2}{4})]\,, && \text{(3.28b)}
\end{aligned}$$

and $\kappa_{ij} = \sum_k V_{k,i}V_{k,j}\left[-i\mathscr{P}\frac{1}{\omega_k-\omega'_{jb}} + \pi\delta(\omega_k-\omega'_{jb})\right] = \frac{1}{2}\gamma_{ij} + i\Delta E_{\rm dyn}^{(ij)} + i\eta_{ij}$, with

$$\begin{aligned}
\gamma_{0\pm} = \;& N_\pm N_0\Bigg\{\Omega_1\Omega_2\left[\left(\mu \pm \frac{\omega_{12}}{2}\right)\gamma_{a_1} - \left(\mu \mp \frac{\omega_{12}}{2}\right)\gamma_{a_2}\right] \\
& + p\left[-\Omega_1^2\left(\mu \pm \frac{\omega_{12}}{2}\right) + \Omega_2^2\left(\mu \mp \frac{\omega_{12}}{2}\right)\right]\sqrt{\gamma_{a_1}\gamma_{a_2}}\Bigg\}\,, && \text{(3.29a)}\\
\gamma_{+-} = \;& N_+N_-\Bigg\{\left(\mu^2 - \frac{\omega_{12}^2}{4}\right)\left[\Omega_1^2\gamma_{a_1} + \Omega_2^2\gamma_{a_2}\right] \\
& + p\Omega_1\Omega_2\left[\left(\mu + \frac{\omega_{12}}{2}\right)^2 + \left(\mu - \frac{\omega_{12}}{2}\right)^2\right]\sqrt{\gamma_{a_1}\gamma_{a_2}}\Bigg\}\,. && \text{(3.29b)}
\end{aligned}$$

Here $p$ denotes the alignment of the matrix elements of the two dipole moments and is given by

$$p = \frac{\vec{p}_{a_1b}\cdot\vec{p}_{a_2b}}{|\vec{p}_{a_1b}||\vec{p}_{a_1b}|}\,. \qquad \text{(3.30)}$$

Note that if we replace $\eta_{ij} = 0$, $\Delta E_{\rm dyn}^{(i)} = \Delta E_{\rm dyn}^{(ij)} = 0$, we get the previous result under the RWA [14, 18]. Since the dynamic energy shifts are now correlated with the decay rates, we would expect quantum interference effects resulting from the dynamic energy shifts. In addition, the couplings between the high dressed levels introduced by the virtual-photon processes will also lead to interference phenomena.

We can redefine the amplitudes as $a_+ = \tilde{a}_+ e^{i\omega'_{+0}t}$, $a_0 = \tilde{a}_0$ and $a_- = \tilde{a}_- e^{i\omega'_{-0}t}$, the

evolution equations are

$$\dot{\tilde{a}}_+ = -(\kappa_+ + i\omega'_{+0})\tilde{a}_+ - \kappa_{+0}\tilde{a}_0 - \kappa_{+-}\tilde{a}_- \,, \tag{3.31a}$$

$$\dot{\tilde{a}}_0 = -\kappa_0\tilde{a}_0 - \kappa_{0+}\tilde{a}_+ - \kappa_{0-}\tilde{a}_- \,, \tag{3.31b}$$

$$\dot{\tilde{a}}_- = -(\kappa_- + i\omega'_{-0})\tilde{a}_- - \kappa_{-+}\tilde{a}_+ - \kappa_{-0}\tilde{a}_0 \,. \tag{3.31c}$$

If we want to have a nonzero upper level population at $t = \infty$, we need a nonzero steady-state solution, which means $\det M = 0$, where

$$M = \begin{pmatrix} \kappa_+ + i\omega'_{+0} & \kappa_{+0} & \kappa_{+-} \\ \kappa_{0+} & \kappa_0 & \kappa_{0-} \\ \kappa_{-+} & \kappa_{-0} & \kappa_- + i\omega'_{-0} \end{pmatrix} . \tag{3.32}$$

If we have the condition $|p| = 1$ and

$$\frac{\Omega_1}{\Omega_2} = p\sqrt{\frac{\gamma_{a_1}}{\gamma_{a_2}}} \,, \tag{3.33}$$

then $\gamma_0 = 0$, and at the same time $\gamma_{0\pm} = 0$. Thus, under the RWA, $\kappa_{\pm 0} = \kappa_{0\pm} = \kappa_0 = 0$, so $\det M = 0$. Therefore, if the initial state has a portion of state $|0\rangle$, a significant amount of population can be trapped in the upper levels provided the driving field is strong enough [18]. One can find that, if the counter-rotating terms are kept in the Hamiltonian, we will have the same condition for elimination of spontaneous emission from level $|0\rangle$, see the Appendix C.

The solutions for $\tilde{a}_i$ are now given by

$$\tilde{a}_i(t) = \sum_{j=1}^{3} \alpha_{ij} e^{-\lambda_j t} \,, \tag{3.34}$$

where the $\lambda_j$'s are the three roots of the secular equation corresponding to the matrix $M$. The coefficients $\alpha_{ij}$ are determined by the initial condition of the atomic state.

The probability amplitude $\beta_k(\infty)$ of the atom being in the lower state with one photon emitted is given by

$$\begin{aligned}
\beta_k(t) &= -i \sum_{i=0,\pm} \int_0^t dt' a_i(t') V_{k,i} \exp[-i(\omega'_{ib} - \omega_k)t'] \\
&= -i \sum_{i=0,\pm} \int_0^t dt' \sum_{j=1}^{3} \alpha_{ij} e^{-\lambda_j t' + i\omega'_{i0} t} V_{k,i} e^{-i(\omega'_{ib} - \omega_k)t'} \\
&= -i \sum_{i=0,\pm} \int_0^t dt' \sum_{j=1}^{3} \alpha_{ij} V_{k,i} e^{-\lambda_j t' - i(\omega'_{b0} - \omega_k)t'} \,. \qquad (3.35)
\end{aligned}$$

The spontaneous emission spectrum is proportional to $|\beta_k(t=\infty)|^2$ [2], with

$$\beta_k = \sum_{j=1}^{3} \frac{i \sum_{i=0,\pm} (V_{k,i} \alpha_{ij})}{-\lambda_j + i\delta_k} \,, \qquad (3.36)$$

where $\delta_k = \omega_k - \omega'_{b0}$.

### *3.3.3 Results*

By adding the driving field, the survival probability of the atomic levels can be controlled. The population evolution of the upper levels for the cases with and without the driving field is shown in figure 3.2. As shown in figure 3.2(a), the dynamic energy shifts and the coupling terms $\eta_{ij}$ introduce an oscillation between the two upper levels $|a_1\rangle$ and $|a_2\rangle$. Once the driving field is added, it brings the oscillations from $|a_1\rangle$ and $|a_2\rangle$ to level $|c\rangle$. Note that the two Rabi oscillations have the same phase. Meanwhile, they also show interference through the dynamic energy shifts. Since the driving field establishes a channel to reach state $|c\rangle$, we also observe a population in state $|c\rangle$; see figure 3.2(b). As the driving field is increased,

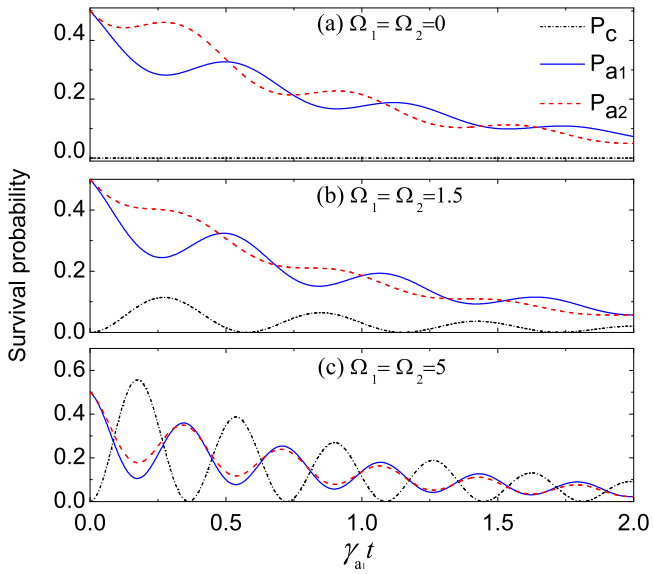


Figure 3.2: Evolution of the population with $a_1(0) = a_2(0) = 1/\sqrt{2}$. The parameters are $\omega_{a_1 b} = 10^4 \gamma_{a_1}$, $\Delta_1 = -\Delta_2 = 5\gamma_{a_1}$, and $\gamma_{a_2} = \gamma_{a_1}$. The driving fields are (a) $\Omega_1 = \Omega_2 = 0$, (b) $\Omega_1 = \Omega_2 = 1.5\gamma_{a_1}$, and (c) $\Omega_1 = \Omega_2 = 5\gamma_{a_1}$.

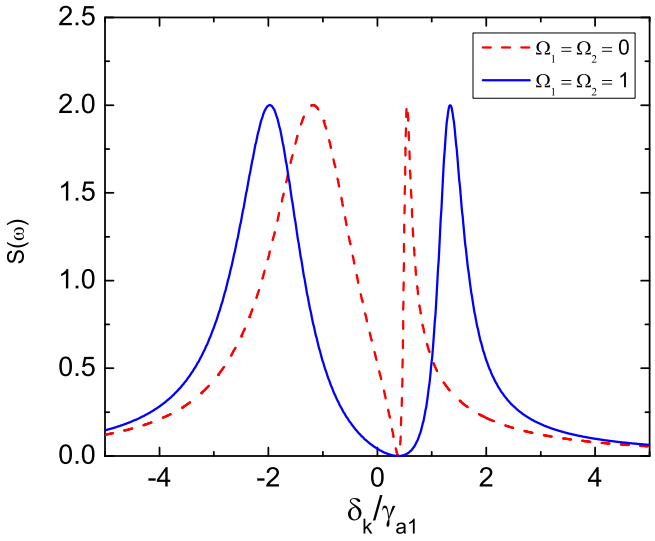


Figure 3.3: Spontaneous emission spectrum for $a_1(0) = a_2(0) = 1/\sqrt{2}$. The parameters are $\omega_{a_1 b} = 10^4 \gamma_{a_1}$ and $\omega_{12} = \gamma_{a_2} = \gamma_{a_1}$. Red dashed line, $\Omega_1 = \Omega_2 = 0$; blue solid line, $\Omega_1 = \Omega_2 = \gamma_{a_1}$.

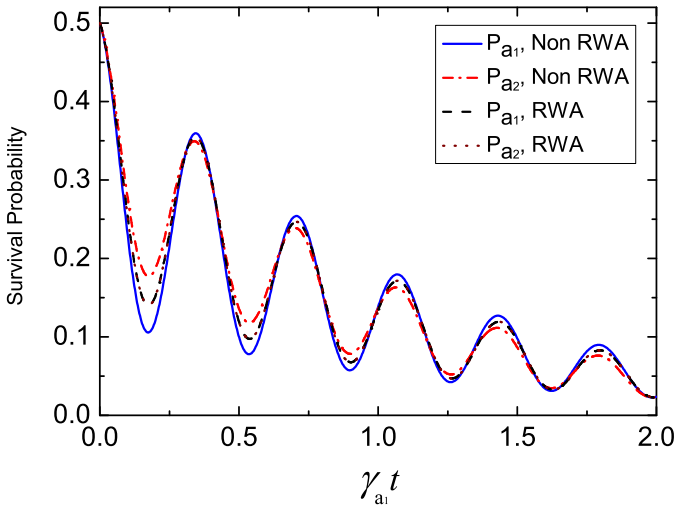


Figure 3.4: Evolution of the population in the upper levels for $a_1(0) = a_2(0) = 1/\sqrt{2}$. The parameters are $\omega_{a_1 b} = 10^4 \gamma_{a_1}$, $\Delta_1 = -\Delta_2 = 5\gamma_{a_1}$, $\Omega_1 = \Omega_2 = 5\gamma_{a_1}$, and $\gamma_{a_2} = \gamma_{a_1}$.

the population evolution pattern is mainly determined by oscillations from $|a_1\rangle$ to $|c\rangle$ and $|a_2\rangle$ to $|c\rangle$ with oscillation between $|a_1\rangle$ and $|a_2\rangle$ because the energy shifts are small perturbations; see figure 3.2(c). The spectrum is reshaped, as shown in figure 3.3.

As we expect, the model also provides us a test for the effect of counter-rotating terms at the time scale of the spontaneous emission [98]. In figure 3.4 we depict the population evolution of $a_1$ and $a_2$ for the cases with and without the energy shifts. We find that the counter-rotating terms play a significant role at the time scale of $1/\gamma_{a_1}$. Here although the trapping conditions equations (3.14) and (3.33) hold with the parameters chosen in figure 3.4, there is no population trapped in the upper levels. This is because the initial state $(1/\sqrt{2})(|a_1\rangle + |a_2\rangle)$ is orthogonal to the dressed state $|0\rangle$. The spectrum is also influenced. In figure 3.5, we show

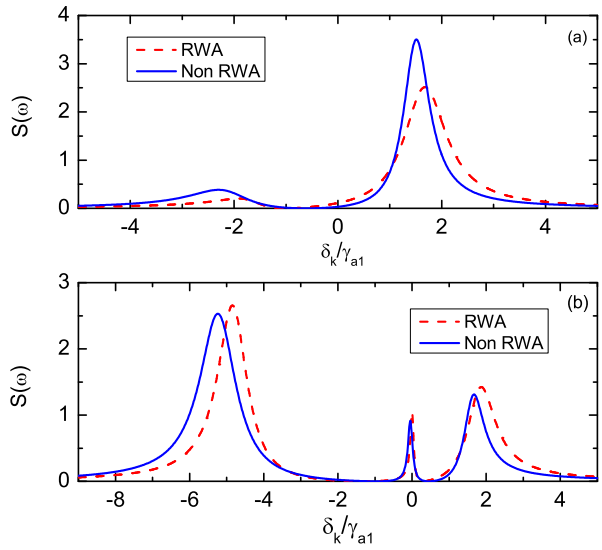


Figure 3.5: Spontaneous emission spectrum. The parameters are $\omega_{a_1 b} = 10^4 \gamma_{a_1}$, (a) $\Omega_1 = \Omega_2 = \Delta_1 = -\Delta_2 = \gamma_{a_2} = \gamma_{a_1}$, (b) $\Omega_1 = \Delta_1 = \gamma_{a_2} = \gamma_{a_1}$, $\Delta_2 = -4\gamma_{a_1}$, $\Omega_2 = 2\gamma_{a_1}$. The atom is initially in level $|a_1\rangle$ for (a) and $(1/\sqrt{2})(|a_1\rangle + |a_2\rangle)$ for (b).

the spectrum of the emitted photon with the atom initially prepared in state $a_1$. In figure 3.5(a), the trapping conditions equations (3.14) and (3.33) are fulfilled, and we observe elimination of the spontaneous emission for the center peak. In figure 3.5(b), the trapping condition equation (3.33) is not satisfied, and the center peak remains there. For both cases, we observe differences between the RWA and non-RWA results. One has to note that the differences are due only to the dynamic energy shifts, as the effects of non-dynamic shifts were removed when we defined $\delta_k = \omega_k - \omega'_{b0}$.

The most interesting feature of this four-level driving system is that the effect of the dynamic shift can be captured even if the transition matrices between the two upper levels $a_1$, $a_2$ and the ground level $b$ are orthogonal. In the previous study of a V-type three level system, it has been shown that the virtual photon process between the two upper levels through the ground level can induce the dynamic energy shift.

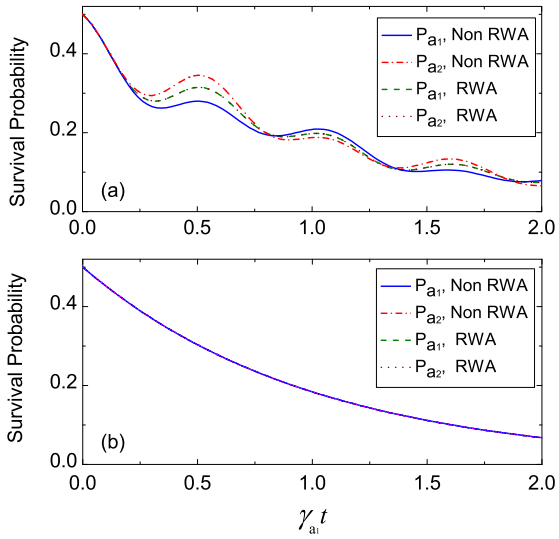


Figure 3.6: Evolution of the population in the upper levels when the two dipoles are orthogonal. The initial state is $(1/\sqrt{2})(|a_1\rangle+|a_2\rangle)$. The parameters are $\omega_{a_1 b} = 10^4\gamma_{a_1}$, $\Delta_1 = -\Delta_2 = 5\gamma_{a_1}$, $\gamma_{a_2} = \gamma_{a_1}$. The driving fields are (a) $\Omega_1 = \Omega_2 = 2\gamma_{a_1}$ and (b) $\Omega_1 = \Omega_2 = 0$.

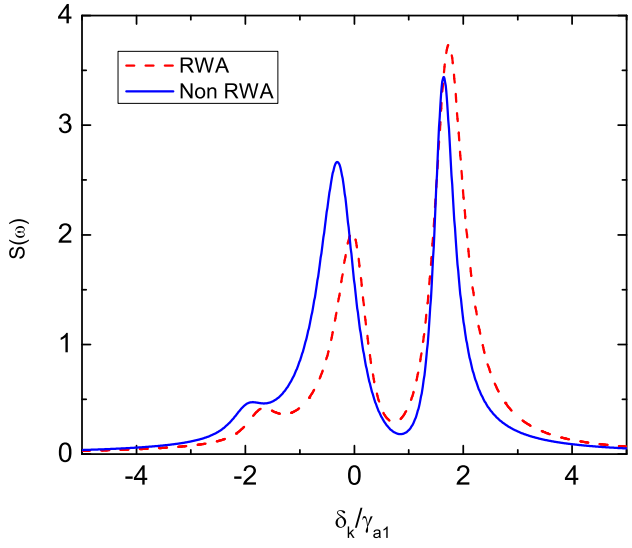


Figure 3.7: Spontaneous emission spectrum when the two dipoles are orthogonal. The parameters are $\omega_{a_1 b} = 10^4\gamma_{a_1}$, $\Omega_1 = \Omega_2 = \Delta_1 = -\Delta_2 = \gamma_{a_2} = \gamma_{a_1}$. The atom is initially in level $|a_1\rangle$.

This shift influences the spectrum of the spontaneous emission from the upper levels. However, this process requires two non-orthogonal transition matrices between the upper levels and the lower level, see figure 3.6(b). If the two dipoles are orthogonal, the virtual-photon processes $a_1 \rightarrow b \rightarrow a_2$ can not happen. So the energy shifts do not exist. In contrast to this scenario, the dynamic energy shifts still survive in our model. This is because the virtual-photon processes $a_1 \rightarrow b \rightarrow a_1$ and $a_2 \rightarrow b \rightarrow a_2$ can introduce couplings between the three dressed upper levels. Therefore, the dynamic energy shifts are non-zero even if the two original transition matrices $\vec{p}_{a_1 b}$ and $\vec{p}_{a_2 b}$ are orthogonal. See figure 3.6(a) for the population in the upper levels and figure 3.7 for the spectrum.

### *3.3.4 Experiment proposal*

Now let us discuss the possible experimental realization of our scheme. We choose $^{87}$Rb to realize our four-level atomic diagram. We first consider the case with parallel dipoles. As in the level diagram proposed in Ref. [98], the levels $|5P_{3/2}, F = 2, m_F = 0\rangle$ and $|5P_{3/2}, F = 1, m_F = 0\rangle$ of $^{87}$Rb can be chosen as the two upper levels $|a_1\rangle$ and $|a_2\rangle$. The $5S_{1/2}$ states can be regarded as the ground state $|b\rangle$. As the lifetime of the $5D$ levels is much longer than that of the $5P$ levels, we can choose $|5D_{3/2}, F = 2, m_F = 1\rangle$ as level $|c\rangle$ and neglect its spontaneous emission. For the case to two orthogonal dipoles, the upper levels $|a_1\rangle$ and $|a_2\rangle$, the lower level $|c\rangle$ and the ground state $|b\rangle$ can be chosen as $|a_1\rangle = |5P_{3/2}, F = 1, m_F = 0\rangle$, $|a_2\rangle = |5P_{3/2}, F = 1, m_F = 1\rangle$, $|c\rangle = |5S_{1/2}, F = 2, m_F = 1\rangle$, and $|b\rangle = |5S_{1/2}, F = 1, m_F = 1\rangle$, respectively. With the selected states, the electric dipole transitions between the two upper levels $a_1$ and $a_2$ and the lower level $c$ are much weaker than the transitions between the two upper levels $a_1$ and $a_2$ and the ground state $b$. Therefore, the spontaneous emissions from states $a_1$ and $a_2$ to state $c$ can be neglected. We can use the Zeeman effect to

select the spectrum corresponding to the relevant transitions. In order to eliminate the Doppler broadening, cold atoms in a magneto-optical trap would be required.

### *3.3.5 Summary*

We studied the quantum interference resulting from energy shifts and its influence on the decay rates and emission spectrum of a four-level atomic system. The effects of counter-rotating terms and the self-energy are included in the dynamic evolution equations by a unitary transformation method. We show that the counter-rotating terms, which are normally neglected in the usual investigation of atomic systems, do produce a significant influence on the evolution of the atomic amplitudes and the emission spectrum. In contrast to the three-level scheme [98], here the effect of counter-rotating terms can be observed in the time scale of the decay rate even when the dipole moments of the two upper levels are orthogonal to each other.

## 3.4 Effect of counter-rotating terms on the spontaneous emission in an anisotropic photonic crystal

### *3.4.1 Motivation*

Various photonic crystal models have been investigated theoretically [92, 96, 99, 100, 101, 102, 103] and experimentally [104, 105, 106]. Among these models is the study of spontaneous emission of a two level atom within a three-dimensional anisotropic photonic crystal under the RWA [92]. The properties of the radiation field, in such photonic crystal, depend on the relative position of the atomic transition frequency and the band edge of the photonic crystal. It is shown that there exist two characteristic atomic transition frequencies. Here one can see three different and distinct regions; (a) above these two frequencies, the emission is purely a propagating wave, (b) a localized field below them, (c) while it is a purely diffusion field between the two frequencies. Clearly, there is no coexistence of localized and propagating

fields. This remark is quite different when it comes to the one-dimensional photonic crystals as they have different density of states [94, 95, 96, 97, 107]. For an anisotropic band gap structure, the density of state is proportional to $(\omega_k - \omega_c)^{1/2}$. In contrast, it is proportional to $(\omega_k - \omega_c)^{-1/2}$ for an isotropic band gap structure and leads to a singularity at the band edge.

Here we not only study the usual spontaneous emission of a two level atom that is embedded in a three-dimensional anisotropic photonic crystal but also considering the with the full counter-rotating terms. The behavior of the emission is similar to the RWA case, i.e., the localized and propagating fields are also separated by two characteristic atomic transition frequencies. However, this two characteristic frequencies are shifted due to the full Lamb shift which is obtained without making RWA.

### *3.4.2 Model and calculation*

We consider a two-level atom coupled to the radiation field in an anisotropic photonic crystal. The excited and ground energy levels of the atom are label as $|1\rangle$ and $|0\rangle$ respectively. The band edge frequency $\omega_c$ of the photonic crystal is chosen to be near the atomic transition frequency $\omega_1$. Without making the RWA, the full Hamiltonian of the system is

$$\hat{H} = \hbar\omega_1|1\rangle\langle 1| + \sum_k \hbar\omega_k b_k^\dagger b_k + \hbar\sum_k g_k(b_k^\dagger + b_k)(|0\rangle\langle 1| + |1\rangle\langle 0|)\,, \quad (3.37)$$

After employing the unitary transformation method, the transformed Hamiltonian takes the form

$$\hat{H} = \hbar(\omega_1 + \Delta\omega_{\rm ndy}^{(1)})|1\rangle\langle 1| + \Delta\omega_{\rm ndy}^{(0)}|0\rangle\langle 0| + \sum_k \hbar\omega_k b_k^\dagger b_k$$

$$+\hbar \sum_k V_k (b_k^\dagger |0\rangle\langle 1| + b_k |1\rangle\langle 0|)\,, \tag{3.38}$$

where the non-dynamic energy shifts are

$$\Delta\omega_{\rm ndy}^{(1)} = \sum_k \frac{g_k^2}{\omega_k} \frac{\omega_1(\omega_1 - \omega_k)}{(\omega_k + \omega_1)^2}\,, \tag{3.39a}$$

$$\Delta\omega_{\rm ndy}^{(0)} = \sum_k \frac{g_k^2}{\omega_k} \frac{\omega_1(\omega_1 + \omega_k)}{(\omega_k + \omega_1)^2}\,, \tag{3.39b}$$

and

$$V_k = \frac{2\omega_1 g_k}{\omega_k + \omega_1}\,. \tag{3.40}$$

Here we have removed the self-energy of the free electron due to the vacuum fluctuations in the non-dynamic shifts.

The dispersion relation in an anisotropic photonic crystal is modified by the periodic dielectric structure. An anisotropic band gap structure is formed on the surface of the the first Brillouin zone of the reciprocal lattice space. The band edge is associated with several symmetry-related points $\mathbf{k}_0^i$. Near each $\mathbf{k}_0^i$, the dispersion relation can be approximated as

$$\omega_k = \omega_c + A|\mathbf{k} - \mathbf{k}_0^i|^2\,. \tag{3.41}$$

The atom is assumed to be initially in the excited state $|1\rangle$ and the radiation field is in the vacuum state. The state vector of the system at an arbitrary time $t$ is

$$|\psi(t)\rangle \;=\; A(t)e^{-i(\omega_1 + \Delta\omega_{\rm ndy}^{(1)})t}|1, \{0\}\rangle + \sum_k B_k(t) e^{-i(\omega_k + \Delta\omega_{\rm ndy}^{(0)})t}|0, \{1_k\}\rangle\,. \tag{3.42}$$

From the Schrödinger equation, we obtain the the following differential equations for

the amplitudes $A(t)$ and $B_k(t)$,

$$\frac{\partial}{\partial t}A(t) = -\sum_k V_k e^{-i(\omega_k-\omega_1')t}B_k(t)\,, \tag{3.43a}$$

$$\frac{\partial}{\partial t}B_k(t) = V_k e^{i(\omega_k-\omega_1')t}A(t)\,. \tag{3.43b}$$

Here $\omega_1' = \omega_1 + \Delta\omega_{\rm ndy}^{(1)} - \Delta\omega_{\rm ndy}^{(0)}$ is the shifted atomic transition frequency.

After making the Laplace transform, we obtain the Laplace transform $\tilde{A}(p)$ for the amplitude $A(t)$,

$$\tilde{A}(p) = (p+\Gamma)^{-1}\,, \tag{3.44}$$

with

$$\begin{aligned}\Gamma &= \sum_k \frac{V_k^2}{p+i(\omega_k-\omega_1')} \\ &= \frac{(\omega_1 d_1)^2}{16\pi^3\epsilon_0\hbar}\int d\mathbf{k}\frac{1}{\omega_k[p+i(\omega_k-\omega_1')]}\Big(\frac{2\omega_1}{\omega_1+\omega_k}\Big)^2\Big[1-\frac{(\mathbf{k}\cdot\mathbf{u}_d)^2}{k^2}\Big]\,.\end{aligned} \tag{3.45}$$

Here we convert the mode sum over the transverse plane wave into integral, i.e., $\sum_k \to [V/(2\pi)^3]\int d\mathbf{k}$. Due to the anisotropy, the integration over $\mathbf{k}$ has to be carried out around the direction of each $\mathbf{k}_0^j$. The angle between the atom dipole vector and the $\mathbf{k}_0^j$ is $\theta_j$. In addition, we can extend the integration over $\mathbf{k}$ to infinity since the frequencies far away form the band edge do not contribute significantly. Detailed calculation is given in Appendix: D.1. We then have

$$\begin{aligned}\Gamma &= -2i\beta^{3/2}\omega_1^2\left[\sqrt{\omega_c}+2\sqrt{\omega_1+\omega_c}+\sqrt{-ip-(\omega_1'-\omega_c)}\right]/\Big\{(\sqrt{\omega_c}+\sqrt{\omega_1+\omega_c})^2 \\ &\quad \left[\sqrt{\omega_1+\omega_c}\sqrt{\omega_c}+\sqrt{-ip-(\omega_1'-\omega_c)}\right]\left[\sqrt{\omega_1+\omega_c}+\sqrt{-ip-(\omega_1'-\omega_c)}\right]^2\Big\}^{-1}\,,\end{aligned} \tag{3.46}$$

with $\beta^{3/2} = [(\omega_1 d_1)^2/8\pi\epsilon_0\hbar A^{3/2}]\sum_j \sin^2\theta_j$. Note here that, in order to ensure the integral in the above equation to be meaningful, the phase angle of $\sqrt{-ip-(\omega_1'-\omega_c)}$ has been defined within $(-\pi/2, \pi/2)$.

The amplitude $A(t)$ is given by the inverse Laplace transform,

$$A(t) = \frac{1}{2\pi i}\int_{\sigma-i\infty}^{\sigma+i\infty} A(p)e^{pt}dp = \frac{1}{2\pi i}\int_{\sigma-i\infty}^{\sigma+i\infty}\frac{e^{pt}}{p+\Gamma}dp\,, \tag{3.47}$$

where the real number $\sigma$ is chosen so that all the singularities of the function $A(s)$ lies to the left of the line $s=\sigma$ in the Bromwich integral.

Following the residue theorem, we have

$$\begin{aligned} A(t) &= \sum_j \frac{e^{x_j^{(1)}t}}{F'(x_j^{(1)})} + \sum_j \frac{e^{x_j^{(2)}t}}{G'(x_j^{(2)})} \\ &+\frac{1}{2\pi i}\int_{\omega_{1c}'-\infty}^{\omega_{1c}'+0} \frac{e^{xt}}{x - \frac{i\beta^{3/2}\cdot 2\omega_1^2(\sqrt{\omega_c}+2\sqrt{\omega_1+\omega_c}-i\sqrt{x+(\omega_1'-\omega_c)})}{\sqrt{\omega_1+\omega_c}(\sqrt{\omega_c}+\sqrt{\omega_1+\omega_c})^2\cdot(\sqrt{\omega_c}-i\sqrt{ix+(\omega_1'-\omega_c)})(\sqrt{\omega_1+\omega_c}-i\sqrt{ix+(\omega_1'-\omega_c)})^2}}dx \\ &-\frac{1}{2\pi i}\int_{\omega_{1c}'-\infty}^{\omega_{1c}'+0} \frac{e^{xt}}{x - \frac{i\beta^{3/2}\cdot 2\omega_1^2(\sqrt{\omega_c}+2\sqrt{\omega_1+\omega_c}+\sqrt{-ix-(\omega_1'-\omega_c)})}{\sqrt{\omega_1+\omega_c}(\sqrt{\omega_c}+\sqrt{\omega_1+\omega_c})^2\cdot(\sqrt{\omega_c}+\sqrt{-ix-(\omega_1'-\omega_c)})(\sqrt{\omega_1+\omega_c}+\sqrt{-ix-(\omega_1'-\omega_c)})^2}}dx\,. \end{aligned} \tag{3.48}$$

The details of the calculation are given in Appendix D.2. Here the functions $F(x)$ and $G(x)$ are defined in equations (D.4) and (D.6), where $x_j^{(1)}$ are the root of the equation $F(x)=0$ in the region $[Re(x)>0$ or $Im(x)>\omega_{ic}']$ as shown in figure D.1(a), and $x_j^{(2)}$ are the root of equation $G(x)=0$ in the region $[Im(x)<\omega_{ic}'$ and $Re(x)<0]$ as shown in figure D.1(b).

With the solved atomic amplitudes, the emitted field $\mathbf{E}(\mathbf{r},t)$ can be calculated as

$$\mathbf{E}(\mathbf{r},t) = \frac{\omega_1 d_1}{16\pi^3\epsilon_0}\mathbf{E}_0(\mathbf{r},t)\int e^{-i(\omega_{\mathbf{q}}t-\mathbf{q}\cdot\mathbf{r})}\left[\int_0^t A(t)e^{i(\omega_{\mathbf{q}}-\omega_1)t'}dt'\right]d\mathbf{q}\,, \quad (3.49)$$

where $\mathbf{E}_0(\mathbf{r},t)=\sum_i e^{i\mathbf{k}_0^i\cdot\mathbf{r}}[\mathbf{u}_1-\mathbf{k}_0^i(\mathbf{k}_0^i\cdot\mathbf{u}_1)/(k_0^i)^2]$.

### *3.4.3 Results*

#### *3.4.3.1 Emitted field*

As expected from equation (3.48), the dynamical properties of the emitted field is strongly related to the roots $x_j^{(1)}$ and $x_j^{(2)}$. We can find from equations (D.4) and (D.6) that the properties of these roots depend on the relative positions of the upper level of the atom and the band edge. Numerical studies reveal that there exists two characteristic frequencies of the relative positions $\Omega_1$ and $\Omega_2$ ($\Omega_1<\Omega_2$). In region I ($\omega_1<\Omega_1$), only one purely imaginary root $x^{(1)}$ exists for $F(x)=0$ in the contoured area as shown in figure D.1(a) while there is no root $x^{(2)}$ for $G(x)=0$ in the contoured area as shown in figure D.1(b). In region II ($\Omega_1\le\omega_1\le\Omega_2$), there is no root for both $x^{(1)}$ and $x^{(2)}$ in the defined contoured areas. In region III ($\omega_1>\Omega_2$), there is no root for $x^{(1)}$ while one and only one complex root with a negative real part exists for $x^{(2)}$. The properties of the roots are the same as in the case when RWA is made. Therefore, upon substituting equation (3.48) into equation (3.49) and following the discussion in Ref. [92], we can write the radiation field as the sum of three parts

$$\mathbf{E}(\mathbf{r},t) = \mathbf{E}_l(\mathbf{r},t)+\mathbf{E}_p(\mathbf{r},t)+\mathbf{E}_d(\mathbf{r},t)\,. \quad (3.50)$$

Here $\mathbf{E}_l(\mathbf{r},t)$ comes from the purely imaginary root for $x^{(1)}$. Thus it is a localized field which exists only if $\omega_1<\Omega_1$. The complex root with a negative real part for $x^{(2)}$ results in a propagating field as denoted by $\mathbf{E}_p(\mathbf{r},t)$. It exists only if $\omega_1>\Omega_2$. So

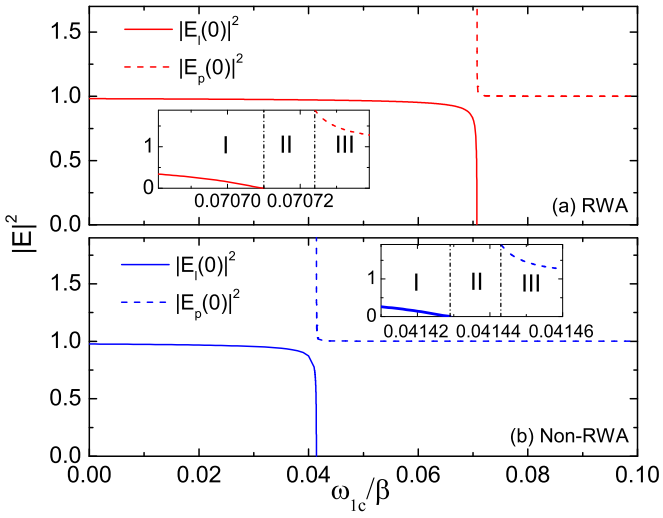


Figure 3.8: The squared amplitude of the localized mode and the propagating mode as function of detuning of resonant frequency from photonic band edge $\omega_1 c$ with $\omega_c = 200\beta$. The top figure corresponds to the case with RWA. The bottom figure corresponds to the case without making RWA. The three ranges I, II and III correspond to the localized modes, diffusion modes and propagating modes, respectively

the localized field and propagating field can not coexist. The diffusion field $\mathbf{E}_d(\mathbf{r}, t)$ comes from the third and fourth terms in equation (3.48). Note that although the behavior of the radiation field is the same as the case when RWA is assumed, the positions of the two characteristic frequencies $\Omega_1$ and $\Omega_2$ are different. Therefore, the regions of the localized, diffusion and propagating field are shifted, as shown in figure 3.8, which will be explained later.

### *3.4.3.2 Population in the upper level*

The evolution of the population in the excited state is

$$P(t) = |A(t)|^2 . \tag{3.51}$$

As discussed in Ref. [92], the propagating and localized field can not coexist in the anisotropic crystal, and the diffusion field is negligibly small when propagating or localized field exists. Therefore, there is no interference and the population in the upper level has no quasi-oscillation. If the emission is a localized field, it dresses the atoms to form a dressed state and leads to a fractionalized steady-state population in the upper level. If only the diffusion field exists, the upper level decays in the manner of a power law. However, if we have only the propagating field, the upper-level population decays exponentially. As shown in figure 3.8, if we take into account the effect of the counter-rotating terms, the regions of the localized, diffusion and propagating fields are shifted with respect to the detuning $\omega_{1c}$.

We, therefore, expect a different behavior for the population in the upper level. When $\omega_{1c} = 0.041436\beta$, the detuning lies in region I in figure 3.8(a) while it lies in region II in figure 3.8(b). So if we include the counter-rotating terms in the Hamiltonian, only diffusion field exists, while RWA predicts a localized field. Consequently, the population in the upper level goes to a constant under RWA, while non-RWA term leads to a power law decay, see figure 3.9(a). When $\omega_{1c} = 0.055\beta$, the detuning lies in region I in figure 3.8(a) while lies in region III in figure 3.8(b). Therefore, the emission is localized if we make RWA, while non-RWA terms predict a propagating field. Therefore the population shows different behaviors: nondecaying under RWA and exponentially decaying if RWA is not made, see figure 3.9(b). When $\omega_{1c} = 0.07072\beta$, the detuning lies in region II in figure 3.8(a) while lies in region III in figure 3.8(b). We expect a diffusion field under RWA and a propagating field without RWA. Correspondingly, the population in the upper level decays polynomially under RWA and exponentially without RWA, see figure 3.9(c).

When time goes to infinity the population in the upper-level can survive only if the emission is a localized field. The steady state atomic population can be obtained

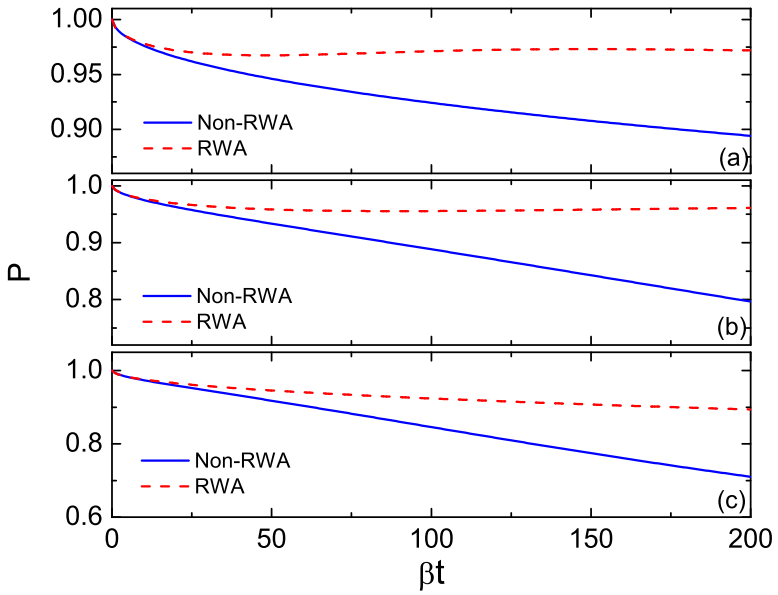


Figure 3.9: The time evolution of the upper-level population with $\omega_c = 200\beta$. figure (a) $\omega_{1c} = 0.041436\beta$, (b) $\omega_{1c} = 0.055\beta$, and (c) $\omega_{1c} = 0.07072\beta$, respectively.

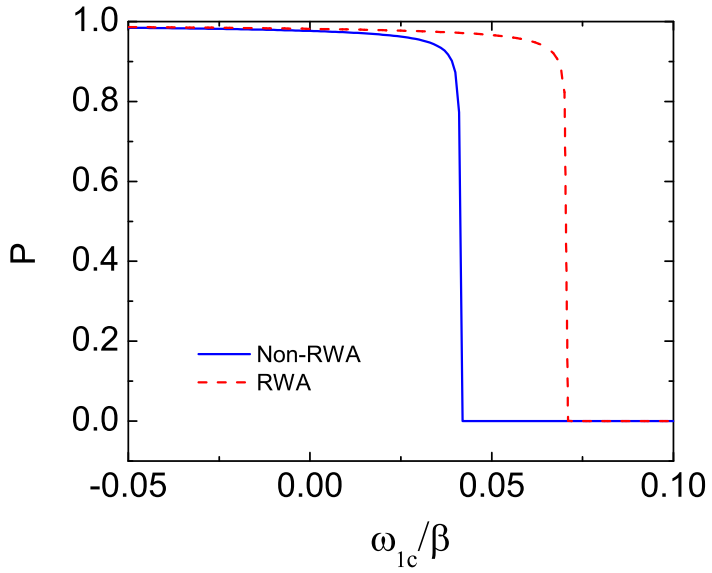


Figure 3.10: The steady-state atomic population in the upper level with respect to the detuning with $\omega_c = 200\beta$.

as

$$P_{\text{steady}} = \left| \frac{1}{F'(x^{(1)})} \right|^2 . \tag{3.52}$$

We expect, from figure 3.8, that there is a shift of the steady-state population with respect to the detuning $\omega_{1c}$ if we consider the effect of the counter-rotating terms, see figure 3.10.

#### *3.4.3.3 Lamb shift*

From the dispersion relation equation (3.41), the density of the field modes is 0 for $\omega_k < \omega_c$. So a naive guess is that $\omega_1 = \omega_c$ is a characteristic point for the behavior of the emission field. If $\omega_1 < \omega_c$, the field should be localized. When $\omega_1 > \omega_c$, the localized field disappears.

However, the strong interaction between the atom and the field shifts the atomic energy levels. When RWA is made, the second order perturbation energy shift is

$$\Delta E_{\text{RWA}} = \sum_k \frac{|\langle 0, \{1_k\}|H_I^{\text{RWA}}|1, \{0\}\rangle|^2}{\hbar(\omega_1 - \omega_k)} = \sum_k \frac{\hbar g_k^2}{\omega_1 - \omega_k} . \tag{3.53}$$

When $\omega_1 = \omega_c = 200\beta$, and substitute for $\omega_k$ from the dispersion relation equation (3.41), we obtain this shift $\Delta E_{\text{RWA}} = -0.0707\hbar\beta$. This shift pushes down the actual transition frequency by an amount of $0.0707\beta$ (See Appendix: D.3 for detailed calculations). Therefore, the field is still localized even if the atomic transition frequency lies above the band edge of the photonic crystal until $\omega_{1c}$ exceeds $0.0707\beta$.

However, this energy shift obtained under RWA is not the whole Lamb shift, because it does not include the shift from the counter-rotating terms. When the counter-rotating terms are included in the Hamiltonian, the transformed Hamiltonian contains non-dynamic energy shifts. In addition, the interaction constant is rescaled

and the interaction Hamiltonian is $H_I = \hbar \sum_k V_k(b_k^\dagger|0\rangle\langle 1| + b_k|1\rangle\langle 0|)$. In this case, the total Lamb shift is given by [47, 98]

$$\begin{aligned} E_{\text{Lamb}} &= \Delta E_{\text{ndy}} + \Delta E_{\text{dyn}} \\ &= \hbar(\Delta\omega_{\text{ndy}}^{(1)} - \Delta\omega_{\text{ndy}}^{(0)}) + \sum_k \frac{|\langle 0, \{1_k\}|H_I|1, \{0\}\rangle|^2}{\hbar(\omega_1 - \omega_k)} \\ &= \sum_k \frac{2\hbar g_k^2 \omega_1}{\omega_1^2 - \omega_k^2}\,. \end{aligned} \tag{3.54}$$

The shift is $\Delta E_{\text{Lamb}} = -0.0414\hbar\beta$. The frequency difference between the atomic transition and the gap edge $\omega_{1c} \approx 0.0414\beta$, which coincides with figure 3.8(b), is a characteristic frequency for the behavior of the emission field. The Lamb shift due to the strong virtual atom-photon interaction results in the peculiar fact that the radiation filed is still localized when the atomic frequency is above the band edge of the photonic crystal until the amount of $0.0414\beta$. In the region $0.0414\beta < \omega_{1c} < 0.0707\beta$, the emission is a propagating mode, which would be a localized mode under RWA.

### *3.4.4 Summary*

We have studied the spontaneous emission of a two-level atom in an anisotropic photonic crystal without making RWA. Similar to the RWA case, there exists two characteristic transition frequencies. Below the two frequencies, the localized field exists while a propagating field shows up above the two frequencies. The localized radiation field exists even if the atomic transition frequency is above the band edge of the photonic crystal. And the localized field cannot coexist with the propagating field. In comparison with the RWA case, the two characteristic frequencies are shifted.

## 3.5 Control of Lamb shift by a driving field

### *3.5.1 Motivation*

Lamb shift is one of the most important quantum electrodynamics effects in atom physics and quantum optics [108]. The energy level shift in hydrogen due to the virtual photon processes measured first by Willis Lamb stimulated the study of the renormalized quantum field theory and confirmed the existence of the quantum vacuum. It was realized early through the work of Bethe [109] that most of the Lamb shift can be explained within the nonrelativistic quantum electrodynamics. There are a number of approaches to the calculation of the Lamb shift. One such approach is due to Feynman [110] and is beautifully reviewed by Milonni [111]. In this approach, it is argued that the presence of an atom inside a box leads to a change of the resonant frequencies from $\omega_k$ to $\omega_k/n(\omega_k)$ where $n(\omega_k)$ is the refractive index at $\omega_k$. This leads to a change of the zero point energy due to the presence of the atom and the calculated change of the energy corresponds to the Lamb shift.

This motivates us to consider a situation where the refractive index $n(\omega_k)$ can be controlled by an external driving field and hence we can coherently control the Lamb shift. Such a situation can for example be realized in a coherently driven system such as in electromagnetically induced transparency [112, 113]. Coherent atomic effects is a hot area of research in quantum optics and have led to a number of interesting and counterintuitive phenomena, such as correlated emission laser [114, 115], lasing without inversion [11, 12, 116] and suppression of atomic decay by spontaneous emission [14].

Here we consider a system where a coherently driven atom can lead to a coherently controlled Lamb shift. It is well known that in order to get the correct Lamb shift we have to include the effect of counter-rotating terms in the interaction

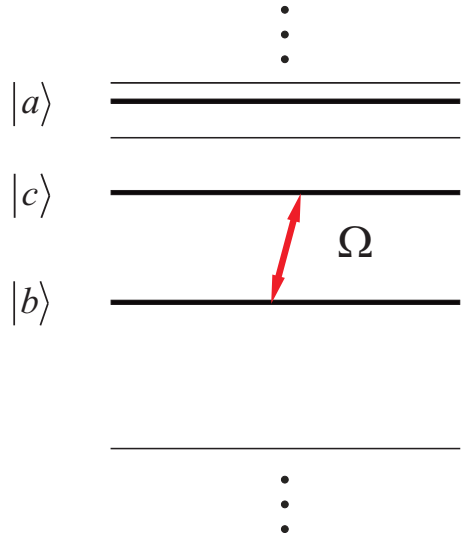


Figure 3.11: The atom configuration.

Hamiltonian between the atom and the electromagnetic vacuum field. In the regular approach of dealing with the quantum interference phenomenon rotating wave approximation(RWA) is often made. We apply the unitary transformation method to a laser driven atomic system and show how the Lamb shift can be affected by the quantum interference between the two-photon channel of the original energy levels and the new channels opened by the pumping laser. This sheds light on the feasibility of coherently controlled Lamb shift by an extra driving laser.

### *3.5.2 Level shifts in a coherently driven atom*

We consider a muti-level atom interacting with the electromagnetic (EM) vacuum field as well as an extra laser field. As shown in figure 3.11, the levels $|b\rangle$ and $|c\rangle$ are coupled via a coherent driving field and we are mainly interested in the Lamb shift of level $|a\rangle$. The two electric dipole allowed transitions within these three levels are $a \leftrightarrow b$ and $c \leftrightarrow b$, but the transition between $|a\rangle$ and $|c\rangle$ is considered to be dipole forbidden due to the selection rules. We suppose here that $E_b < E_c$, and the

transition matrix $\mathbf{p}_{ab}$ and $\mathbf{p}_{bc}$ are perpendicular to each other. This is not difficult to choose in real system. For example, in hydrogen atom, if we label the energy levels as $(n, l, m)$, with $n$ being the principal quantum number, $l$ being the orbital quantum number and $m$ being the magnetic quantum number, we can select $|a\rangle$, $|b\rangle$, and $|c\rangle$ to be $(2, 1, 1)$, $(1, 0, 0)$ and $(2, 1, -1)$ states, respectively. The laser field $\mathbf{A}_L(\mathbf{r}, t) = \mathbf{A}_D(\mathbf{r}) \exp(-i\omega_D t)$ is chosen to be parallel to $\mathbf{p}_{bc}$ and is almost resonant with the $|b\rangle$ and $|c\rangle$ transition, but with large detuning with respect to other levels. So it is reasonable to suppose that the laser couples only levels $|b\rangle$ and $|c\rangle$. With the Rabi frequency associated with the driving field defined as $\Omega = \mathbf{A}_D(\mathbf{r}) \cdot \mathbf{p}_{bc}$, the total Hamiltonian of the atom, the vacuum field and the driving field is given as follows:

$$\begin{aligned} H &= E_a|a\rangle\langle a| + E_b|b\rangle\langle b| + E_c|c\rangle\langle c| + \sum_{i\neq a,b,c} E_i|i\rangle\langle i| + \sum_k \hbar\omega_k b_k^\dagger b_k \\ &+\hbar\Omega\big[\exp(i\omega_D t)|b\rangle\langle c| + |c\rangle\langle b|\exp(-i\omega_D t)\big] \\ &+ \sum_k \hbar g_{k,cb}\big(b_k^\dagger + b_k\big)\big(|b\rangle\langle c| + |c\rangle\langle b|\big) + \sum_k \hbar g_{k,ab}\big(b_k^\dagger + b_k\big)\big(|a\rangle\langle b| + |b\rangle\langle a|\big) \\ &+ \sum_{n=a,b,c}\sum_{i\neq a,b,c}\sum_k \hbar g_{k,ni}\big(b_k^\dagger + b_k\big)\big(|n\rangle\langle i| + |i\rangle\langle n|\big) \\ &+ \sum_{i\neq a,b,c}\sum_{j\neq a,b,c}\sum_k \hbar g_{k,ij}\big(b_k^\dagger + b_k\big)\big(|i\rangle\langle j| + |j\rangle\langle i|\big)\,. \end{aligned} \tag{3.55}$$

Here $E_l$ is the energy for level $|l\rangle$, and $b_k^\dagger$ ($b_k$) is the creation (annihilation) operator of EM mode with frequency $\omega_k$ ($k$ including the polarization). Notice that we have made RWA for the driving field induced coupling with $|b\rangle$ and $|c\rangle$.

In the above Hamiltonian, we have divided all the energy levels into two groups: the three levels $\{|a\rangle, |b\rangle, |c\rangle\}$ and other levels labeled as $|i\rangle$. Since the coupling between the levels $|b\rangle$ and $|c\rangle$ is dominated by the strong coherent field and the transition $a \leftrightarrow c$ is forbidden, we can remove the terms in the fourth line (the interaction between $|b\rangle$ and $|c\rangle$ coupled to the vacuum field) and part of the sixth

line (the coupling between $|b\rangle(|c\rangle)$ and the other levels). In addition, as we are interested in the Lamb shift of the state $|a\rangle$, all terms in the last line (the coupling within other levels) can also been neglected. We also make a unitary transformation $U_0 = |a\rangle\langle a| + |b\rangle\langle b| + \exp(-i\omega_D t)|c\rangle\langle c|$ with $\omega_D = \omega_{cb} - \Delta$, where $\omega_{cb} = (E_c - E_b)/\hbar$ and $\Delta$ is the detuning. The resulting Hamiltonian is

$$\begin{aligned} H_{\text{eff}} &= E_a|a\rangle\langle a| + E_b|b\rangle\langle b| + (\hbar\Delta + E_b)\,|c\rangle\langle c| + \hbar\Omega\,(|b\rangle\langle c| + |c\rangle\langle b|) \\ &+ \sum_{i\neq a,b,c} E_i|i\rangle\langle i| + \sum_k \hbar\omega_k b_k^\dagger b_k + \sum_k \hbar g_{k,ab}\big(b_k^\dagger + b_k\big)\big(|a\rangle\langle b| + |b\rangle\langle a|\big) \\ &+ \sum_{i\neq a,b,c}\sum_k \hbar g_{k,ai}\big(b_k^\dagger + b_k\big)\big(|a\rangle\langle i| + |i\rangle\langle a|\big). \end{aligned} \tag{3.56}$$

The analysis can be considerably simplified if we diagonalize the subspace corresponding to the states $|b\rangle$ and $|c\rangle$. This yields the dressed states $|b'\rangle$ and $|c'\rangle$ with energies and the corresponding states given by

$$E_{b'} = E_b + \frac{\hbar}{2}\left(\Delta - \sqrt{\Delta^2 + 4\Omega^2}\right), \tag{3.57a}$$

$$E_{c'} = E_b + \frac{\hbar}{2}\left(\Delta + \sqrt{\Delta^2 + 4\Omega^2}\right), \tag{3.57b}$$

$$|b'\rangle = \begin{pmatrix} \cos\theta \\ -\sin\theta \end{pmatrix}, \quad |c'\rangle = \begin{pmatrix} \sin\theta \\ \cos\theta \end{pmatrix}, \tag{3.57c}$$

where

$$\cos\theta = \sqrt{\frac{\left(\Delta + \sqrt{\Delta^2 + 4\Omega^2}\right)^2}{\left(\Delta + \sqrt{\Delta^2 + 4\Omega^2}\right)^2 + 4\Omega^2}}. \tag{3.58}$$

In terms of the dressed states, the Hamiltonian equation (3.56) can be rewritten

as

$$
\begin{aligned}
H_{\text{eff}} = \;& H_0' + H_1', && \text{(3.59a)}\\
H_0' = \;& E_a|a\rangle\langle a| + E_{b'}|b'\rangle\langle b'| + E_{c'}|c'\rangle\langle c'| + \sum_{i\neq a,b',c'} E_i|i\rangle\langle i| + \sum_k \hbar\omega_k b_k^\dagger b_k, && \text{(3.59b)}\\
H_1' = \;& \sum_k \hbar g_{k,ab'}\left(b_k^\dagger + b_k\right)\left(|a\rangle\langle b'| + |b'\rangle\langle a|\right) + \sum_k \hbar g_{k,ac'}\left(b_k^\dagger + b_k\right)\left(|a\rangle\langle c'| + |c'\rangle\langle a|\right)\\
& + \sum_{i\neq a,b',c'}\sum_k \hbar g_{k,ai}\left(b_k^\dagger + b_k\right)\left(|a\rangle\langle i| + |i\rangle\langle a|\right), && \text{(3.59c)}
\end{aligned}
$$

where

$$
g_{k,ab'} = g_{k,ab}\cos\theta, \qquad g_{k,ac'} = g_{k,ab}\sin\theta. \tag{3.60}
$$

Performing the unitary transformation and subtracting the free-electron self-energy, the first order terms (of order $g_k$), are given by

$$
\begin{aligned}
H_1'' \;=\; & \sum_{E_\beta<E_a}\sum_k \frac{2g_{k,a\beta}\xi_{k,a\beta}}{\omega_k}(E_a - E_\beta)\left(|\beta\rangle\langle a|b_k^\dagger + |a\rangle\langle\beta|b_k\right)\\
& + \sum_{E_\beta>E_a}\sum_k \frac{2g_{k,a\beta}\xi_{k,a\beta}}{\omega_k}(E_\beta - E_a)\left(|a\rangle\langle\beta|b_k^\dagger + |\beta\rangle\langle a|b_k\right). \qquad \text{(3.61)}
\end{aligned}
$$

Here we choose the index $\beta$ to describe the atomic levels in the new dressed basis $\{a, b', c', ...\}$, and

$$
\xi_{k,a\beta} \;=\; \frac{\omega_k}{\omega_k + |E_a - E_\beta|/\hbar}. \tag{3.62}
$$

The second order terms are

$$
H_2'' - E_{\text{se}} \;=\; -\sum_{\beta\neq a}\sum_k \frac{\hbar g_{k,a\beta}^2}{\omega_k}\left(2\xi_{k,a\beta} - \xi_{k,a\beta}^2 - 1 - \frac{E_\beta - E_a}{\hbar\omega_k}\xi_{k,a\beta}^2\right)|a\rangle\langle a|
$$

$$-\sum_{\beta\neq a}\sum_{k}\frac{\hbar g_{k,a\beta}^2}{\omega_k}\left(2\xi_{k,a\beta}-\xi_{k,a\beta}^2-1-\xi_{k,a\beta}^2\frac{E_a-E_\beta}{\hbar\omega_k}\right)|\beta\rangle\langle\beta| \\ +V_{nd}\,. \tag{3.63}$$

where $V_{nd}$ contains the non-diagonal terms, $|a\rangle\langle\beta|$ ($\beta\neq a$) for the atom and $b_k^\dagger b_{k'}^\dagger$, $b_k b_{k'}$ $b_k^\dagger b_{k'}$ and $b_k b_{k'}^\dagger (k\neq k')$ for the EM field. Since we are interested in the energy and the decay rate of the single level, and the contribution of these non-diagonal terms would be at least third order in $g_k$ and can be neglected, we drop $V_{nd}$ in the following calculation.

The summation $\sum_k$ can be replaced by the integral:

$$\sum_k \frac{g_{k,a\beta}^2}{\omega_k}h(\omega_k)=\frac{2\alpha\mathbf{p}_{a\beta}^2}{3\pi(mc)^2}\int_0^\infty d\omega_k h(\omega_k), \tag{3.64}$$

where $h(\omega_k)$ is any function of $\omega_k$ and $\alpha$ is the fine structure constant. Summarizing over $k$, we have

$$\begin{aligned} H_2''-E_{\rm se} &= \frac{2\alpha}{3\pi(mc)^2}\left[\sum_{E_\beta<E_a}2\mathbf{p}_{a\beta}^2\hbar\omega_{a\beta}+\sum_{\beta\neq a}\mathbf{p}_{a\beta}^2(E_\beta-E_a)\ln\frac{\omega_c+\omega_{a\beta}}{\omega_{a\beta}}\right]|a\rangle\langle a| \\ &+\frac{2\alpha}{3\pi(mc)^2}\sum_{E_\beta>E_a}\left[2\mathbf{p}_{a\beta}^2\hbar\omega_{a\beta}+\mathbf{p}_{a\beta}^2(E_a-E_\beta)\ln\frac{\omega_c+\omega_{a\beta}}{\omega_{a\beta}}\right]|\beta\rangle\langle\beta| \\ &+\frac{2\alpha}{3\pi(mc)^2}\sum_{E_\beta<E_a}\mathbf{p}_{a\beta}^2(E_a-E_\beta)\ln\frac{\omega_c+\omega_{a\beta}}{\omega_{a\beta}}|\beta\rangle\langle\beta|, \end{aligned} \tag{3.65}$$

where $\omega_{a\beta}=|E_\beta-E_a|/\hbar>0$ is the transition frequency between levels $|a\rangle$ and $|\beta\rangle$. The transformed Hamiltonian can be written as $H_T=H_0''+H_1''$, where $H_0''=H_0'+H_2''-E_{\rm se}$ is the unperturbed part, and $H_1''$ in equation(13) represents the perturbation.

The second-order perturbed energy of level $a$ due to the transformed interaction

Hamiltonian $H_1''$ is

$$\begin{aligned}\Delta E_a^{(a)} &= \sum_\beta \sum_k \frac{|\langle \beta, 1_k | H_1'' | a, vac\rangle|^2}{E_a - E_\beta - \hbar\omega_k} = \sum_{E_\beta < E_a} \sum_k \frac{4\hbar g_{k,a\beta}^2 \xi_{k,a\beta}^2 \omega_{a\beta}^2}{\omega_k^2(\omega_{a\beta} - \omega_k)} \\ &\simeq -\frac{2\alpha}{3\pi(mc)^2} \sum_{E_\beta < E_a} 2\mathbf{p}_{a\beta}^2 \hbar\omega_{a\beta}\,, \end{aligned} \tag{3.66}$$

where $|a, vac\rangle$ corresponds to the atom in level $a$ and no photon, and the intermediate state $|\beta, 1_k\rangle$ corresponds to the atom in level $\beta$ and one photon in mode $k$. When summing over $k$, we simplify the result using the fact that the UV cutoff $\omega c \approx mc^2$ is much larger than the atomic level energy and get the second line.

Now the Lamb shift of level $a$ is given by

$$\begin{aligned} E_a^{\text{Lamb}} &= E_a'' - E_a + \Delta E_a^{(2)} = \frac{2\alpha}{3\pi(mc)^2} \sum_{\beta \neq a} \mathbf{p}_{a\beta}^2 (E_\beta - E_a) \ln \frac{\omega_c + \omega_{a\beta}}{\omega_{a\beta}} \\ &\simeq \frac{2\alpha}{3\pi(mc)^2} \sum_{\beta \neq a} \mathbf{p}_{a\beta}^2 (E_\beta - E_a) \ln \frac{\omega_c}{\omega_{a\beta}}\,. \end{aligned} \tag{3.67}$$

In the last step, we utilize the fact that $\omega_c \ll \omega_{a\beta}$.

It is clear from comparison of equation (3.67) with the Lamb shift without the driving field that the only difference between the two cases is that bases $b$ and $c$ are shifted to the dressed bases $b'$ and $c'$ when adding the driving laser. The Lamb shift is therefore changed accordingly, and the resulting change in the Lamb shift of level a due to the addition of the driving field is therefore given by

$$\begin{aligned} \Delta E_a^{\text{Lamb}} &= \frac{2\alpha}{3\pi(mc)^2} \left[ \mathbf{p}_{ab'}^2 (E_b' - E_a) \ln \frac{\omega_c}{|E_b' - E_a|} + \mathbf{p}_{ac'}^2 (E_c' - E_a) \ln \frac{\omega_c}{|E_c' - E_a|} \right] \\ &\quad - \frac{2\alpha}{3\pi(mc)^2} \mathbf{p}_{ab}^2 (E_b - E_a) \ln \frac{\omega_c}{|E_b - E_a|} \\ &= \chi \Big\{ \cos^2\theta \hbar \Big[ \omega_{ab} - \frac{1}{2}\big(\Delta - \sqrt{\Delta^2 + 4\Omega^2}\big) \Big] \ln \frac{\omega_{ab} - \frac{1}{2}\big(\Delta - \sqrt{\Delta^2 + 4\Omega^2}\big)}{\omega_{ab}} \end{aligned}$$

$$+\sin^2\theta\hbar\Big[\omega_{ab}-\frac{1}{2}\big(\Delta+\sqrt{\Delta^2+4\Omega^2}\big)\Big]\ln\frac{\omega_{ab}-\frac{1}{2}\big(\Delta+\sqrt{\Delta^2+4\Omega^2}\big)}{\omega_{ab}}\Big\}, \tag{3.68}$$

where $\chi = 2\alpha\mathbf{p}_{ab}^2/(3\pi m^2c^2)$. In the first line, the contribution proportional to $\mathbf{p}_{ac}^2$ is missing, as the coupling between level a and level c is dipole forbidden, $\mathbf{p}_{ac}^2 = 0$. This is the main result of this paper. Since this change of the Lamb shift depends on the Rabi frequency and the detuning of the driving filed (mainly the Rabi frequency, see figure 3.12), we can coherently control the Lamb shift by changing the laser field. In particular, for those levels which initially have a zero Lamb shift (for example the 2P state for hydrogen atom), we can produce a tunable Lamb shift. In the case of resonant driving field, $\Delta = 0$, we obtain $\cos^2\theta = 1/2$. The additional Lamb shift by the driving field is then

$$\Delta E_a^{\text{Lamb}} = \frac{1}{2}\chi\hbar\omega_{ab}\left[\left(1+\frac{\Omega}{\omega_{ab}}\right)\ln\left(1+\frac{\Omega}{\omega_{ab}}\right)+\left(1-\frac{\Omega}{\omega_{ab}}\right)\ln\left(1-\frac{\Omega}{\omega_{ab}}\right)\right]. \tag{3.69}$$

We note that in the above discussion, we do not make any assumption about the energy relation between $E_a$ and $E_b(E_c)$, since the Lamb shift is due to the processes of emission and reabsorption of the virtual vacuum photons between level $|a\rangle$ and any other possible levels as long as the dipole moment is nonzero.

Next we suppose that level $|b\rangle$ is the ground state of the atom and $E_a > E_c' > E_b'$. We study the influence on the decay rate of the level $|a\rangle$ of the driving filed. The total Hamiltonian is $H_T = H_0'' + H_1''$ and it is in the form of the RWA. There are two decay channels for the electron in level $|a\rangle$, i.e., $a \to b'$ and $a \to c'$. The effective

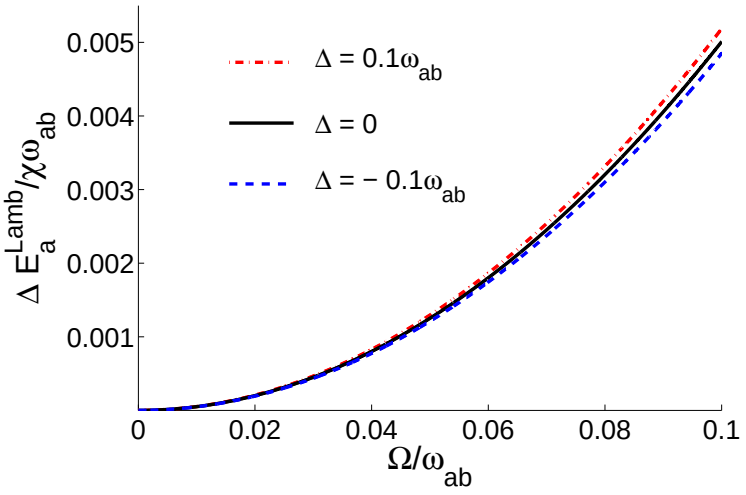


Figure 3.12: Additional Lamb shift by the driving field.

decay rate of the energy level $|a\rangle$ for a short time is [46]

$$\gamma(\tau) \;=\; 2\pi \int d\omega \Big[ G'_{ab'}(\omega) F(\omega - \omega_{ab'}, \tau) + G'_{ac'}(\omega) F(\omega - \omega_{ac'}, \tau) \Big], \qquad (3.70)$$

where

$$G'_{ai'}(\omega) = \frac{2\alpha}{3\pi (mc)^2} \frac{4\omega_{ai'}^2}{(\omega + \omega_{ai'})^2} \mathbf{p}_{ai'}^2 \omega, \qquad (3.71)$$

$$F(\omega - \omega_{ai'}, \tau) = 2 \frac{\sin^2[\frac{\omega - \omega_{ai'}}{2}\tau]}{\pi \tau (\omega - \omega_{ai'})^2}, \qquad (3.72)$$

with $i' = b', c'$. If there is no driving field, $\Omega = 0$, we have $\cos\theta = 1$. We then have $G'_{ac'} = 0$ and $\omega_{ab'} = \omega_{ab}$, and the decay rate goes back to the same form as in [46]. In the long time limit, $F(\omega - \omega_{ai'}, \tau) \to \delta(\omega - \omega_{ai'})$, the decay rate is given by

$$\gamma(\Delta, \Omega) = 2\pi \frac{2\alpha}{3\pi (mc)^2} \mathbf{p}_{ab}^2 (\cos^2\theta \omega_{ab'} + \sin^2\theta \omega_{ac'}). \qquad (3.73)$$

If the driving field is at resonance, $\cos^2\theta = 1/2$, $\omega_{ab'} = \omega_{ab} - \Omega$, $\omega_{ac'} = \omega_{ab} + \Omega$, and we obtain

$$\gamma(\Omega) = 2\pi \frac{2\alpha}{3\pi(mc)^2} \mathbf{p}_{ab}^2 \omega_{ab}. \tag{3.74}$$

In this case, the driving field has no effect on the decay rate. This coincides with the result in [117], where the RWA of the coupling between the atom and vacuum field is made at the beginning. This result can be understood from the observation that, in the long time limit, the counter-rotating terms have no influence on the decay.

As we mentioned in the introduction, this problem is motivated by Feynman's derivation of the Lamb shift. In this interpretation, a dilute gas with $N$ atoms per unit volume in a box of volume $V$ is considered [111]. Since the dimension of the box determines the allowed wavelengths in the box, the frequencies would be effected by the refractive index associated with the atomic gas, see figure 3.13. Thus the presence of the atomic gas changes the zero-point field energy by

$$\Delta E = \sum_{\mathbf{k}} \frac{1}{2} \frac{\hbar\omega_k}{n(\omega_k)} - \sum_{\mathbf{k}} \frac{1}{2}\hbar\omega_k \cong -\sum_{\mathbf{k}} \big[n(\omega_k) - 1\big] \frac{1}{2}\hbar\omega_k, \tag{3.75}$$

for $n(\omega_k) \cong 1$, where $n(\omega_k)$ is the refraction index of the atomic gas at $\omega_k$. For a dilute gas of atoms in level $|a\rangle$,

$$n \cong 1 + \frac{4\pi N}{3\hbar} \sum_l \frac{\omega_{al} |\mathbf{d}_{al}|^2}{\omega_{al}^2 - \omega_k^2}, \tag{3.76}$$

where $\mathbf{d}_{al}$ is $a \leftrightarrow l$ transition dipole moment. Then by subtracting from this expression the change of the zero-point energy due to free electrons with the same density, we can get an observable energy shift for the atomic level $|a\rangle$.

For the case of atom gas with the driving field considered above, we notice that

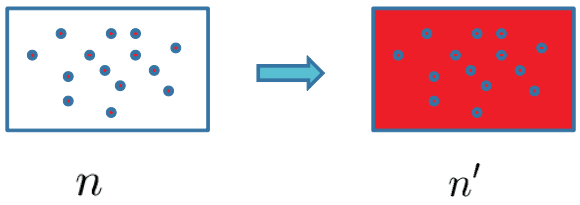


Figure 3.13: Schematic of Feynman's interpretation of the Lamb shift.

the refractive index of the gas with the atom in level $|a\rangle$ changes into

$$n' \cong n + \frac{4\pi N}{3\hbar}\left(\sum_{\beta=b',c'}\frac{\omega_{a\beta}|\mathbf{d}_{a\beta}|^2}{\omega_{a\beta}^2-\omega_k^2}-\frac{\omega_{ab}|\mathbf{d}_{ab}|^2}{\omega_{ab}^2-\omega_k^2}\right). \tag{3.77}$$

Thus the change of the zero-point energy due to the presence of the driving field is given by

$$\Delta E_a = -\sum_{\mathbf{k}}\frac{\hbar\omega_k}{2}\frac{4\pi N}{3\hbar}\left(\sum_{\beta=b',c'}\frac{\omega_{a\beta}|\mathbf{d}_{a\beta}|^2}{\omega_{a\beta}^2-\omega_k^2}-\frac{\omega_{ab}|\mathbf{d}_{ab}|^2}{\omega_{ab}^2-\omega_k^2}\right). \tag{3.78}$$

As the box contains only one atom, we have $NV = 1$. After summing over $\mathbf{k}$ and recalling that $|\mathbf{p}_{al}|^2 = m^2\omega_{al}^2|\mathbf{x}_{al}|^2 = (m^2\omega_{al}^2/e^2)|\mathbf{d}_{al}|^2$, we get the same Lamb shift as derived above.

### *3.5.3 Summary*

We studied the effect of the driving laser on the Lamb shift. First we change the picture of the system from the bare atom and laser field to a dressed state. Then a unitary transformation is made on the original Hamiltonian which is then transformed into the form of RWA. We can directly show that the Lamb shift depends on the Rabi frequency and the detunning of the driving field. This relation provides a way to control the Lamb shift coherently.

# 4. SINGLE ATOM LOCALIZATION VIA RESONANCE FLUORESCENCE PHOTON STATISTICS *

## 4.1 Introduction

The recent interest in mesoscopic and nanoscopic physics asks for an accurate control of the position of the interacting components [118]. In particular, the methods to achieve high spatial resolution in position measurement via optical techniques draw great attention [119]. Many schemes have been proposed to overcome the well-known Rayleigh diffraction limit and achieve subwavelength localization of microscopic objects. One class of schemes is proposed to make use of the properties of the far-field light emitted or scattered by the particles driven by a standing-wave laser field. In these schemes, the position information of the atom is encoded into the atomic dynamics via the position dependent standing-wave field intensity. The observable for decoding the position information can be quadrature phases of light fields [120, 121, 122], long-lived atomic states [123, 124], spontaneously emitted light [125, 126, 127], absorption of probe light [128] or a combination of these ideas [129]. It is also suggested to measure the distance between two adjacent two-level atoms via the resonance fluorescence spectrum [130] and the intensity-intensity correlation function [131].

We propose a scheme to localize a single atom fixed in a standing wave based on the photon statistics in resonance fluorescence [52, 53, 54]. This scheme is different from similar schemes where an atom with an extended wavefunction in the transverse direction passes through a standing wave and is localized. Possible realizations of

*Reprinted with permission from "Single-atom localization via resonance-fluorescence photon statistics," by Shuai Yang, M. Al-Amri, and M. Suhail Zubairy, 2012, *Phys. Rev. A*, vol. 85, p. 023831, copyright [2012] by American Physical Society.

our present scheme include small clusters and atom impurities, etc. In such systems, the atom can be viewed as a "point-like" particle and the atomic spread is not a problem. The photon number statistics depends on the atom position through the position related Rabi oscillations introduced by the standing wave field. So the recorded photon number will provide us information of the position of the atom. Furthermore, as the standing wave is a sinusoid function, the change of the Rabi frequency at the nodes is sharp which means a tiny change of the position will cause a dramatic response of the statistics. The accuracy of the localization would be high close to the nodes. Motivated from this idea, we study the position distribution of a two-level atom driven by a standing-wave field conditioned on the photon statistics measurement of the resonance fluorescence. We note that the best localization occurs when the atom is at the nodes of the standing-wave field which is complementary to our previous scheme [125, 126, 127].

The section is organized as follows. In 4.2, we briefly introduce our scheme of localizing a two-level atom. In 4.3, we present the photon statistics of the resonance fluorescence from the driven two-level atom. In 4.4, we present the strategy and accuracy of our localization scheme. Finally we present some concluding remarks in 4.5.

## 4.2 Localization scheme

We consider a two-level atom placed at some unknown position inside a standing-wave field with wavelength $\lambda$. The field is along the $x$ direction and interacts with the atomic transition resonantly. The atom undergoes Rabi oscillations introduced by the standing-wage driving field. The Rabi frequency is given by

$$\Omega(x) = \Omega_0 \sin kx \,, \tag{4.1}$$

where $k = 2\pi/\lambda$ and $\Omega_0$ are the wave vector and maximal intensity of the standing-wave driving field, respectively. The spontaneously emitted photons via resonance fluorescence are recorded by a $4\pi$ detector. The photon statistics of the detected photons depends on the position of the atom via the position-dependent Rabi frequency. Thus the probability of measuring $n$ photons with the atom being located at position $x$ fulfills a joint probability distribution $p(x, n)$.

Our aim is to estimate the position of the atom based on the detection of the emitted photons, i.e., we determine the conditional position distribution $p(x|n)$ of finding the atom at position $x$ in the standing-wave, given that we have recorded $n$ number of photons from the resonance fluorescence.

To find this conditional position probability distribution we make use of the Bayes' theorem and obtain

$$p(x|n) = \frac{p(x)p(n|x)}{p(n)} = \frac{p(x)p(n|x)}{\int dx p(n|x)} \,. \tag{4.2}$$

Here $p(x)$ is the position distribution of the atom within a wavelength which reveals our initial information of the atom's position. Also $p(n|x)$ is the conditional spontaneously emitted photon number distribution when the atom is located at position $x$. It is viewed as the prior information since it can be calculated from theory and then be tested in experiment. Here $p(n) = \int dx p(n|x)$ denotes the marginal photon statistics. It can also be viewed as the normalization probability.

After the measurement, we obtain the photon number and then the information of the atom's position is extracted from the conditional probability distribution $p(x|n)$. The position of the atom can be estimated with the average value

$$\bar{x} = \int dx x p(x|n) \,. \tag{4.3}$$

The accuracy of this estimation is quantified by the standard deviation

$$\Delta(x) = \int dx(x-\bar{x})^2 p(x|n)\,. \tag{4.4}$$

## 4.3 Photon statistics in resonance fluorescence

The photon number statistics $p(n|x)$ in resonance fluorescence of our target atom located at the position $x$ in the standing-wave is given by [53]

$$\begin{aligned} p(n|x) &= \frac{\beta^n \Omega^{2n-2} e^{-\beta t}}{(n!)^2 \tilde{\Omega}^{3n+2}} \sum_{k=0}^{n} \sum_{L=0}^{k} \frac{\tilde{\Omega} t t^{k-L}}{(k-L)!L!} \Big( c_{nk} a_L + D_{nk} \Big\{ b_L^+ \cos\left[\tilde{\Omega}t + \pi(n-k)/2\right] \\ &\quad - b_L^- \sin\left[\tilde{\Omega}t + \pi(n-k)/2\right] \Big\} \Big)\,, \end{aligned} \tag{4.5}$$

where $t$ is the recording time of the detector, $\beta$ is the spontaneous emission rate, $\tilde{\Omega} = [\Omega(x)^2 - \beta^2]^{1/2}$, and

$$C_{nk} = (-1)^{\frac{n-k}{2}} \sum_{m=0}^{n-k} \frac{(-1)^m (n+m)!(2n-k-m)!}{m!(n-k-m)!} \tag{4.6}$$

$$D_{nk} = (-1)^{n+1} \sum_{m=0}^{n-k} \frac{(n+m)!(2n-k-m)!}{2^{n+m} m!(n-k-m)!}\,, \tag{4.7}$$

are numerical coefficients with $n-k$ being even($C_{nk} = 0$ for $n-k$ odd). And

$$a_L = \frac{d^L g(-\beta)}{ds^L}, \tag{4.8}$$

$$b_L^+ = \frac{1}{2}\left[\frac{d^L g(s_+)}{ds^L} + \frac{d^L g(s_-)}{ds^L}\right], \tag{4.9}$$

$$b_L^- = -\frac{i}{2}\left[\frac{d^L g(s_+)}{ds^L} - \frac{d^L g(s_-)}{ds^L}\right], \tag{4.10}$$

with $s_\pm = -\beta \pm i\tilde{\Omega}$ and

$$g(s) = \left[(s+2\beta)(s+\beta)+\Omega^2\right]\left[s(s+\beta)(1+w_0)-\Omega v_0 s+\Omega^2\right]. \quad (4.11)$$

Here $v_0$ and $w_0$ are the coefficients that depend on the initial state of the atom. For the atom initially in the steady state, we have

$$v_0 = \frac{2\beta\Omega^2}{2\beta^2+\Omega^2},\ w_0 = -\frac{2\beta^2}{2\beta^2+\Omega^2}. \quad (4.12)$$

We note that equation (4.5) describes the photon statistics only for non-zero photon number case. The probability that no photon has been measured is given by

$$\begin{aligned} p(0|x) &= \frac{e^{-\beta t}}{\alpha^2+\gamma^2}\Big\{ \left[\Omega(\Omega+\beta v_0)+\alpha^2\right]\cosh\alpha t - \left[\Omega(\Omega+\beta v_0)-\gamma^2\right]\cos\gamma t \\ &\quad -\beta\alpha w_0 \sinh\alpha t - \beta\gamma w_0 \sin\gamma t\Big\}, \end{aligned} \quad (4.13)$$

where

$$\alpha = \sqrt{\frac{1}{2}\left[\beta^2-\Omega^2+(\beta^2-\Omega^2)^{1/2}\right]}, \quad (4.14)$$

$$\gamma = \sqrt{\frac{1}{2}\left[\beta^2+\Omega^2+(\beta^2-\Omega^2)^{1/2}\right]}. \quad (4.15)$$

The photon statistics in resonance fluorescence as given in equations (4.5) and (4.13) now depends on the position of the atom through the position-dependent Rabi frequency $\Omega$. Further, as the standing-wave is a sinusoid function, the change of the Rabi frequency at the nodes would be abrupt for large $\Omega_0$. This means that a tiny change of the atom's position can cause a sharp change of the Rabi frequency and thus a dramatic difference in the photon statistics.

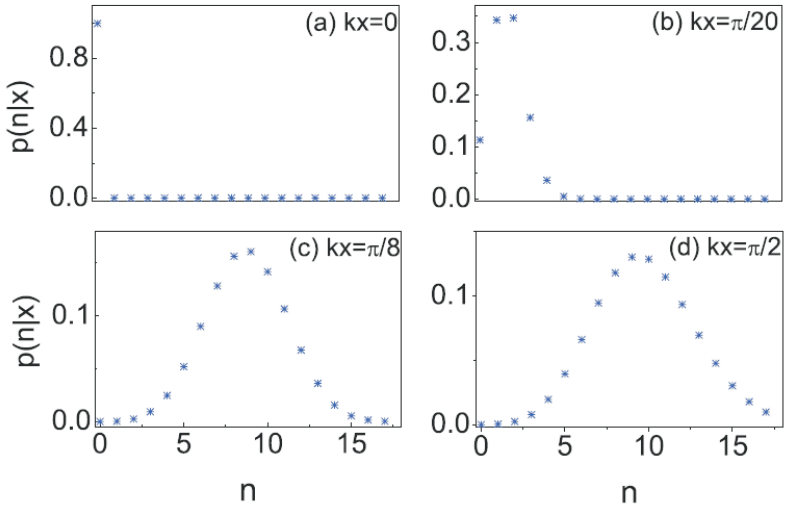


Figure 4.1: The photon statistics $p(n|x)$ for fixed atom positions (a) $kx = 0$, (b) $kx = \pi/20$, (c) $kx = \pi/8$, and (d) $kx = \pi/2$. The other parameters are $\Omega_0 = 10\beta$ and $\beta t = 10$.

## 4.4 Results and discussion

### *4.4.1 Position-dependent resonance fluorescence photon statistics*

As discussed before, the photon statistics of the spontaneously emitted photons depends on the position of the atom inside the standing-wave field. To show this dependence explicitly, we plot the conditional probability distribution $p(n|x)$ for four different positions of the atom inside the standing-wave field; $kx =$ (a) 0, (b) $\pi/20$, (c) $\pi/8$, and (d) $\pi/2$, see figure 4.1. Here we consider a strong driving field intensity $\Omega_0 = 10\beta$ and a long measuring time $\beta t = 10$.

As shown in figure 4.1(a), when the atom is placed at $x = 0$, the photon number distribution is unity at $n = 0$ and zero at $n > 0$. This position corresponds to the node of the standing-wave field where the Rabi frequency is zero and therefore no spontaneous emission takes place. When the position of the atom is moved from $kx = 0$ to $\pi/20$, the atom experiences a weak Rabi frequency. Due to this weak

Rabi oscillation there is a probability that a small number of photons are emitted and then recorded by the detector. As a result the photon statistics exhibits a non-zero structure with a very small average number of photons, see figure 4.1(b). As the position of the atom shifts toward the anti-node to $kx = \pi/8$ and then $\pi/2$, the strength of the Rabi frequency increases. Therefore, a relatively large average number of photons would be measured, see figure 4.1(c) and (d). It is now clear that the average number of photons recorded by the detector depends on the position of the atom. It is small when the atom is at or very close to the nodes and large when the atom is far from the nodes.

### *4.4.2 Conditional position probability distribution*

We next study the behavior of the conditional position probability distribution $p(x|n)$ following equation (4.2). Since we have no past information about the position of the atom before the measurement, it would be reasonable to assume a uniform distribution of $p(x)$ within the unit wavelength $[-\pi, \pi]$ as

$$p(x) = \frac{1}{2\pi}\,. \tag{4.16}$$

It follows, on substituting equations (4.5), (4.13), and (4.16) into equation (4.2), that the conditional position probability $p(x|n)$ provides the information about the atom's position. In figure 4.2, we plot $p(x|n)$ for six different cases of photon numbers $n$ recorded during the measuring time $t$. It is observed that if the detector does not record any photon ((a) $n = 0$), a sharp probability distribution centered at the nodes is expected. This steep peak arises due to the following considerations. First, the Rabi frequency is zero at the nodes and thus the distribution peaks at $x = 0$. Second, as the maximal intensity of the sinusoidal standing-wave is large, the Rabi frequency changes abruptly when close to the node. Third, the measuring time is long. So even

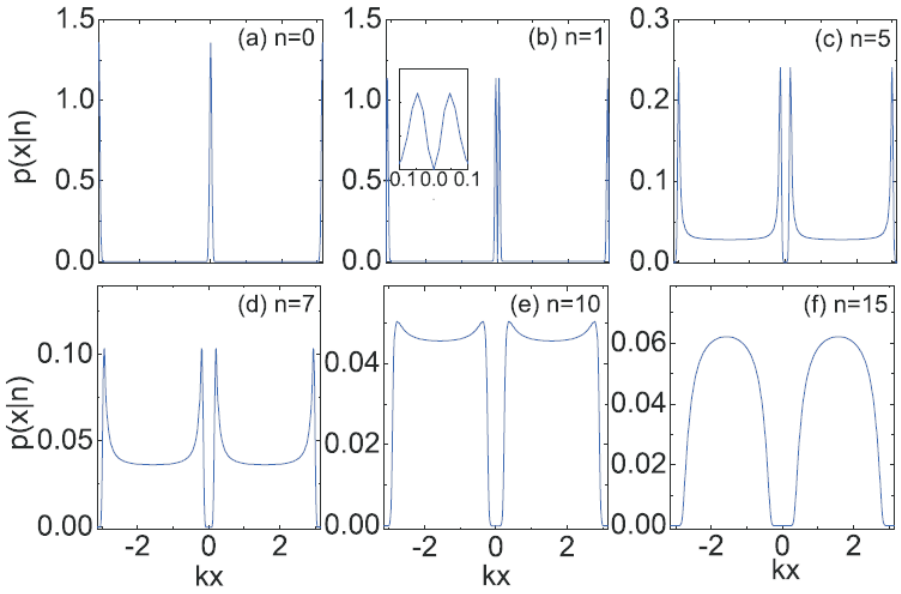


Figure 4.2: The conditional position probability distribution $p(x|n)$ versus normalized position of the atom inside the standing-wave field ($kx = -\pi$ to $\pi$) for (a) $n = 0$, (b) $n = 1$, (c) $n = 5$, (d) $n = 7$, (e) $n = 10$, and (f) $n = 15$. The other parameters are the same as in figure 4.1.

a slight deviation from the node will bring enough Rabi oscillations and therefore emitted photons.

However, the probability of the atom located at the node reduces to zero when the detector records $n = 1$ number of photons, see figure 4.2(b). This is because there is no chance for the atom to emit a photon if it is located at the node where the Rabi frequecy is zero, see figure 4.1(a). The peaks are still very close to the nodes and very sharp. In figures 4.2(c) and (d), we plot the conditional position probability distribution when the detector records $n = 5$ and $n = 7$ number of photons, respectively. The localization peaks are moved away from the nodes. Meanwhile the probability of the atom located at other positions beyond the peak increases. Thus the localization accuracy degrades.

As shown in figures 4.2 (e) and (f), the probability of finding the atom at the anti-

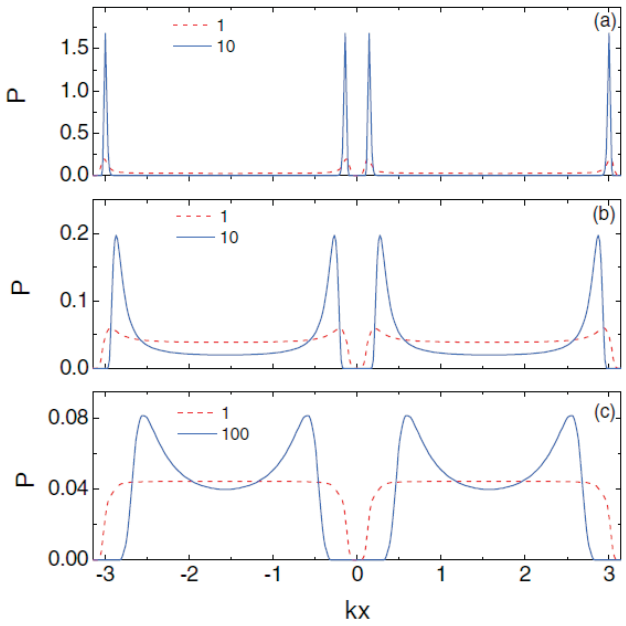


Figure 4.3: The conditional position probability distribution for different number of measurements when the atom is located at (a) $kx = \pi/20$, (b) $kx = \pi/10$ and (c) $kx = \pi/4$. The red dashed lines correspond to the case when one measurement is made. The blue solid lines correspond to the case when 10 measurements are made in (a) and (b) and the case when 100 measurements are made in (c). The other parameters are the same as in figure 4.1.

nodes $kx = \pm\pi/2$ of the standing-wave field increases significantly if more photons are detected. This is in accordance with the figures 4.1(c) and (d) where we observe large average number of photons when the atom locates near the anti-node. When the recorded photon number is $n = 15$, there are two broad localization peaks in figure 4.2(f) centered at the anti-nodes of the standing-wave field. The peaks are quite broad because the Rabi frequency decreases slowly as the atom moves away from the anti-nodes.

From these observations we conclude that the spatial resolution of single atom localization is bad if the photon numbers are large and the accuracy is good if the number of photons being recorded is small.

Note that here we suppose that we have no prior information about the position of the atom and therefore we assume a uniform distribution of $p(x)$ as shown in equation (4.16). If some position information is acquired before the measurement, a better resolution can be expected. With this in mind, instead of making only one measurement, we make a series of measurements and record the photon number each time, we can update the probability distribution $p(x)$ in equation (4.2) with the conditional probability distribution $p(x|n)$ from previous measurements. After using equation (4.2) iteratively, we can achieve a narrower conditional probability distribution of the atom position.

In figure 4.3, we draw the conditional probability distribution for different number of measurements when the atom is fixed at different positions. Note that as the number of emitted photon is random, the measured photon numbers may be different for different experiments, the results shown in this figure have been averaged over 100 experiments. Figure 4.3 (a) corresponds to the case when the atom is actually located at $kx = \pi/20$. The red dashed line shows the conditional position distribution when only one measurement is made while the blue solid line shows the result when ten measurements are made. By comparing the two lines, we can conclude that making more measurements improves the resolution of the localization. This is also demonstrated in figure 4.3 (b) $kx = \pi/10$ and (c) $kx = \pi/4$. However, when the atom is located at $kx = \pi/4$, the resolution is still bad even if 100 measurements are made. This is because the change of the driving field with the position of the atom gets slow when the atom is close to anti-nodes and the difference between the photon statistics for different positions will accordingly become tiny, as shown in figures 4.1 (c) and (d).

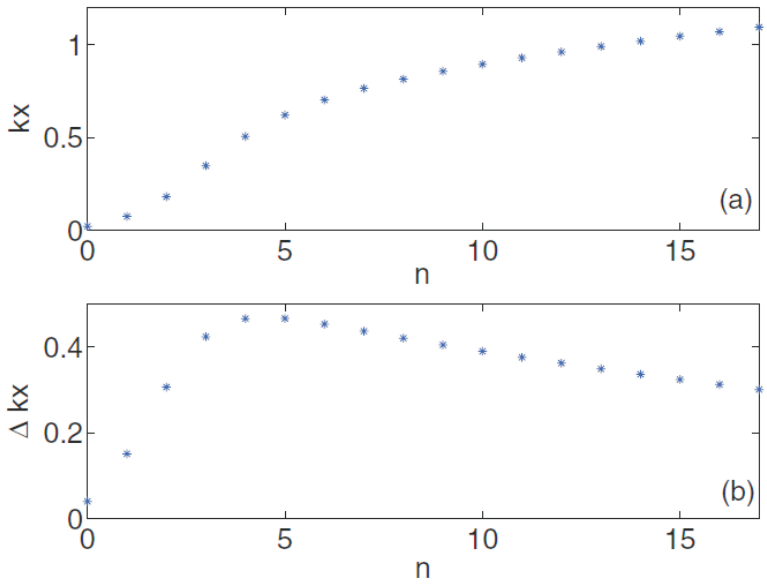


Figure 4.4: (a) The estimated position of the atom within unit wavelength domain of the standing-wave field and (b) deviation from the estimated position versus number of photons measured. The other parameters are the same as in figure 4.1.

### *4.4.3 Strategy*

In figure 4.4, following the definition of equations (4.3) and (4.4), we plot (a) the estimated position and (b) the accuracy of the localization predicted from the conditional position probability distribution $p(x|n)$. It shows clearly that when there is no photon being recorded, the atom is localized precisely at the nodes of the standing-wave field. If the signal of the detector is strong which means that large number of photons are detected, it is hard to give an accurate description of the position of the atom.

In the light of our analysis above we address the localization strategy. For an atom located in a standing-wave driving field, we first measure the emitted photons in a relatively long time. If a weak signal is reported, we would conclude that the atom is localized at a position close to the nodes of the standing-wave field, i.e., at

$kx = n\pi$ ($n = 0, \pm 1$). On the other hand, if the detector records large number of photons, the atom is located close to the anti-nodes. However, the accuracy is bad for this case. In order to localize the atom precisely, we tune the relative phase of the two counter-propagating fields forming the standing-wave and thus the position of the node along the $x-$axis is scanned. When the signal becomes almost negligible, the atom is located to the nodes of the standing-wave with good accuracy. Current technology provides us high accuracy controlled by piezoelectric ceramics and we can ignore the error brought by tuning the position of the nodes. So we adjust the phase of the standing-wave until there is no signal when we localize the atom. Note that the characteristic of this scheme is in contrast with the previous localization scheme [125, 126, 127] based on the spectrum of the emitted photon where the best localization happens at the anti-nodes. In addition, in the previous scheme, the precision in localization depends on the manipulation of the vacuum-field detuning which is rather difficult to control experimentally. The present scheme for the single atom localization is based on zero photon counting and therefore much easier for implementation.

One may propose another localization scheme by recording the fluorescence photons for many times following the analysis of the conditional probability with many measurements as shown in figure 4.3. With the recorded photon numbers, equation (4.2) is iteratively utilized. Then we are able to localize the atom from the conditional probability distribution. However, as a photon number discrimination detector is required, this scheme is not realistic with current technology. In our strategy a photon number discrimination detector is unnecessary. We only need a $4\pi$ detector to record the photons. If it happens that no photon is recorded, the atom is then localized at the node of the field.

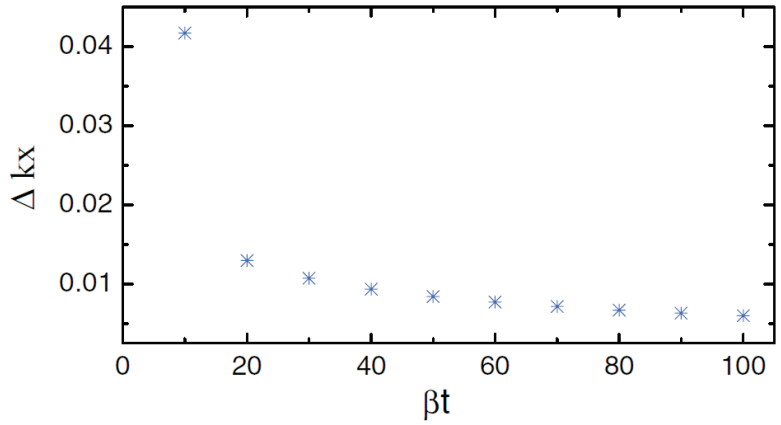


Figure 4.5: The deviation from the estimated position of the atom versus detector measuring time when no photon is recorded. The other parameters are the same as in figure 4.1.

### *4.4.4 Effect of the detector efficiency*

The accuracy of our localization scheme can be improved by increasing the strength of the standing-wave driving field and prolonging the measuring time of the detector. When the atom is near the nodes, the change of the Rabi frequency brought by the deviation of atom position is proportional to the maximal intensity of the standing-wave field. Therefore, increase of the strength of the field will result in a more sensitive response of the photon statistics and thus better discrimination of the atom localization. Strong driving field also increases the number of Rabi cycles leading to a higher probability of spontaneous emission unless the atom is located at the node. Long measuring time means more Rabi cycles during the recording and therefore increasing the possibility to record more photons unless the atom is at the node. We show in figure 4.5 how the accuracy of the atom localization is improved with prolonged detector recording time.

This property can also be used to overcome the impair of the accuracy from bad

detector efficiency. In the above discussion we assume a perfect detector efficiency which is unrealistic in experiments. First, the detector has blind response, i.e., the photon hits the detector but the detector gets no response. Also it is impossible to build up the idealized $4\pi$ detector which enclose the whole cavity and atom. Since the direction distribution of the spontaneous emission is uniform and we are interested in the photon number only, we can include the missing records in the open angles to the whole detector efficiency. With bad detector efficiency, even if the atom is located close to the anti-node we will still have considerable probability to detect quite weak signal. According to our scheme, this misleading reading locates the atom at the nodes. This situation definitely reduces the localization accuracy. We next explain how to overcome this difficulty.

We assume that the detector has an efficiency $\eta$ for single photon detection. If $m$ photons are emitted by the atom then due to efficiency of the detector the probability for detecting $n$ photons is $C(m,k)\eta^n(1-\eta)^{m-n}$. So the conditional probability for the detector to record $n$ photons at a given time $t$ when the atom is at some position $x$ is given by

$$p_e(n|x) = \sum_{m\geq n} p(m|x)\begin{pmatrix} m \\ n \end{pmatrix}\eta^n(1-\eta)^{m-n}. \tag{4.17}$$

On substituting equation (4.17) into equation (4.2), the conditional position probability distribution with $n$ number of photons being detected becomes

$$p_e(x|n) = \frac{p(x)\sum_{m\geq n} p(m|x)\begin{pmatrix} m \\ n \end{pmatrix}\eta^n(1-\eta)^{m-n}}{\sum_x \sum_{m\geq n} p(m|x)\begin{pmatrix} m \\ n \end{pmatrix}\eta^n(1-\eta)^{m-n}}. \tag{4.18}$$

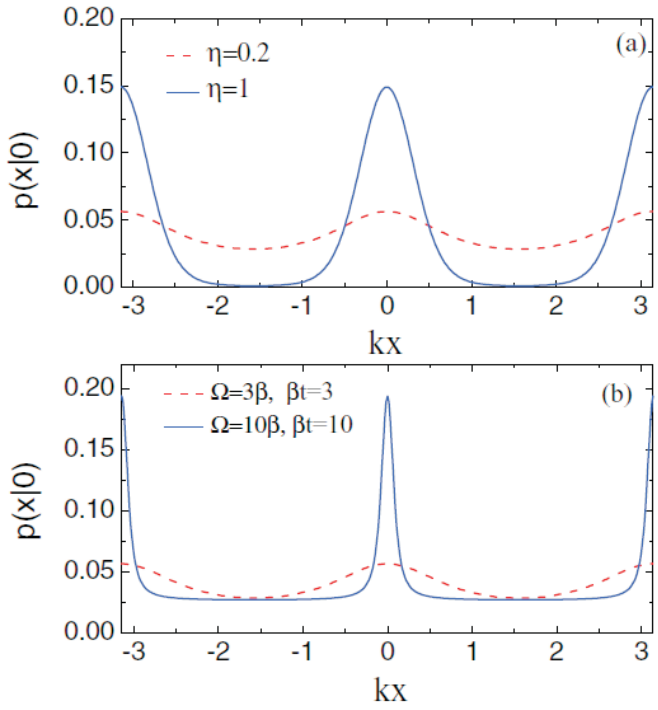


Figure 4.6: The position probability distribution for no counting $p(x|0)$ versus $kx$ for (a) different detector efficiencies (i) $\eta = 0.2$ (ii) and $\eta = 1.0$. The driving field strength $\Omega_0 = 3\beta$ and the measuring time $\beta t = 3$. (b) different combinations of the driving field strength and the measuring time (i) $\Omega_0 = 3\beta$, $\beta t = 3$ and (ii) $\Omega_0 = 10\beta$, $\beta t = 10$. Here $\eta = 0.2$.

The effect of the detector efficiency on single atom position measurement is presented in figure 4.6(a). Here, we plot the conditional position probability distribution when no photon is emitted for two different detector efficiencies, i.e., $\eta = 0.2$ (red dashed line) and $\eta = 1.0$ (blue solid line). This clearly shows that bad detector efficiency degrades the precision in the atom localization.

In figure 4.6(b), we compare the conditional probability distribution $p_e(x|0)$ for different dimensionless measuring time $\beta t$ and different strengths of the driving field intensity $\Omega_0$. It shows that by increasing the measuring time and the strength of the driving field, the peak of the conditional probability of the atom position is narrowed

and thus the localization accuracy is improved.

## 4.5 Summary

In this section, we present a subwavelength atom localization scheme for an atom located in a standing-wave field. The strategy is based on the observation that the photon statistics of resonance fluorescence depends on the position-dependent Rabi frequency. Therefore the photon statistics changes dramatically across the standing-wave driving field when we choose an intense driving field and long recording time. The precise localization of the atom takes place at positions close the nodes of the standing-wave field. We also show that the losing accuracy caused by bad detector efficiency can be retrieved by increasing either the driving field strength or the measuring time or both.

# 5. CONCLUSION

In this dissertation, we studied the applications of quantum interference and coherence in the following aspects.

In section 2, we studied the optical properties of the combined cavity-cold atoms system. The atom-photon interaction provides the optical lattice to the atoms and affects the mechanical motion of the atoms. In turn, atoms induce a position dependent phase shift on the cavity field. This highly intrinsic nonlinearity leads bistability for both the intra-cavity photon number and atomic state. We first showed that the bistability of the intra-cavity photon number with respect to the input intensity along the cavity axis can be controlled by a second laser field added perpendicular to the cavity axis [45]. For low transverse pumping, the intra-cavity photon number shows clear bistability for a particular range of the input pump along the cavity axis. When increasing the transverse pumping field, the range of the bistable behavior is diminished. In particular, above a critical value of the transverse pumping, the bistable behavior disappears. This is because the scattered photons from the transverse pumping excluded the existence of the lower branch. This result provides the possibility of realizing a controllable optical switch. For this, the two stable branches of the output photon number conditioned on the parallel input field act as the optical switch. The transverse pump can then be used to enable or disable this switch. If the switch is disabled, only one of the two possible switch states can be realized, independent of the input field. We verify the operation of the switch using numerical solutions of the underlying GP equation, and additionally we interpret the results based on the DMA method.

Next, we explored the dynamic behavior of the optical bistability induced by the

pumping field along the cavity axis. We investigated the switching behavior of the intra-cavity photon number from one branch to the other. We found that the way of adding the field is crucial to the switching close to the critical transition point. If the pump field is added adiabatically, the jumping happens exactly at the critical point [59]. If the pump field is added abruptly, the system may jump to the upper branch even if the pump field intensity is less than the critical transition point. This behavior is similar to the anomalous switching of the dispersive optical bistability [44]. It was shown that the condensate can be mapped to a nonlinear spring and the potential energy of the spring is determined by the intensity of the pumping field. The anomalous switching can then be understood in a ball-bowl picture. In this picture, the condensate is like a small ball sliding in a frictionless bowl whose shape is determined by the functional of the potential. When the potential has only minimum, there no bistability, while bistability emerges if there are two minimums in the potential. Suppose there is no pumping field, the shape of the ball is parabolic and the ball is staying at the bottom of the bowl. If the field is added adiabatically, the shape of the bowl changes gradually and the ball will stay at the bottom of the bowl. Then at some intensity, a second but lower well appears and the ball keeps on staying at the bottom of the initial well which is higher. If the field is increased further, the lower well gets deeper and the upper well is raised. At the critical point, the minimum of the upper well coincides with the unstable peak of the barrier in the middle. Therefore the upper well disappears. The ball falls down to the deeper well which corresponds to the higher branch. When the field is added abruptly to some certain value from zero, the situation is much different. The ball lies at the bottom of the bottom of the parabolic bowl. Then shape of bowl changed immediately. The ball then starts to oscillate in the bowl. If the intensity of the field lies in the bistable region but far from the critical point, the ball will be confined in the upper basin

of the double well as the barrier in the middle is higher than the initial position. However, for some values of the bistable region close to the critical point, the the barrier in the middle of the double well is lower than the initial position. Therefore, the ball can pass the barrier and slide to the deeper basin. With this picture in mind, we also showed that different initial conditions and damping rates may affect this anomalous switching behavior.

In the end of section 2, we proposed an interesting scheme which realizes an effective Dicke Hamiltonian with a quantum-degenerate Fermi gas in an optical cavity. We showed that, as the same as a BEC in an optical cavity, the self-organization phase transition of a 1-D Fermi gas can also be mapped to the Dicke-phase transition. However, in the Boson case, the atom-atom interaction affects the critical value of the transition. In our Fermi gas case, the atom-atom interaction due to the $s$-wave scattering is excluded directly by the Pauli exclusion principle. Therefore, our proposal makes it possible to directly compare the theoretical and experimental critical values of the Dicke quantum phase transition.

In section 3, we utilized a unitary transformation method to study the effect of counter-rotating terms on the controlling of spontaneous emission. This unitary transformation method transforms the Hamiltonian to the RWA form while including the effect of counter-rotating terms and and subtracting the free electron self-energy from the Hamiltonian. In traditional studies of spontaneous emission modification via quantum interference, the imaginary parts in the dynamic equations which result in energy shifts were discarded in the long time limit and the Markov approximation. However, if two decay channels are correlated, this energy shifts and decay processes are correlated. We showed this effect in a four-level atom system [48]. In different from the three-level atom case studied in [98], this effect will be revealed in our scheme even if the two dipole transitions from the upper levels to the ground level

are orthogonal.

We then showed the effect of the counter-rotating terms of the spontaneous emission from an atom embedded in a three-dimensional anisotropic photonic crystal. The properties of the radiation field, in such a photonic crystal, depend on the relative position of the atomic transition frequency and the band edge of the photonic crystal. It is shown that there exist two characteristic atomic transition frequencies. Here one can see three different and distinct regions; (a) above these two frequencies, the emission is purely a propagating wave, (b) a localized field below them, (c) while it is a purely diffusion field between the two frequencies. And there is no coexistence of localized and propagating fields. It is shown that a localized field exists even if the atomic frequency is higher than the band edge of the photonic crystal. This is because the strong interaction between the atom and electromagnetic radiation shifts the atomic energy level. However, previous studies neglected the counter-rotating terms which results in an incomplete calculation in the energy shifts. With the unitary transformation method, we studies the properties of the emitted field. We found that the behavior of the emission is similar to the RWA case, i.e., the localized and propagating fields are also separated by two characteristic atomic transition frequencies. However, this two characteristic frequencies are shifted due to the full Lamb shift which is obtained without making RWA [49].

At the end of this section, we explored the unitary transformation method to show how the Lamb shift can be controlled by a driving field. In Feynman's interpretation, it is argued that the presence of an atom inside a box leads to a change of the resonant frequencies from $\omega_k$ to $\omega_k/n(\omega_k)$ where $n(\omega_k)$ is the refractive index at $\omega_k$. This leads to a change of the zero point energy due to the presence of the atom and the calculated change of the energy corresponds to the Lamb shift. We control the refractive index $n(\omega_k)$ can be controlled by an external driving field which is added to

other two levels of the atom [50]. Therefore the Lamb shift is coherently controlled.

In section 4, we proposed a scheme to localize a single atom fixed in a standing wave to subwavelength level based on the photon statistics in resonance fluorescence [48]. Possible realizations of our present scheme include small clusters and atom impurities, etc. In such systems, the atom can be viewed as a "point-like" particle and the atomic spread is not a problem. In history, experimental verification of the antibunching property of resonance fluorescence light provided the first nonclassical effect of light. The sub-Poissonian statistics of the emitted light depends on the intensity of the pumping field. Therefore, the photon number statistics of the resonance fluorescence light in our scheme depends on the atom position through the position related Rabi oscillations introduced by the standing wave field. The recorded photon number provides us information of the position of the atom. We showed that the atom's conditional position distribution on the measured photon number is sharpest when the photon number is zero. This is because standing wave is a sinusoid function and the change of the Rabi frequency at the nodes is sharpest. So a tiny change of the position will cause a dramatic response of the statistics. Thus the accuracy of the localization is high close to the nodes. We also show that the losing accuracy caused by bad detector efficiency can be retrieved by increasing either the driving field strength or the measuring time or both.

# REFERENCES


[1] R. P. Feynman, R. B. Leighton, and M. L. Sands, *The Feynman lectures on physics*. Redwood City: Addison-Wesley, 1989.

[2] M. O. Scully and M. S. Zubairy, *Quantum Optics*. Cambridge: Cambridge University Press, 1997.

[3] R. H. Brown and R. Q. Twiss, "Correlation between photons in two coherent beams of light," *Nature*, vol. 177, no. 4497, pp. 27–29, 1956.

[4] R. J. Glauber, "The quantum theory of optical coherence," *Phys. Rev.*, vol. 130, pp. 2529–2539, Jun 1963.

[5] H. J. Kimble, M. Dagenais, and L. Mandel, "Photon antibunching in resonance fluorescence," *Phys. Rev. Lett.*, vol. 39, pp. 691–695, Sep 1977.

[6] C. M. Caves, "Quantum-mechanical noise in an interferometer," *Phys. Rev. D*, vol. 23, pp. 1693–1708, Apr 1981.

[7] M. Xiao, L.-A. Wu, and H. J. Kimble, "Precision measurement beyond the shot-noise limit," *Phys. Rev. Lett.*, vol. 59, pp. 278–281, Jul 1987.

[8] K.-J. Boller, A. Imamolu, and S. E. Harris, "Observation of electromagnetically induced transparency," *Phys. Rev. Lett.*, vol. 66, pp. 2593–2596, May 1991.

[9] J. E. Field, K. H. Hahn, and S. E. Harris, "Observation of electromagnetically induced transparency in collisionally broadened lead vapor," *Phys. Rev. Lett.*, vol. 67, pp. 3062–3065, Nov 1991.

[10] O. Kocharovskaya and Y. Khanin, "Coherent amplication of an ultrashort pulse in a 3-level medium without a population-inversion," *JETP Lett.*, vol. 48, pp. 630–634, Dec 10 1988.

[11] S. E. Harris, "Lasers without inversion: Interference of lifetime-broadened resonances," *Phys. Rev. Lett.*, vol. 62, pp. 1033–1036, Feb 1989.

[12] M. O. Scully, S.-Y. Zhu, and A. Gavrielides, "Degenerate quantum-beat laser: Lasing without inversion and inversion without lasing," *Phys. Rev. Lett.*, vol. 62, pp. 2813–2816, Jun 1989.

[13] S.-Y. Zhu, R. C. F. Chan, and C. P. Lee, "Spontaneous emission from a three-level atom," *Phys. Rev. A*, vol. 52, pp. 710–716, Jul 1995.

[14] S.-Y. Zhu and M. O. Scully, "Spectral line elimination and spontaneous emission cancellation via quantum interference," *Phys. Rev. Lett.*, vol. 76, pp. 388–391, Jan 1996.

[15] H. Lee, P. Polynkin, M. O. Scully, and S.-Y. Zhu, "Quenching of spontaneous emission via quantum interference," *Phys. Rev. A*, vol. 55, pp. 4454–4465, Jun 1997.

[16] P. Zhou and S. Swain, "Ultranarrow spectral lines via quantum interference," *Phys. Rev. Lett.*, vol. 77, pp. 3995–3998, Nov 1996.

[17] P. Zhou and S. Swain, "Quantum interference in resonance fluorescence for a driven v atom," *Phys. Rev. A*, vol. 56, pp. 3011–3021, Oct 1997.

[18] P. R. Berman, "Analysis of dynamical suppression of spontaneous emission," *Phys. Rev. A*, vol. 58, pp. 4886–4891, Dec 1998.

[19] C. H. Keitel, "Narrowing spontaneous emission without intensity reduction," *Phys. Rev. Lett.*, vol. 83, pp. 1307–1310, Aug 1999.

[20] F. Plastina and F. Piperno, "Suppression of decay via magnetic coherence in a V-type three-level system," *Phys. Rev. A*, vol. 62, p. 053801, Oct 2000.

[21] G. S. Agarwal, "Anisotropic vacuum-induced interference in decay channels," *Phys. Rev. Lett.*, vol. 84, pp. 5500–5503, Jun 2000.

[22] E. Paspalakis and P. L. Knight, "Phase control of spontaneous emission," *Phys. Rev. Lett.*, vol. 81, pp. 293–296, Jul 1998.

[23] S.-y. Gao, F.-l. Li, and S.-y. Zhu, "Quantum interference and phase-dependent spectrum of resonance fluorescence of a three-level v-type atom," *Phys. Rev. A*, vol. 66, p. 043806, Oct 2002.

[24] Y. Niu and S. Gong, "Enhancing kerr nonlinearity via spontaneously generated coherence," *Phys. Rev. A*, vol. 73, p. 053811, May 2006.

[25] J.-W. Pan, Z.-B. Chen, C.-Y. Lu, H. Weinfurter, A. Zeilinger, and M. Żukowski, "Multiphoton entanglement and interferometry," *Rev. Mod. Phys.*, vol. 84, pp. 777–838, May 2012.

[26] P. Meystre, *Atom optics*. Springer series on atomic, optical, and plasma physics, New York: AIP Press/Springer, 2001.

[27] M. H. Anderson, J. R. Ensher, M. R. Matthews, C. E. Wieman, and E. A. Cornell, "Observation of bose-einstein condensation in a dilute atomic vapor," *Science*, vol. 269, no. 5221, pp. 198–201, 1995.

[28] K. B. Davis, M. O. Mewes, M. R. Andrews, N. J. van Druten, D. S. Durfee, D. M. Kurn, and W. Ketterle, "Bose-einstein condensation in a gas of sodium atoms," *Phys. Rev. Lett.*, vol. 75, pp. 3969–3973, Nov 1995.

[29] W. Ketterle, "Nobel lecture: When atoms behave as waves: Bose-einstein condensation and the atom laser," *Rev. Mod. Phys.*, vol. 74, pp. 1131–1151, Nov 2002.

[30] M. Lewenstein, A. Sanpera, V. Ahufinger, B. Damski, A. Sen(De), and U. Sen, "Ultracold atomic gases in optical lattices: mimicking condensed matter physics and beyond," *Advances in Physics*, vol. 56, no. 2, pp. 243–379, 2007.

[31] P. Domokos and H. Ritsch, "Collective cooling and self-organization of atoms in a cavity," *Phys. Rev. Lett.*, vol. 89, p. 253003, Dec 2002.

[32] A. T. Black, H. W. Chan, and V. Vuletić, "Observation of collective friction forces due to spatial self-organization of atoms: From rayleigh to bragg scattering," *Phys. Rev. Lett.*, vol. 91, p. 203001, Nov 2003.

[33] J. K. Asbóth, P. Domokos, H. Ritsch, and A. Vukics, "Self-organization of atoms in a cavity field: Threshold, bistability, and scaling laws," *Phys. Rev. A*, vol. 72, p. 053417, Nov 2005.

[34] A. Vukics, C. Maschler, and H. Ritsch, "Microscopic physics of quantum self-organization of optical lattices in cavities," *New Journal of Physics*, vol. 9, no. 8, p. 255, 2007.

[35] C. Maschler, I. B. Mekhov, and H. Ritsch, "Ultracold atoms in optical lattices generated by quantized light fields," *The European Physical Journal D*, vol. 46, no. 3, pp. 545–560, 2008.

[36] D. Nagy, G. Szirmai, and P. Domokos, "Self-organization of a bose-einstein condensate in an optical cavity," *The European Physical Journal D*, vol. 48, no. 1, pp. 127–137, 2008.

[37] R. H. Dicke, "Coherence in spontaneous radiation processes," *Phys. Rev.*, vol. 93, pp. 99–110, Jan 1954.

[38] K. Hepp and E. H. Lieb, "On the superradiant phase transition for molecules in a quantized radiation field: the dicke maser model," *Ann. Phys.*, vol. 76, no. 2, pp. 360 – 404, 1973.

[39] Y. K. Wang and F. T. Hioe, "Phase transition in the dicke model of superradiance," *Phys. Rev. A*, vol. 7, pp. 831–836, Mar 1973.

[40] K. Baumann, C. Guerlin, F. Brennecke, and T. Esslinger, "Dicke quantum phase transition with a superfluid gas in an optical cavity," *Nature*, vol. 464, pp. 1301–U1, Apr 29 2010.

[41] D. Nagy, G. Kónya, G. Szirmai, and P. Domokos, "Dicke-model phase transition in the quantum motion of a bose-einstein condensate in an optical cavity," *Phys. Rev. Lett.*, vol. 104, p. 130401, Apr 2010.

[42] S. G. K. W. Murch, K. L. Moore and D. M. Stamper-Kurn, "Observation of quantum-measurement backaction with an ultracold atomic gas," *Nat Phys*, vol. 4, pp. 561 – 564, May 2008.

[43] F. Brennecke, S. Ritter, T. Donner, and T. Esslinger, "Cavity optomechanics with a bose-einstein condensate," *Science*, vol. 322, no. 5899, pp. 235–238, 2008.

[44] S. Yang, M. Al-Amri, and M. S. Zubairy, "Anomalous switching of optical bistability in a bose-einstein condensate," *Phys. Rev. A*, vol. 87, p. 033836, Mar 2013.

[45] S. Yang, M. Al-Amri, J. Evers, and M. S. Zubairy, "Controllable optical switch using a bose-einstein condensate in an optical cavity," *Phys. Rev. A*, vol. 83, p. 053821, May 2011.

[46] H. Zheng, S. Y. Zhu, and M. S. Zubairy, "Quantum zeno and anti-zeno effects: Without the rotating-wave approximation," *Phys. Rev. Lett.*, vol. 101, p. 200404, Nov 2008.

[47] Z.-H. Li, D.-W. Wang, H. Zheng, S.-Y. Zhu, and M. S. Zubairy, "Effect of the counterrotating-wave terms on the spontaneous emission from a multilevel atom," *Phys. Rev. A*, vol. 80, p. 023801, Aug 2009.

[48] S. Yang, J. Xu, S.-Y. Zhu, and M. S. Zubairy, "Effect of energy shifts on the spontaneous emission modification via quantum interference," *Phys. Rev. A*, vol. 85, p. 062516, Jun 2012.

[49] S. Yang, M. Al-Amri, S.-Y. Zhu, and M. S. Zubairy, "Effect of counter-rotating terms on the spontaneous emission in an anisotropic photonic crystal," *Phys. Rev. A*, vol. 87, p. 033818, Mar 2013.

[50] S. Yang, H. Zheng, R. Hong, S.-Y. Zhu, and M. S. Zubairy, "Control of the lamb shift by a driving field," *Phys. Rev. A*, vol. 81, p. 052501, May 2010.

[51] P. Knight and P. Milonni, "The rabi frequency in optical spectra," *Physics Reports*, vol. 66, no. 2, pp. 21 – 107, 1980.

[52] L. Mandel, "Sub-poissonian photon statistics in resonance fluorescence," *Opt. Lett.*, vol. 4, pp. 205–207, Jul 1979.

[53] R. J. Cook, "Photon number statistics in resonance fluorescence," *Phys. Rev. A*, vol. 23, pp. 1243–1250, Mar 1981.

[54] D. Lenstra, "Photon-number statistics in resonance fluorescence," *Phys. Rev. A*, vol. 26, pp. 3369–3377, Dec 1982.

[55] S. Yang, M. Al-Amri, and M. S. Zubairy, "Single-atom localization via resonance-fluorescence photon statistics," *Phys. Rev. A*, vol. 85, p. 023831, Feb 2012.

[56] S. Gupta, K. L. Moore, K. W. Murch, and D. M. Stamper-Kurn, "Cavity nonlinear optics at low photon numbers from collective atomic motion," *Phys. Rev. Lett.*, vol. 99, p. 213601, Nov 2007.

[57] J. A. Sauer, K. M. Fortier, M. S. Chang, C. D. Hamley, and M. S. Chapman, "Cavity qed with optically transported atoms," *Phys. Rev. A*, vol. 69, p. 051804, May 2004.

[58] S. Ritter, F. Brennecke, K. Baumann, T. Donner, C. Guerlin, and T. Esslinger, "Dynamical coupling between a bose-einstein condensate and a cavity optical lattice," *Applied Physics B*, vol. 95, no. 2, pp. 213–218, 2009.

[59] J. M. Zhang, F. C. Cui, D. L. Zhou, and W. M. Liu, "Nonlinear dynamics of a cigar-shaped bose-einstein condensate in an optical cavity," *Phys. Rev. A*, vol. 79, p. 033401, Mar 2009.

[60] Y. Dong, J. Ye, and H. Pu, "Multistability in an optomechanical system with a two-component bose-einstein condensate," *Phys. Rev. A*, vol. 83, p. 031608, Mar 2011.

[61] S. Slama, S. Bux, G. Krenz, C. Zimmermann, and P. W. Courteille, "Superradiant rayleigh scattering and collective atomic recoil lasing in a ring cavity," *Phys. Rev. Lett.*, vol. 98, p. 053603, Feb 2007.

[62] F. Hopf, P. Meystre, P. Drummond, and D. Walls, "Anomalous switching in dispersive optical bistability," *Optics Communications*, vol. 31, no. 2, pp. 245 – 250, 1979.

[63] L. Lugiato, M. Milani, and P. Meystre, "Analytical description of anomalous switching in dispersive optical bistability," *Optics Communications*, vol. 40, no. 4, pp. 307 – 311, 1982.

[64] P. Muruganandam and S. Adhikari, "Fortran programs for the time-dependent gross-pitaevskii equation in a fully anisotropic trap," *Computer Physics Communications*, vol. 180, no. 10, pp. 1888 – 1912, 2009.

[65] R. Roy and M. S. Zubairy, "Beyond the mean-field theory of dispersive optical bistability," *Phys. Rev. A*, vol. 21, pp. 274–280, Jan 1980.

[66] K. Zhang, W. Chen, M. Bhattacharya, and P. Meystre, "Hamiltonian chaos in a coupled bec˘optomechanical-cavity system," *Phys. Rev. A*, vol. 81, p. 013802, Jan 2010.

[67] K. Hepp and E. Lieb, "Superrradiant phase-transition for molecules in a quantized radiation field-Dicke maser model," *Ann. Phys.*, vol. 76, no. 2, pp. 360–404, 1973.

[68] K. Hepp and E. H. Lieb, "Equilibrium statistical mechanics of matter interacting with the quantized radiation field," *Phys. Rev. A*, vol. 8, pp. 2517–2525, Nov 1973.

[69] Carmicha.HJ, C. Gardiner, and D. Walls, "Higher-order corrections to Dicke superradiant phase-transition," *Phys. Lett. A*, vol. A 46, no. 1, pp. 47–48, 1973.

[70] C. Emary and T. Brandes, "Quantum chaos triggered by precursors of a quantum phase transition: The dicke model," *Phys. Rev. Lett.*, vol. 90, p. 044101, Jan 2003.

[71] C. Emary and T. Brandes, "Chaos and the quantum phase transition in the dicke model," *Phys. Rev. E*, vol. 67, p. 066203, Jun 2003.

[72] N. Lambert, C. Emary, and T. Brandes, "Entanglement and the phase transition in single-mode superradiance," *Phys. Rev. Lett.*, vol. 92, p. 073602, Feb 2004.

[73] N. Lambert, C. Emary, and T. Brandes, "Entanglement and entropy in a spin-boson quantum phase transition," *Phys. Rev. A*, vol. 71, p. 053804, May 2005.

[74] K. W. K. Rzążewski and W. Żakowicz, "Phase transitions, two-level atoms, and the $A^2$ term," *Phys. Rev. Lett.*, vol. 35, pp. 432–434, Aug 1975.

[75] J. M. Knight, Y. Aharonov, and G. T. C. Hsieh, "Are super-radiant phase transitions possible?," *Phys. Rev. A*, vol. 17, pp. 1454–1462, Apr 1978.

[76] I. Bialynicki-Birula and K. Rzążewski, "No-go theorem concerning the superradiant phase transition in atomic systems," *Phys. Rev. A*, vol. 19, pp. 301–303, Jan 1979.

[77] K. Rzążewski and K. Wódkiewicz, "Comment on "instability and entanglement of the ground state of the dicke model"," *Phys. Rev. Lett.*, vol. 96, p. 089301, Feb 2006.

[78] K. Rzążewski and K. Wódkiewicz, "Stability of matter interacting with photons," *Phys. Rev. A*, vol. 43, pp. 593–594, Jan 1991.

[79] J. Keeling, "Coulomb interactions, gauge invariance, and phase transitions of the Dicke model," *J. Phys.: Condens. Matt.*, vol. 19, Jul 25 2007.

[80] A. Vukics and P. Domokos, "Adequacy of the dicke model in cavity qed: A counter-no-go statement," *Phys. Rev. A*, vol. 86, p. 053807, Nov 2012.

[81] F. Dimer, B. Estienne, A. S. Parkins, and H. J. Carmichael, "Proposed realization of the dicke-model quantum phase transition in an optical cavity qed system," *Phys. Rev. A*, vol. 75, p. 013804, Jan 2007.

[82] P. Nataf and C. Ciuti, "No-go theorem for superradiant quantum phase transitions in cavity QED and counter-example in circuit QED," *Nat. Comm.*, vol. 1, Sep 2010.

[83] B. M. Garraway, "The Dicke model in quantum optics: Dicke model revisited," *Phil. Trans. R. Soc. A*, vol. 369, pp. 1137–1155, Mar 28 2011.

[84] F. Bloch, "Stopping power of atoms with several electrons," *Z. Phys.*, vol. 81, pp. 363–376, May 1933.

[85] S. Tomonaga, "Remarks on Blochs method of sound waves applied to many-Fermion problems," *Prog. Theor. Phys.*, vol. 5, no. 4, pp. 544–569, 1950.

[86] R. Kanamoto and P. Meystre, "Optomechanics of a quantum-degenerate fermi gas," *Phys. Rev. Lett.*, vol. 104, p. 063601, Feb 2010.

[87] R. Kanamoto and P. Meystre, "Optomechanics of ultracold atomic gases," *Physica Scripta*, vol. 82, no. 3, p. 038111, 2010.

[88] E. M. Purcell, H. C. Torrey, and R. V. Pound, "Resonance absorption by nuclear magnetic moments in a solid," *Phys. Rev.*, vol. 69, pp. 37–38, Jan 1946.

[89] P. R. Berman, *Cavity quantum electrodynamics*. Boston: Academic Press, 1994.

[90] J. D. Joannopoulos, *Photonic crystals : molding the flow of light*. Princeton: Princeton University Press, 2nd ed., 2008.

[91] P. Russell, "Photonic crystal fibers," *Science*, vol. 299, no. 5605, pp. 358–362, 2003.

[92] Y. Yang and S.-Y. Zhu, "Spontaneous emission from a two-level atom in a three-dimensional photonic crystal," *Phys. Rev. A*, vol. 62, p. 013805, Jun 2000.

[93] I. Takahashi and K. Ujihara, "Theory of spontaneous emission in an optical cavity," *Phys. Rev. A*, vol. 56, pp. 2299–2307, Sep 1997.

[94] S. John and J. Wang, "Quantum electrodynamics near a photonic band gap: Photon bound states and dressed atoms," *Phys. Rev. Lett.*, vol. 64, pp. 2418–2421, May 1990.

[95] S. John and J. Wang, "Quantum optics of localized light in a photonic band gap," *Phys. Rev. B*, vol. 43, pp. 12772–12789, Jun 1991.

[96] S. John and T. Quang, "Localization of superradiance near a photonic band gap," *Phys. Rev. Lett.*, vol. 74, pp. 3419–3422, Apr 1995.

[97] S. John and T. Quang, "Collective switching and inversion without fluctuation of two-level atoms in confined photonic systems," *Phys. Rev. Lett.*, vol. 78, pp. 1888–1891, Mar 1997.

[98] Z.-H. Li, D.-W. Wang, H. Zheng, S.-Y. Zhu, and M. S. Zubairy, "Quantum interference due to energy shifts and its effect on spontaneous emission," *Phys. Rev. A*, vol. 82, p. 050501, Nov 2010.

[99] K. Sakoda, "Group-theoretical classification of eigenmodes in three-dimensional photonic lattices," *Phys. Rev. B*, vol. 55, pp. 15345–15348, Jun 1997.

[100] I. Alvarado-Rodriguez, P. Halevi, and A. S. Sánchez, "Dipole radiation in a one-dimensional photonic crystal: te polarization," *Phys. Rev. E*, vol. 63, p. 056613, Apr 2001.

[101] Y. Yang, S.-Y. Zhu, and M. Zubairy, "Quantum interference-enhanced spontaneous emission and population oscillation in photonic crystals," *Optics Communications*, vol. 166, no. 16, pp. 79 – 84, 1999.

[102] Y. Yang, M. Fleischhauer, and S.-Y. Zhu, "Spontaneous emission from a two-level atom in two-band anisotropic photonic crystals," *Phys. Rev. A*, vol. 68, p. 043805, Oct 2003.

[103] N. Vats, S. John, and K. Busch, "Theory of fluorescence in photonic crystals," *Phys. Rev. A*, vol. 65, p. 043808, Mar 2002.

[104] S. Noda, K. Tomoda, N. Yamamoto, and A. Chutinan, "Full three-dimensional photonic bandgap crystals at near-infrared wavelengths," *Science*, vol. 289, no. 5479, pp. 604–606, 2000.

[105] M. A. T. Noda, Susumu Fujita, "Spontaneous-emission control by photonic crystals and nanocavities," *Nat Photon*, vol. 1, pp. 449–458, 2007.

[106] M. Fujita, S. Takahashi, Y. Tanaka, T. Asano, and S. Noda, "Simultaneous inhibition and redistribution of spontaneous light emission in photonic crystals," *Science*, vol. 308, no. 5726, pp. 1296–1298, 2005.

[107] S. John and T. Quang, "Quantum optical spin-glass state of impurity two-level atoms in a photonic band gap," *Phys. Rev. Lett.*, vol. 76, pp. 1320–1323, Feb 1996.

[108] W. E. Lamb and R. C. Retherford, "Fine structure of the hydrogen atom by a microwave method," *Phys. Rev.*, vol. 72, pp. 241–243, Aug 1947.

[109] H. A. Bethe, "The electromagnetic shift of energy levels," *Phys. Rev.*, vol. 72, pp. 339–341, Aug 1947.

[110] E. A. Power, "Zero-point energy and the lamb shift," *Am. J. Phys*, vol. 34, pp. 516–518, 1966.

[111] P. W. Milonni, *The quantum vacuum : an introduction to quantum electrodynamics*. Boston: Academic Press, 1994.

[112] M. Fleischhauer, A. Imamoglu, and J. P. Marangos, "Electromagnetically induced transparency: Optics in coherent media," *Rev. Mod. Phys.*, vol. 77, pp. 633–673, Jul 2005.

[113] S. Harris, "Electromagnetically induced transparency," *Phys. Today*, vol. 50, pp. 36–42, Jul 1997.

[114] M. O. Scully, "Correlated spontaneous-emission lasers: Quenching of quantum fluctuations in the relative phase angle," *Phys. Rev. Lett.*, vol. 55, pp. 2802–2805, Dec 1985.

[115] M. O. Scully and M. S. Zubairy, "Theory of the quantum-beat laser," *Phys. Rev. A*, vol. 35, pp. 752–758, Jan 1987.

[116] A. S. Zibrov, M. D. Lukin, D. E. Nikonov, L. Hollberg, M. O. Scully, V. L. Velichansky, and H. G. Robinson, "Experimental demonstration of laser oscillation without population inversion via quantum interference in rb," *Phys. Rev. Lett.*, vol. 75, pp. 1499–1502, Aug 1995.

[117] P. Facchi and S. Pascazio, "Spontaneous emission and lifetime modification caused by an intense electromagnetic field," *Phys. Rev. A*, vol. 62, p. 023804, Jul 2000.

[118] K. Johnson, J. Thywissen, N. Dekker, K. Berggren, A. Chu, R. Younkin, and M. Prentiss, "Localization of metastable atom beams with optical standing

waves: Nanolithography at the Heisenberg limit," *Science*, vol. 280, pp. 1583–1586, Jun 5 1998.

[119] J. Thomas and L. Wang, "Precision position measurement of moving atoms," *Physics Reports*, vol. 262, no. 6, pp. 311 – 366, 1995.

[120] P. Storey, M. Collett, and D. Walls, "Measurement-induced diffraction and interference of atoms," *Phys. Rev. Lett.*, vol. 68, pp. 472–475, Jan 1992.

[121] P. Storey, M. Collett, and D. Walls, "Atomic-position resolution by quadrature-field measurement," *Phys. Rev. A*, vol. 47, pp. 405–418, Jan 1993.

[122] R. Quadt, M. Collett, and D. F. Walls, "Measurement of atomic motion in a standing light field by homodyne detection," *Phys. Rev. Lett.*, vol. 74, pp. 351–354, Jan 1995.

[123] S. Kunze, K. Dieckmann, and G. Rempe, "Diffraction of atoms from a measurement induced grating," *Phys. Rev. Lett.*, vol. 78, pp. 2038–2041, Mar 1997.

[124] F. Le Kien, G. Rempe, W. P. Schleich, and M. S. Zubairy, "Atom localization via ramsey interferometry: A coherent cavity field provides a better resolution," *Phys. Rev. A*, vol. 56, pp. 2972–2977, Oct 1997.

[125] A. M. Herkommer, W. P. Schleich, and M. S. Zubairy, "Autler-townes microscopy on a single atom," *Journal of Modern Optics*, vol. 44, no. 11-12, pp. 2507–2513, 1997.

[126] S. Qamar, S.-Y. Zhu, and M. S. Zubairy, "Atom localization via resonance fluorescence," *Phys. Rev. A*, vol. 61, p. 063806, May 2000.

[127] S. Qamar, S.-Y. Zhu, and M. Zubairy, "Precision localization of single atom using autler-townes microscopy," *Optics Communications*, vol. 176, pp. 409 – 416, 2000.

[128] E. Paspalakis and P. L. Knight, "Localizing an atom via quantum interference," *Phys. Rev. A*, vol. 63, p. 065802, May 2001.

[129] H. Nha, J.-H. Lee, J.-S. Chang, and K. An, "Atomic-position localization via dual measurement," *Phys. Rev. A*, vol. 65, p. 033827, Feb 2002.

[130] J.-T. Chang, J. Evers, M. O. Scully, and M. Suhail Zubairy, "Measurement of the separation between atoms beyond diffraction limit," *Phys. Rev. A*, vol. 73, p. 031803, Mar 2006.

[131] J.-T. Chang, J. Evers, and M. S. Zubairy, "Distilling two-atom distance information from intensity-intensity correlation functions," *Phys. Rev. A*, vol. 74, p. 043820, Oct 2006.

# APPENDIX A

## DERIVATION OF THE DISCRETE MODE HAMILTONIAN

The derivation of the discrete mode Hamiltonian equation. (2.20) follows from equations. (2.13) and (2.19) as

$$
\begin{aligned}
\hat{H} = & \int dx \left[\sqrt{\frac{1}{L}}\hat{c}_0^\dagger + \sqrt{\frac{2}{L}}\cos(kx)\hat{c}_1^\dagger + \sqrt{\frac{2}{L}}\cos(2kx)\hat{c}_2^\dagger\right]\left[\frac{-1}{2m}\frac{d^2}{d^2x} + U_0\cos^2(kx)\hat{a}^\dagger\hat{a}\right. \\
& \left.+\eta_\perp\cos(kx)(\hat{a}^\dagger+\hat{a})\right]\left[\sqrt{\frac{1}{L}}\hat{c}_0 + \sqrt{\frac{2}{L}}\cos(kx)\hat{c}_1 + \sqrt{\frac{2}{L}}\cos(2kx)\hat{c}_2\right] + \Delta_c\hat{a}^\dagger\hat{a} \\
& + \eta_\parallel(\hat{a}^\dagger+\hat{a}) \\
= & \int dx \left[\sqrt{\frac{1}{L}}\hat{c}_0^\dagger + \sqrt{\frac{2}{L}}\cos(kx)\hat{c}_1^\dagger + \sqrt{\frac{2}{L}}\cos(2kx)\hat{c}_2^\dagger\right]\left[\sqrt{\frac{1}{L}}\cos^2(kx)U_0\hat{a}^\dagger\hat{a}\hat{c}_0\right. \\
& + \sqrt{\frac{1}{L}}\cos(kx)\eta_\perp(\hat{a}^\dagger+\hat{a})\hat{c}_0 + \frac{k^2}{2m}\sqrt{\frac{2}{L}}\cos(kx)\hat{c}_1 + \sqrt{\frac{2}{L}}\cos^3(kx)U_0\hat{a}^\dagger\hat{a}\hat{c}_1 \\
& + \sqrt{\frac{2}{L}}\cos^2(kx)\eta_\perp(\hat{a}^\dagger+\hat{a})\hat{c}_1 + \sqrt{\frac{2}{L}}\cos(kx)\cos(2kx)\eta_\perp(\hat{a}^\dagger+\hat{a})\hat{c}_2 \\
& \left.+\sqrt{\frac{2}{L}}\cos^2(kx)\cos(2kx)U_0\hat{a}^\dagger\hat{a}\hat{c}_2\right] + \frac{4k^2}{2m}\sqrt{\frac{2}{L}}\cos(2kx)\hat{c}_2 + \Delta_c\hat{a}^\dagger\hat{a} + \eta_\parallel(\hat{a}^\dagger+\hat{a}) \\
= & \frac{U_0}{2}\hat{a}^\dagger\hat{a}\hat{c}_0^\dagger\hat{c}_0 + \frac{U_0}{2\sqrt{2}}\hat{a}^\dagger\hat{a}\hat{c}_2^\dagger\hat{c}_0 + \frac{\eta_\perp}{\sqrt{2}}(\hat{a}^\dagger+\hat{a})\hat{c}_1^\dagger\hat{c}_0 + \frac{k^2}{2m}\hat{c}_1^\dagger\hat{c}_1 + \frac{3U_0}{4}\hat{a}^\dagger\hat{a}\hat{c}_1^\dagger\hat{c}_1 \\
& + \frac{\eta_\perp}{\sqrt{2}}(\hat{a}^\dagger+\hat{a})\hat{c}_0^\dagger\hat{c}_1 + \frac{\eta_\perp}{2}(\hat{a}^\dagger+\hat{a})\hat{c}_2^\dagger\hat{c}_1 + \frac{4k^2}{2m}\hat{c}_2^\dagger\hat{c}_2 + \frac{U_0}{2\sqrt{2}}\hat{a}^\dagger\hat{a}\hat{c}_0^\dagger\hat{c}_2 \\
& + \frac{U_0}{2}\hat{a}^\dagger\hat{a}\hat{c}_2^\dagger\hat{c}_2 + \frac{\eta_\perp}{2}(\hat{a}^\dagger+\hat{a})\hat{c}_1^\dagger\hat{c}_2 + \Delta_c\hat{a}^\dagger\hat{a} + \eta_\parallel(\hat{a}^\dagger+\hat{a}) \\
= & \omega_r\hat{c}_1^\dagger\hat{c}_1 + 4\omega_r\hat{c}_2^\dagger\hat{c}_2 + \frac{U_0}{4}\hat{a}^\dagger\hat{a}\Big[\sqrt{2}(\hat{c}_0^\dagger\hat{c}_2 + \hat{c}_2^\dagger\hat{c}_0) + 2N + \hat{c}_1^\dagger\hat{c}_1\Big] \\
& + \frac{\eta_\perp}{2}(\hat{a}^\dagger+\hat{a})\Big[\sqrt{2}(\hat{c}_0^\dagger\hat{c}_1 + \hat{c}_1^\dagger\hat{c}_0) + (\hat{c}_1^\dagger\hat{c}_2 + \hat{c}_2^\dagger\hat{c}_1)\Big] + \Delta_c\hat{a}^\dagger\hat{a} + \eta_\parallel(\hat{a}^\dagger+\hat{a}). \qquad \text{(A.1)}
\end{aligned}
$$

The atom-atom interaction contains terms such as $\hat{c}_1^\dagger \hat{c}_1 \hat{c}_0^\dagger \hat{c}_0$, which mixes the discrete modes we retain and other modes we discard and impairs the DMP method. The energy scale of the atom atom interactions on the order of the chemical potential $\mu = (3g\omega/4)^{2/3}$(in units of $\omega_r$), we can neglect it on the time scale of $1/\omega_r$ when $\mu \ll 1$. This condition is fulfilled in current experiment [43].

# APPENDIX B

# DERIVATION OF THE FERMION HAMILTONIAN

## B.1 Commutation relation $[\hat{d}_q, \hat{d}_q^\dagger]$

We prove the commutation relations $[\hat{d}_q, \hat{d}_q^\dagger] = 1$, where $\hat{d}_q$ and $\hat{d}_q^\dagger$ are defined in equation(2.46).

$$
\begin{aligned}
[\hat{d}_q, \hat{d}_q^\dagger] =& \beta_q^2 \sum_{k,k'>0} (\hat{f}_k^\dagger \hat{f}_{k+q} \hat{f}_{k'}^\dagger \hat{f}_{k'-q} - \hat{f}_{k'}^\dagger \hat{f}_{k'-q} \hat{f}_k^\dagger \hat{f}_{k+q}) \\
=& \beta_q^2 \sum_{k,k'>0} (\hat{f}_k^\dagger \hat{f}_{k'-q} \delta_{k+q,k'} - \hat{f}_k^\dagger \hat{f}_{k'}^\dagger \hat{f}_{k+q} \hat{f}_{k'-q} - \hat{f}_{k'}^\dagger \hat{f}_{k'-q} \hat{f}_k^\dagger \hat{f}_{k+q}) \\
=& \beta_q^2 \sum_{k,k'>0} (\hat{f}_k^\dagger \hat{f}_{k'-q} \delta_{k+q,k'} - \hat{f}_{k'}^\dagger \hat{f}_k^\dagger \hat{f}_{k'-q} \hat{f}_{k+q} - \hat{f}_{k'}^\dagger \hat{f}_{k'-q} \hat{f}_k^\dagger \hat{f}_{k+q}) \\
=& \beta_q^2 \sum_{k,k'>0} (\hat{f}_k^\dagger \hat{f}_{k'-q} \delta_{k+q,k'} - \hat{f}_{k'}^\dagger \hat{f}_{k+q} \delta_{k,k'-q} + \hat{f}_{k'}^\dagger \hat{f}_{k'-q} \hat{f}_k^\dagger \hat{f}_{k+q} - \hat{f}_{k'}^\dagger \hat{f}_{k'-q} \hat{f}_k^\dagger \hat{f}_{k+q}) \\
=& \beta_q^2 \sum_{k>0} (\hat{f}_k^\dagger \hat{f}_k - \hat{f}_{k+q}^\dagger \hat{f}_{k+q}) = \beta_q^2 \sum_{k>0}^{q} \hat{f}_k^\dagger \hat{f}_k \simeq \beta_q^2 \frac{qL}{2\pi} = 1 \,.
\end{aligned} \tag{B.1}
$$

## B.2 Effective Hamiltonian

Next we prove that $\sum_k \epsilon(k) \hat{f}_k^\dagger \hat{f}_k \to \sum_{q>0} \hbar v_F q (\hat{d}_q^\dagger \hat{d}_q + \hat{d}_{-q}^\dagger \hat{d}_{-q})$.

First, following the definition in equation (2.46), we have

$$
\begin{aligned}
\sum_{q>0} \hat{\rho}_{-q}^+ \hat{\rho}_q^+ =& \sum_{q>0} \sum_{k>0} \sum_{k'>0} \hat{f}_k^\dagger \hat{f}_{k-q} \hat{f}_{k'}^\dagger \hat{f}_{k'+q} \\
=& \sum_{q>0} \sum_{k>q} \hat{f}_k^\dagger \hat{f}_{k-q} \hat{f}_{k-q}^\dagger \hat{f}_k + \sum_{q>0} \left( \sum_{k>0} \sum_{k'>0} \right)' \hat{f}_k^\dagger \hat{f}_{k-q} \hat{f}_{k'}^\dagger \hat{f}_{k'+q} \,.
\end{aligned} \tag{B.2}
$$

In the above summation, the prime means that terms with $k' = k - q$ are omitted. In

the last line of the equation above, the first term corresponds to the diagonal parts and the second term corresponds to the off-diagonal parts. For the diagonal term $D^+$, we have

$$\begin{aligned} D^+ =& \sum_{q>0}\sum_{k>q} \hat{f}_k^\dagger \hat{f}_{k-q} \hat{f}_{k-q}^\dagger \hat{f}_k = \sum_{q>0}\sum_{k>q} \hat{f}_k^\dagger \hat{f}_k (1 - \hat{f}_{k-q}^\dagger \hat{f}_{k-q}) \\ =& \sum_{k>q}\sum_{q>0} (\hat{f}_k^\dagger \hat{f}_k - \hat{f}_{k-q}^\dagger \hat{f}_{k-q} \hat{f}_k^\dagger \hat{f}_k) \,. \end{aligned} \tag{B.3}$$

We now notice that

$$\sum_{k>q}\sum_{q>0} \hat{f}_k^\dagger \hat{f}_k = \sum_{k>0}\sum_{0<q<k} \hat{f}_k^\dagger \hat{f}_k = \sum_{k>0} \frac{kL}{2\pi} \hat{f}_k^\dagger \hat{f}_k \,, \tag{B.4}$$

and

$$\begin{aligned} \sum_{k>q}\sum_{q>0} \hat{f}_{k-q}^\dagger \hat{f}_{k-q} \hat{f}_k^\dagger \hat{f}_k =& \sum_{k>0}\sum_{0<q<k} n_{k-q} n_k = \frac{1}{2}\left[ \left( \sum_{k>0} n_k \right)^2 + \sum_{k>0} n_k^2 \right] \\ =& \frac{1}{2} N_{\max}(N_{\max}+1) \,, \end{aligned} \tag{B.5}$$

so,

$$D^+ = \sum_{k>0} \frac{kL}{2\pi} \hat{f}_k^\dagger \hat{f}_k - \frac{1}{2} N_{\max}(N_{\max}+1) \,. \tag{B.6}$$

For the off-diagonal term,

$$\begin{aligned} C^+ =& \sum_{q>0} \left( \sum_{k>0}\sum_{k'>0} \right)' \hat{f}_k^\dagger \hat{f}_{k-q} \hat{f}_{k'}^\dagger \hat{f}_{k'+q} = \sum_{q<0} \left( \sum_{k'>0}\sum_{k>0} \right)' \hat{f}_{k'}^\dagger \hat{f}_{k'+q} \hat{f}_k^\dagger \hat{f}_{k-q} \\ =& \sum_{q<0} \left( \sum_{k>0}\sum_{k'>0} \right)' \hat{f}_k^\dagger \hat{f}_{k-q} \hat{f}_{k'}^\dagger \hat{f}_{k'+q} = \frac{1}{2} \sum_{q} \left( \sum_{k>0}\sum_{k'>0} \right)' \hat{f}_k^\dagger \hat{f}_{k-q} \hat{f}_{k'}^\dagger \hat{f}_{k'+q} \,. \end{aligned} \tag{B.7}$$

Notice that

$$C^+ = -\frac{1}{2}\sum_q \left(\sum_{k>0}\sum_{k'>0}\right)' \hat{f}^\dagger_{k'}\hat{f}_{k-q}\hat{f}^\dagger_k\hat{f}_{k'+q}\,. \tag{B.8}$$

Then if we define $k-q = k'-s$, we have

$$C^+ = -\frac{1}{2}\sum_s \left(\sum_{k>0}\sum_{k'>0}\right)' \hat{f}^\dagger_{k'}\hat{f}_{k'-s}\hat{f}^\dagger_k\hat{f}_{k+s}\,. \tag{B.9}$$

Therefore we have

$$C^+ = -C^+ = 0\,. \tag{B.10}$$

In the same way, we have, for $\sum_q \rho^-_q\rho^-_{-q}$,

$$\begin{aligned} D^- &= \sum_{k<0}\frac{|k|L}{2\pi}\hat{f}^\dagger_k\hat{f}_k - \frac{1}{2}N_{\max}(N_{\max}+1)\,, \\ C^- &= 0\,. \end{aligned} \tag{B.11}$$

Therefore, we have

$$\begin{aligned} &\sum_{q>0}\hbar v_F q\left(\hat{d}^\dagger_q\hat{d}_q + \hat{d}^\dagger_{-q}\hat{d}_{-q}\right) = \sum_{q>0}\hbar v_F\frac{2\pi}{L}\left(\hat{\rho}^+_{-q}\hat{\rho}^+_q + \hat{\rho}^-_q\hat{\rho}^-_{-q}\right) \\ =&\sum_k \hbar|k|v_F\hat{f}^\dagger_k\hat{f}_k - \hbar v_F\frac{2\pi}{L}N_{\max}(N_{\max}+1) \\ =&\sum_k \hbar|k|v_F\hat{f}^\dagger_k\hat{f}_k - 2\hbar v_F k_F(N_{\max}+1)\,. \end{aligned} \tag{B.12}$$

The second term corresponds to the energy of the ground state, which is a constant. So $\sum_{q>0}\hbar v_F q(\hat{d}^\dagger_q\hat{d}_q + \hat{d}^\dagger_{-q}\hat{d}_{-q})$ describes the kinetic energy of the excitation.

# APPENDIX C

## TRAPPING CONDITION WITHOUT THE RWA

First, let us note that, if we have $\omega_{a_1 b},\ \omega_{a_2 b} \gg |\omega_{a_1 b} - \omega_{a_2 b}|$, then

$$\frac{\gamma_{a_1}}{\gamma_{a_2}} \simeq \frac{|\vec{p}_{a_1 b}|^2}{|\vec{p}_{a_2 b}|^2}\,. \tag{C.1}$$

If we include the counter-rotating terms, $\kappa_0 = \frac{1}{2}\gamma_0 + i\Delta E^{(0)}_{\rm dyn}$ and $\kappa_{0\pm} = \frac{1}{2}\gamma_{0\pm} + i\Delta E^{(0\pm)}_{\rm dyn} + i\eta_{0\pm}$. And we have that

$$\begin{aligned}
\Delta E^{(0)}_{\rm dyn} &= \sum_k \mathscr{P}\frac{V^2_{k,0}}{\omega'_{0b} - \omega_k} \\
&= \sum_k \mathscr{P}\frac{4\omega^2_{0b} g^2_{k,0}}{(\omega_k + \omega_{0b})^2(\omega'_{0b} - \omega_k)} \\
&= N_0^2 \sum_k \mathscr{P}[\Omega_2^2 g_k^{(1)2} + \Omega_1^2 g_k^{(2)2} - 2\Omega_1\Omega_2 g_k^{(1)} g_k^{(2)}]\frac{4\omega^2_{0b}}{(\omega_k + \omega_{0b})^2(\omega'_{0b} - \omega_k)} \\
&= N_0^2[\Omega_2^2\gamma_{a_1} + \Omega_1^2\gamma_{a_2} - 2p\Omega_1\Omega_2\sqrt{\gamma_{a_1}\gamma_{a_2}}] \sum_k \mathscr{P}\frac{g_k^{(1)2}}{\gamma_{a_1}}\frac{4\omega^2_{0b}}{(\omega_k + \omega_{0b})^2(\omega'_{0b} - \omega_k)}\,, \qquad \text{(C.2a)} \\
\Delta E^{(0\pm)}_{\rm dyn} &= \sum_k \mathscr{P}\frac{V_{k,0}V_{k,\pm}}{\omega'_{0b} - \omega_k} = \sum_k \mathscr{P}\frac{4\omega_{0b}\omega_{\pm b} g_{k,0} g_{k,\pm}}{(\omega_k + \omega_{0b})(\omega_k + \omega_{\pm b})(\omega'_{0b} - \omega_k)} \\
&= N_\pm N_0 \sum_k \mathscr{P}\Bigg\{\Omega_1\Omega_2\left[\left(\mu \pm \frac{\omega_{12}}{2}\right) g_k^{(1)2} - \left(\mu \mp \frac{\omega_{12}}{2}\right) g_k^{(2)2}\right] + \left[\Omega_2^2\left(\mu \mp \frac{\omega_{12}}{2}\right)\right. \\
&\quad \left. -\Omega_1^2\left(\mu \pm \frac{\omega_{12}}{2}\right) g_k^{(1)} g_k^{(2)}\right]\Bigg\}\frac{4\omega_{0b}\omega_{0\pm}}{(\omega_k + \omega_{0b})(\omega_k + \omega_{\pm b})(\omega'_{0b} - \omega_k)} \\
&= N_\pm N_0\Bigg\{\Omega_1\Omega_2\left[\left(\mu \pm \frac{\omega_{12}}{2}\right)\gamma_{a_1} - \left(\mu \mp \frac{\omega_{12}}{2}\right)\gamma_{a_2}\right] + p\left[\Omega_2^2\left(\mu \mp \frac{\omega_{12}}{2}\right)\right. \\
&\quad \left. -\Omega_1^2\left(\mu \pm \frac{\omega_{12}}{2}\right)\sqrt{\gamma_{a_1}\gamma_{a_2}}\right]\Bigg\} \sum_k \mathscr{P}\frac{g_k^{(1)2}}{\gamma_{a_1}}\frac{4\omega_{0b}\omega_{0\pm}}{(\omega_k + \omega_{0b})(\omega_k + \omega_{\pm b})(\omega'_{0b} - \omega_k)}\,, \qquad \text{(C.2b)}
\end{aligned}$$

$$
\begin{aligned}
\eta_{0\pm} &= \sum_k \frac{g_{k,0}g_{k,\pm}}{\omega_k}\frac{2\omega_0\omega_\pm - \omega_k(\omega_0+\omega_\pm)}{2(\omega_0+\omega_k)(\omega_\pm+\omega_k)} \\
&= N_\pm N_0 \sum_k \Bigg\{ \Omega_1\Omega_2 \left[\left(\mu \pm \frac{\omega_{12}}{2}\right) g_k^{(1)2} - \left(\mu \mp \frac{\omega_{12}}{2}\right) g_k^{(2)2}\right] + \left[\Omega_2^2\left(\mu \mp \frac{\omega_{12}}{2}\right)\right. \\
&\quad \left. -\Omega_1^2\left(\mu \pm \frac{\omega_{12}}{2}\right) g_k^{(1)} g_k^{(2)}\right] \Bigg\} \frac{1}{\omega_k}\frac{2\omega_0\omega_\pm - \omega_k(\omega_0+\omega_\pm)}{2(\omega_0+\omega_k)(\omega_\pm+\omega_k)} \\
&= N_\pm N_0 \Bigg\{ \Omega_1\Omega_2 \left[\left(\mu \pm \frac{\omega_{12}}{2}\right)\gamma_{a_1} - \left(\mu \mp \frac{\omega_{12}}{2}\right)\gamma_{a_2}\right] + p\left[\Omega_2^2\left(\mu \mp \frac{\omega_{12}}{2}\right)\right. \\
&\quad \left. -\Omega_1^2\left(\mu \pm \frac{\omega_{12}}{2}\right)\sqrt{\gamma_{a_1}\gamma_{a_2}}\right] \Bigg\} \sum_k \frac{g_k^{(1)2}}{\gamma_{a_1}}\frac{1}{\omega_k}\frac{2\omega_0\omega_\pm - \omega_k(\omega_0+\omega_\pm)}{2(\omega_0+\omega_k)(\omega_\pm+\omega_k)}\,. \qquad \text{(C.2c)}
\end{aligned}
$$

So when the condition as shown in Eq. (3.33) holds, $\gamma_0 = \gamma_{0\pm} = 0$, and $\Delta E^{(0)}_{\rm dyn} = \Delta E^{(0\pm)}_{\rm dyn} = \eta_{0\pm} = 0$. Therefore $\det M = 0$ and the trapping condition remains the same as when we use the RWA.

# APPENDIX D

# LAPLACE TRANSFORM AND ENERGY SHIFTS

## D.1 Calculation of Γ

It follows from Eq. (10) that

$$\begin{aligned}\Gamma &= \sum_k \frac{V_k^2}{p + i(\omega_k - \omega_1')} \\ &= \frac{(\omega_1 d_1)^2}{16\pi^3\epsilon_0\hbar} \sum_j \int_j d\mathbf{k} \Big(\frac{2\omega_1}{\omega_1 + \omega_k}\Big)^2 \frac{1}{\omega_k} \Big[1 - \frac{(\mathbf{k}\cdot\mathbf{u}_d)^2}{k^2}\Big] \frac{1}{p - i(\omega_1' - \omega_k)} \,. \quad \text{(D.1)}\end{aligned}$$

If the density of the state is broadband, such as in vacuum, the Weisskopf-Wigner approximation is valid and one can use the first order pole contribution of $p$ to calculate the above integration. However, the density of the electromagnetic modes of the photonic crystal changes rapidly in the vicinity of the band edge, the Weisskopf-Wigner perturbation theory is inadequate. We have to perform an exact integration in Eq. (D.1). Therefore we substitute the dispersion relation as described in Eq. (3.41) in Eq. (D.1)

$$\begin{aligned}\Gamma &= \frac{(\omega_1 d_1)^2}{16\pi^3\epsilon_0\hbar} \sum_j (\sin\theta_j)^2 \int_j d\mathbf{k} \Big(\frac{2\omega_1}{\omega_1 + \omega_c + A|\mathbf{k} - \mathbf{k}_0^i|^2}\Big)^2 \frac{1}{\omega_c + A|\mathbf{k} - \mathbf{k}_0^i|^2} \\ &\quad \frac{1}{p + iA|\mathbf{k} - \mathbf{k}_0^i|^2 + i(\omega_c - \omega_1')} \\ &= \frac{(\omega_1 d_1)^2}{16\pi^3\epsilon_0\hbar} \sum_j (\sin\theta_j)^2 \int_j d\mathbf{q} \Big(\frac{2\omega_1}{\omega_1 + \omega_c + Aq^2}\Big)^2 \frac{1}{\omega_c + Aq^2} \frac{1}{p + i(\omega_c - \omega_1') + iAq^2} \\ &= \frac{(\omega_1 d_1)^2}{4\pi^2\epsilon_0\hbar} \sum_j (\sin\theta_j)^2 \int_j dq \Big(\frac{2\omega_1}{\omega_1 + \omega_c + Aq^2}\Big)^2 \frac{q^2}{\omega_c + Aq^2} \frac{1}{p + i(\omega_c - \omega_1') + iAq^2}\end{aligned}$$

$$
\begin{aligned}
&= -2i\beta^{3/2}\int_j dx\Big(\frac{2\omega_1}{\omega_1+\omega_c+x^2}\Big)^2\frac{x^2}{\omega_c+x^2}\frac{1}{-i(p+i\omega_c-i\omega_1')+x^2}\\
&= -2i\beta^{3/2}\omega_1^2\left[\sqrt{\omega_c}+2\sqrt{\omega_1+\omega_c}+\sqrt{-ip-(\omega_1'-\omega_c)}\right]/\Big\{(\sqrt{\omega_c}+\sqrt{\omega_1+\omega_c})^2\\
&\quad\left[\sqrt{\omega_1+\omega_c}\sqrt{\omega_c}+\sqrt{-ip-(\omega_1'-\omega_c)}\right]\left[\sqrt{\omega_1+\omega_c}+\sqrt{-ip-(\omega_1'-\omega_c)}\right]^2\Big\}^{-1}.
\end{aligned}
\tag{D.2}
$$

## D.2 The inverse Laplace transform

According to Eq. (3.47), we proceed the inverse Laplace transform as follows. Since $\sqrt{-ix-(\omega_1'-\omega_c)}$ is not single valued, we cut the complex plane along $(\omega_{1c}'i, -\infty i)$. We then choose the integration contour as shown in figure D.1(a). According to the residue theorem,

$$
A(t)=\sum_j\frac{e^{x_j^{(1)}t}}{F'(x_j^{(1)})}-\frac{1}{2\pi i}\left[\int_{\omega_{1c}'i-\infty}^{\omega_{1c}'i+0}+\int_{\omega_{1c}'i+0}^{-\infty i+0}\right]\frac{e^{xt}}{x+\Gamma}dx, \tag{D.3}
$$

where

$$
\begin{aligned}
F(x) &\equiv x-\left[i\beta^{3/2}\cdot 2\omega_1^2(\sqrt{\omega_c}+2\sqrt{\omega_1+\omega_c}+\sqrt{-ix-(\omega_1'-\omega_c)})\right]\Big\{\sqrt{\omega_1+\omega_c}\\
&\quad\cdot\left(\sqrt{\omega_c}+\sqrt{\omega_1+\omega_c}\right)^2\left[\sqrt{\omega_c}+\sqrt{-ix-(\omega_1'-\omega_c)}\right]\left[\sqrt{\omega_1+\omega_c}\right.\\
&\quad\left.+\sqrt{-ix-(\omega_1'-\omega_c)}\right]^2\Big\}^{-1},\\
F'(x) &= \frac{dF}{dx},
\end{aligned}
\tag{D.4}
$$

and $x_j^{(1)}$ is the root of the equation $F(x)=0$ in the region as the contour shown in figure D.1(a). The last term of Eq. (D.3) can be calculated as follows

$$
\int_{\omega_{1c}'i+0}^{-\infty i+0}\frac{e^{xt}}{x+\Gamma}dx
$$

$$
\begin{aligned}
&= \int_{\omega'_{1c}i+0}^{-\infty i+0} \frac{e^{xt}}{x - \frac{i\beta^{3/2}\cdot 2\omega_1^2(\sqrt{\omega_c}+2\sqrt{\omega_1+\omega_c}+\sqrt{-ix-(\omega'_1-\omega_c)})}{\sqrt{\omega_1+\omega_c}(\sqrt{\omega_c}+\sqrt{\omega_1+\omega_c})^2\cdot(\sqrt{\omega_c}+\sqrt{-ix-(\omega'_1-\omega_c)})(\sqrt{\omega_1+\omega_c}+\sqrt{-ix-(\omega'_1-\omega_c)})^2}} dx \\
&= \int_{\omega'_{1c}i}^{-\infty i} \frac{e^{xt}}{x - \frac{i\beta^{3/2}\cdot 2\omega_1^2(\sqrt{\omega_c}+2\sqrt{\omega_1+\omega_c}-i\sqrt{ix+(\omega'_1-\omega_c)})}{\sqrt{\omega_1+\omega_c}(\sqrt{\omega_c}+\sqrt{\omega_1+\omega_c})^2\cdot(\sqrt{\omega_c}-i\sqrt{ix+(\omega'_1-\omega_c)})(\sqrt{\omega_1+\omega_c}-i\sqrt{ix+(\omega'_1-\omega_c)})^2}} dx \\
&= -\int_{\omega'_{1c}i-\infty}^{-\infty i} \frac{e^{xt}}{x - \frac{i\beta^{3/2}\cdot 2\omega_1^2(\sqrt{\omega_c}+2\sqrt{\omega_1+\omega_c}-i\sqrt{x+(\omega'_1-\omega_c)})}{\sqrt{\omega_1+\omega_c}(\sqrt{\omega_c}+\sqrt{\omega_1+\omega_c})^2\cdot(\sqrt{\omega_c}-i\sqrt{ix+(\omega'_1-\omega_c)})(\sqrt{\omega_1+\omega_c}-i\sqrt{ix+(\omega'_1-\omega_c)})^2}} dx \\
&\quad -\sum_j \frac{e^{x_j^{(2)}t}}{G'(x_j^{(2)})}\,, \qquad \text{(D.5)}
\end{aligned}
$$

where

$$
\begin{aligned}
G(x) &\equiv x - \left[i\beta^{3/2}\cdot 2\omega_1^2(\sqrt{\omega_c}+2\sqrt{\omega_1+\omega_c}-i\sqrt{ix+(\omega'_1-\omega_c)})\right]\Big\{\sqrt{\omega_1+\omega_c} \\
&\quad \cdot\left(\sqrt{\omega_c}+\sqrt{\omega_1+\omega_c}\right)^2\left[\sqrt{\omega_c}-i\sqrt{ix+(\omega'_1-\omega_c)}\right]\left[\sqrt{\omega_1+\omega_c}\right. \\
&\quad \left.-i\sqrt{ix+(\omega'_1-\omega_c)}\right]^2\Big\}^{-1}, \\
G'(x) &= \frac{dG}{dx}\,, \qquad \text{(D.6)}
\end{aligned}
$$

and $x_j^{(2)}$ is the root of the equation $G(x)=0$ in the region as the contour shown in figure D.1(b). Note that in Eq. (D.5), we integrate along the left edge of $(\omega'_{1c}i, -\infty i)$ instead of the right edge. Thus, $\sqrt{-ix-(\omega'_1-\omega_c)}$ turns to $-i\sqrt{ix+(\omega'_1-\omega_c)}$.

From equations (D.3) and (D.5), we then have

$$
\begin{aligned}
A(t) &= \sum_j \frac{e^{x_j^{(1)}t}}{F'(x_j^{(1)})} + \sum_j \frac{e^{x_j^{(2)}t}}{G'(x_j^{(2)})} \\
&+\frac{1}{2\pi i}\int_{\omega'_{1c}i-\infty}^{\omega'_{1c}i+0} \frac{e^{xt}}{x - \frac{i\beta^{3/2}\cdot 2\omega_1^2(\sqrt{\omega_c}+2\sqrt{\omega_1+\omega_c}-i\sqrt{x+(\omega'_1-\omega_c)})}{\sqrt{\omega_1+\omega_c}(\sqrt{\omega_c}+\sqrt{\omega_1+\omega_c})^2\cdot(\sqrt{\omega_c}-i\sqrt{ix+(\omega'_1-\omega_c)})(\sqrt{\omega_1+\omega_c}-i\sqrt{ix+(\omega'_1-\omega_c)})^2}} dx
\end{aligned}
$$

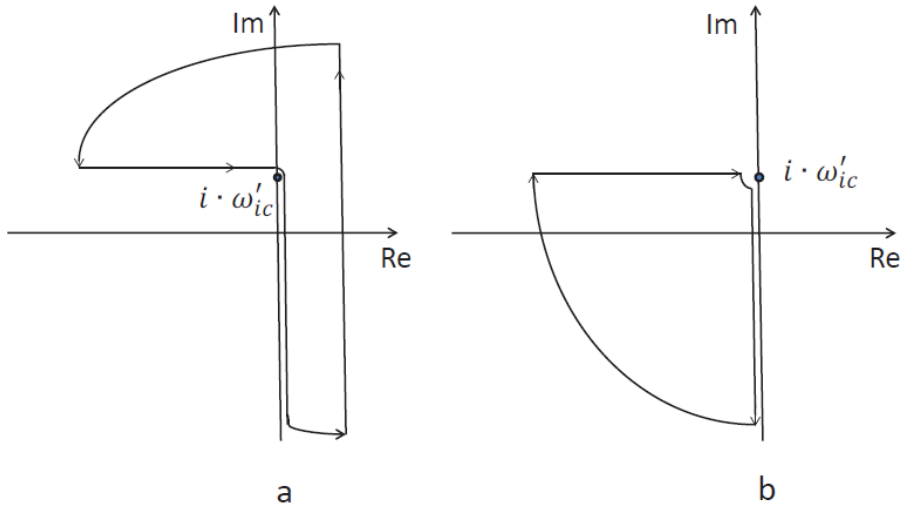


Figure D.1: (a) The integration contour of Eq. (D.3). (b) The integration contour of Eq. (D.5)

$$-\frac{1}{2\pi i}\int_{\omega'_{1c}i-\infty}^{\omega'_{1c}i+0} \frac{e^{xt}}{x-\frac{i\beta^{3/2}\cdot 2\omega_1^2(\sqrt{\omega_c}+2\sqrt{\omega_1+\omega_c}+\sqrt{-ix-(\omega'_1-\omega_c)})}{\sqrt{\omega_1+\omega_c}(\sqrt{\omega_c}+\sqrt{\omega_1+\omega_c})^2\cdot(\sqrt{\omega_c}+\sqrt{-ix-(\omega'_1-\omega_c)})(\sqrt{\omega_1+\omega_c}+\sqrt{-ix-(\omega'_1-\omega_c)})^2}}dx\,. \tag{D.7}$$

## D.3 Energy shifts

The total Lamb shift for a level $i$, composed of the non-dynamic energy shift and the dynamic energy shift, is given by [47]

$$\begin{aligned}\Delta E^i_{\rm Lamb} &= \Delta E^i_{\rm ndy}+\Delta E^i_{\rm dyn}\\ &= \sum_k\sum_{j\neq i}\frac{\hbar g_k^2}{\omega_k}\frac{\omega_{ji}(\omega_{ji}+\omega_k)}{(\omega_k+|\omega_{ji}|)^2}+\sum_k\sum_{j<i}\frac{4\omega_{ij}^2}{(\omega_{ij}+\omega_k)^2}\frac{\hbar g_k^2}{\omega_{ij}-\omega_k}\\ &= \sum_k\sum_{j\neq i}\frac{\hbar g_k^2}{\omega_k}\frac{\omega_{ij}}{\omega_{ij}-\omega_k}\,.\end{aligned} \tag{D.8}$$

As for the two level atom in the photonic crystal, $\omega_k = \omega_c + A|\mathbf{k} - \mathbf{k}_0^i|^2$. When $\omega_1 = \omega_c = 200\beta$, the non-dynamic energy shift is given by

$$\begin{aligned}
\Delta E_{\rm ndy} &= \hbar(\Delta\omega^{(1)}_{\rm ndy} - \Delta\omega^{(0)}_{\rm ndy}) = \sum_k \frac{\hbar g_k^2}{\omega_k}\left[\frac{-\omega_1(-\omega_1+\omega_k)}{(\omega_k+\omega_1)^2} - \frac{\omega_1(\omega_1+\omega_k)}{(\omega_k+\omega_1)^2}\right] \\
&= -\sum_k \frac{2\hbar g_k^2\omega_1}{(\omega_k+\omega_1)^2} = -\frac{\hbar(\omega_1 d_1)^2}{16\pi^3\epsilon_0\hbar}\int d\mathbf{k}\Big[1 - \frac{(\mathbf{k}\cdot\mathbf{u}_d)^2}{k^2}\Big]\frac{2\omega_1}{\omega_k(\omega_1+\omega_k)^2} \\
&= -\frac{\hbar(\omega_1 d_1)^2}{4\pi^2\epsilon_0\hbar}\sum_j \sin^2\theta_j \int dq \frac{2\omega_1 q^2}{(\omega_c + Aq^2)(\omega_1+\omega_c+Aq^2)^2} \\
&= -\frac{\hbar\beta^{3/2}}{\pi}\int dx \frac{4\omega_1 x^2}{(\omega_c+x^2)(\omega_1+\omega_c+x^2)^2} \\
&= -0.0085\hbar\beta\,. \qquad \text{(D.9)}
\end{aligned}$$

Here $x = \sqrt{A}q$.

The dynamic shift is given by

$$\begin{aligned}
\Delta E_{\rm dyn} &= \sum_k \frac{4\omega_1^2}{(\omega_1+\omega_k)^2}\frac{\hbar g_k^2}{\omega_1-\omega_k} \\
&= \frac{\hbar\beta^{3/2}}{\pi}\int dx \frac{8\omega_1^2 x^2}{(\omega_c+x^2)(\omega_1+\omega_c+x^2)^2(\omega_1-\omega_c-x^2)} \\
&= -0.0328\hbar\beta\,. \qquad \text{(D.10)}
\end{aligned}$$

Similarly, the total Lamb shift is

$$\begin{aligned}
\Delta E_{\rm Lamb} &= \sum_k \frac{\hbar g_k^2}{\omega_k}\left(\frac{\omega_1}{\omega_1-\omega_k} - \frac{-\omega_1}{-\omega_1-\omega_k}\right) = \sum_k \frac{2g_k^2\omega_1}{\omega_1^2-\omega_k^2} \\
&= \frac{\hbar\beta^{3/2}}{\pi}\int dx \frac{4\omega_1 x^2}{(\omega_c+x^2)(\omega_1+\omega_c+x^2)(\omega_1-\omega_c-x^2)} \\
&= -0.0414\hbar\beta\,. \qquad \text{(D.11)}
\end{aligned}$$

If the RWA is made, one can not get the full Lamb shift. Specifically, there is no

non-dynamic shift, and the dynamic shift is

$$\Delta E_{\mathrm{RWA}} = \sum_k \frac{\hbar g_k^2}{\omega_1 - \omega_k} = \frac{\beta^{3/2}}{\pi} \int dx \frac{2x^2}{(\omega_c + x^2)(\omega_1 - \omega_c - x^2)} \,. \qquad \text{(D.12)}$$